

1 **Selective inhibition reveals the regulatory function of DYRK2**
2 **in protein synthesis and calcium entry**

3

4 Tiantian Wei^{1,2,3#}, Jue Wang^{4#}, Ruqi Liang^{1,2,4#}, Wendong Chen^{5#}, Yilan Chen⁶, Mingzhe Ma⁴,
5 An He⁷, Yifei Du⁴, Wenjing Zhou⁸, Zhiying Zhang¹, Xin Zeng^{1,4}, Chu Wang^{1,4}, Jin Lu^{9,10}, Xing
6 Guo¹¹, Xiaowei Chen^{1,8}, Youjun Wang⁶, Ruijun Tian^{5,6*}, Junyu Xiao^{1,2,3,12*}, Xiaoguang Lei^{1,2,4,13*}

7

8 ¹The State Key Laboratory of Protein and Plant Gene Research, School of Life Sciences,
9 Peking University, Beijing, China.

10 ²Peking-Tsinghua Center for Life Sciences, Peking University, Beijing 100871, China.

11 ³Academy for Advanced Interdisciplinary Studies, Peking University, Beijing 100871, China.

12 ⁴Beijing National Laboratory for Molecular Sciences, Key Laboratory of Bioorganic Chemistry
13 and Molecular Engineering of Ministry of Education, College of Chemistry and Molecular
14 Engineering, Peking University, Beijing 100871, China.

15 ⁵SUSTech Academy for Advanced Interdisciplinary Studies, Southern University of Science
16 and Technology, Shenzhen 518055, China.

17 ⁶Beijing Key Laboratory of Gene Resource and Molecular Development, Key Laboratory of
18 Cell Proliferation and Regulation Biology, Ministry of Education, College of Life Sciences,
19 Beijing Normal University, Beijing 100875, China

20 ⁷Department of Chemistry, Southern University of Science and Technology, Shenzhen 518055,
21 China.

22 ⁸Institute of Molecular Medicine, Peking University, Beijing 100871, China.

23 ⁹Peking University Institute of Hematology, People's Hospital, Beijing 100044, China.

24 ¹⁰Collaborative Innovation Center of Hematology, Suzhou 215006, China.

25 ¹¹Life Sciences Institute, Zhejiang University, Hangzhou, 310058 China.

26 ¹²Beijing Advanced Innovation Center for Genomics (ICG), Peking University, Beijing 100871,

27 China.

28 ¹³Institute for Cancer Research, Shenzhen Bay Laboratory, Shenzhen, 518107, China

29 #These authors contributed equally

30 *Corresponding authors: Ruijun Tian (tianrj@sustech.edu.cn), Junyu Xiao

31 (junyuxiao@pku.edu.cn), Xiaoguang Lei (xglei@pku.edu.cn)

32

33

34 **Abstract:**

35 The dual-specificity tyrosine phosphorylation-regulated kinase DYRK2 has emerged
36 as a critical regulator of cellular processes. We took a chemical biology approach to gain
37 further insights into its function. We developed C17, a potent small-molecule DYRK2
38 inhibitor, through multiple rounds of structure-based optimization guided by several
39 co-crystallized structures. C17 displayed an effect on DYRK2 at a single-digit nanomolar
40 IC₅₀ and showed outstanding selectivity for the human kinome containing 467 other
41 human kinases. Using C17 as a chemical probe, we further performed quantitative
42 phosphoproteomic assays and identified several novel DYRK2 targets, including
43 eukaryotic translation initiation factor 4E-binding protein 1 (4E-BP1) and stromal
44 interaction molecule 1 (STIM1). DYRK2 phosphorylated 4E-BP1 at multiple sites, and the
45 combined treatment of C17 with AKT and MEK inhibitors showed synergistic 4E-BP1
46 phosphorylation suppression. The phosphorylation of STIM1 by DYRK2 substantially
47 increased the interaction of STIM1 with the ORAI1 channel, and C17 impeded the
48 store-operated calcium entry process. These studies collectively further expand our
49 understanding of DYRK2 and provide a valuable tool to pinpoint its biological function.

50

51 **Keywords:** DYRK2 , Kinase inhibitor , Quantitative phosphoproteomics , 4E-binding
52 protein 1 , stromal interaction molecule 1

53

54 Dual-specificity tyrosine phosphorylation-regulated kinases (DYRKs) belong to the
55 CMGC group of kinases together with other critical human kinases, such as
56 cyclin-dependent kinases (CDKs) and mitogen-activated protein kinases (MAPKs)
57 (Aranda et al., 2011; Becker and Joost, 1999; Manning et al., 2002). DYRKs uniquely
58 phosphorylate tyrosine residues within their activation loops *in cis* during biosynthesis,
59 although mature proteins display exclusive serine/threonine kinase activities (Lochhead et
60 al., 2005). There are five DYRKs in humans: DYRK1A, DYRK1B, DYRK2, DYRK3, and
61 DYRK4. DYRK1A has been extensively studied due to its potential function in the
62 pathogenesis of Down syndrome and neurodegenerative disorders (Becker and Sippl,
63 2011; Wegiel et al., 2011). DYRK3 has been shown to function as a central “dissolvase” to
64 regulate the formation of membrane-less organelles (Rai et al., 2018; Wippich et al.,
65 2013). On the other hand, DYRK2 is a crucial regulator of 26S proteasome activity (Guo
66 et al., 2016).

67 The 26S proteasome degrades the majority of proteins in human cells and plays a
68 central role in many cellular processes, including the regulation of gene expression and
69 cell division (Collins and Goldberg, 2017; Coux et al., 1996). Recent discoveries have
70 revealed that the 26S proteasome is subjected to intricate regulation by reversible
71 phosphorylation (Guo et al., 2017; Guo et al., 2016; Liu et al., 2020). DYRK2
72 phosphorylates the Rpt3 subunit in the regulatory particle of the proteasome at Thr25,
73 leading to the upregulation of proteasome activity (Guo et al., 2016). DYRK2 is
74 overexpressed in several tumors, including triple-negative breast cancer and multiple
75 myeloma, which are known to rely heavily on proteasome activity for progression, and
76 perturbation of DYRK2 activity impedes cancer cell proliferation and inhibits tumor growth
77 (Banerjee et al., 2018; Banerjee et al., 2019).

78 Our knowledge of the physiological functions of DYRK2 remains in its infancy, and
79 DYRK2 likely has cellular targets in addition to Rpt3. Substrates of many kinases,
80 especially Ser/Thr kinases, remain insufficiently identified. A major obstacle to discovering
81 physiologically relevant substrates of a kinase is the lack of highly specific chemical
82 probes that allow precise modulation of kinase function. Some DYRK2 inhibitors have
83 been reported; however, these compounds also inhibit other kinases, mostly other DYRK

84 family members, to various degrees (Chaikuad et al., 2016; Jouanne et al., 2017). We
 85 have recently identified LDN192960 as a selective DYRK2 inhibitor and showed that
 86 LDN192960 could alleviate multiple myeloma and triple-negative breast cancer
 87 progression by inhibiting DYRK2-mediated proteasome phosphorylation (Banerjee et al.,
 88 2019). To obtain even more potent and selective DYRK2 inhibitors, we applied a
 89 structure-guided approach to further engineer chemical compounds based on the
 90 LDN192960 scaffold. One of the best compounds we generated, compound C17 (C17),
 91 displays an effect on DYRK2 at a single-digit nanomolar IC₅₀ with moderate to excellent
 92 selectivity against kinases closely related to DYRK2. Using this potent DYRK2 inhibitor as
 93 a tool, we treated U266 cells with C17. We performed quantitative phosphoproteomic
 94 analyses, which led to identifying several novel DYRK2 targets, including eukaryotic
 95 translation initiation factor 4E-binding protein 1 (4E-BP1) and stromal interaction molecule
 96 1 (STIM1). These results demonstrate that DYRK2 plays critical regulatory roles in
 97 multiple cellular processes, including protein translation and store-operated calcium entry,
 98 and indicate that C17 can serve as a valuable probe for the study of DYRK2 function.

99

100

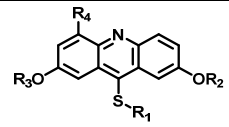
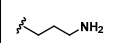
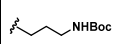
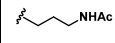
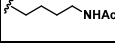
Table 1

101 **Table 1.** The Inhibitory activity and selectivity of acridine analogs of DYRK2.

102 **Table 1-source data 1**

103 Raw data of inhibitors against kinases for Table 1.

104

Cmpd.					IC ₅₀ at molecular level (nM)						Selectivity				
	R ₁	R ₂	R ₃	R ₄	DYRK2	DYRK1A	DYRK1B	DYRK3	Haspin	MARK3	DYRK2& DYRK1A	DYRK2& DYRK1B	DYRK2& DYRK3	DYRK2& Haspin	DYRK2& MARK3
LDN192 960		-CH ₃	-CH ₃	-H	53 ± 2	1859 ± 30	2900 ± 39	22 ± 4	18 ± 2	611 ± 19	35	55	-	-	12
1		-CH ₃	-CH ₃	-H	38 ± 2	651 ± 29	1401 ± 91	115 ± 4	34 ± 3	36 ± 2	17	17	3	-	-
2		-CH ₃	-CH ₃	-H	31 ± 1	731 ± 36	1477 ± 128	94 ± 9	27 ± 3	27 ± 5	24	48	3	-	-
3		-CH ₃	-CH ₃	-H	41 ± 2	1018 ± 78	2495 ± 88	157 ± 18	24 ± 1	33 ± 7	25	61	4	-	-

4		-CH ₃	-CH ₃	-H	53 ± 2	964 ± 14	1386 ± 21	234 ± 10	30 ± 1	96 ± 3	18	26	4	-	2
5		-CH ₃	-CH ₃	-H	89 ± 2	1026 ± 96	3488 ± 86	311 ± 22	53 ± 4	91 ± 5	12	39	3	-	1
6		-CH ₃	-CH ₃	-H	20 ± 3	889 ± 131	697 ± 67	110 ± 11	45 ± 3	100 ± 4	44	35	6	2	5
7		-CH ₃	-CH ₃	-CH ₂ OH	13 ± 1	2844 ± 49	2049 ± 116	26 ± 2	65 ± 5	107 ± 4	219	158	2	5	8
8		-CH ₃	-CH ₃	-COOH	342 ± 77	7713 ± 1249	6311 ± 1380	8009 ± 130	308 ± 26	1613 ± 24	23	18	23	-	5
9		-CH ₃	-CH ₃	-CH ₂ NH ₂	797 ± 26	8774 ± 508	7799 ± 81	665 ± 28	716 ± 48	3390 ± 301	11	10	-	-	4
10		-CH ₃	-CH ₃	-CF ₃ H	522 ± 210	53206 ± 16384	47964 ± 3582	402 ± 13	163 ± 21	460 ± 25	102	92	-	-	-
11		-Bn	-CH ₃	-H	646 ± 164	139908 ± 677	4975 ± 328	2026 ± 600	1608 ± 52	555 ± 36	217	8	3	3	-
12		-Bn	-CH ₃	-H	427 ± 109	12504 ± 3260	8203 ± 674	539 ± 353	1085 ± 139	1062 ± 54	29	19	1	3	2
13		-Bn	-CH ₃	-H	124 ± 27	21608 ± 3431	2812 ± 543	1142 ± 129	1588 ± 40	359 ± 17	174	23	9	13	3
14		-iPr	-CH ₃	-H	85 ± 17	984 ± 127	3787 ± 234	93 ± 28	300 ± 21	215 ± 12	12	45	1	4	3
15		-Bn	-Bn	-H	623 ± 18	19244 ± 1551	21110 ± 1388	496 ± 36	18643 ± 1365	1183 ± 127	31	34	-	30	2
16		-CH ₃	-CH ₃	-CH ₂ OH	25 ± 9	2243 ± 74	2257 ± 279	33 ± 6	90 ± 9	134 ± 8	90	90	1	4	5
17		-CH ₃	-CH ₃	-CH ₂ OH	9 ± 2	2145 ± 100	2272 ± 134	68 ± 5	26 ± 5	87 ± 7	240	252	8	3	10
18		-CH ₃	-CH ₃	-CH ₂ OH	18 ± 2	1250 ± 95	1222 ± 168	73 ± 13	16 ± 3	116 ± 13	69	68	4	-	6
19		-CH ₃	-CH ₃	-CH ₂ OH	23 ± 3	1531 ± 52	3443 ± 294	108 ± 17	50 ± 1	210 ± 4	67	150	5	2	9
20		-CH ₃	-CH ₃	-CH ₂ NC(NH) ₂	1498 ± 104	21536 ± 1910	25850 ± 1571	8477 ± 655	26509 ± 733	25335 ± 1385	14	16	6	18	17
21					159 ± 7	3014 ± 137	3514 ± 511	69 ± 6	1564 ± 252	1315 ± 87	19	22	-	10	8
22					3761 ± 202	24733 ± 1669	25948 ± 540	2426 ± 257	9750 ± 127	16770 ± 1788	7	7	-	3	4

105

106 Results

107 **Structure-based optimization of DYRK2 inhibitors**

108 LDN192960 was identified as a DYRK2 inhibitor (Banerjee et al., 2019; Cuny et al.,
109 2010; Cuny et al., 2012). It occupies the ATP-binding pocket of DYRK2 and mediates
110 extensive hydrophobic and hydrogen bond interactions (Banerjee et al., 2019).
111 Nevertheless, LDN192960 also inhibits other DYRK2-related kinases, especially Haspin
112 and DYRK3 (Banerjee et al., 2019). To generate DYRK2 inhibitors with better selectivity,
113 we synthesized a series of new compounds based on the same acridine core structure
114 (Table 1). The amine side chain was first changed to a protected amine (compounds 1-3),
115 a cyano group (compound 4), or a cyclic amine (compounds 5-6) (Figure 1—figure
116 supplement 1A, Table 1). Among these candidates, compound 6 exhibited the most potent
117 inhibitory effect towards DYRK2, with an *in vitro* IC₅₀ of 17 nM. In comparison,
118 LDN192960 showed an IC₅₀ of 53 nM when the same protocol was used (Table
119 1)—treating HEK293T cells transiently expressing DYRK2 with increasing concentrations
120 of compound 6 efficiently inhibited Rpt3-Thr25 phosphorylation, with the maximal effect
121 observed at an inhibitor concentration of less than 3 μM (Figure 1—figure supplement 1B).
122 Notably, compound 6 also displays good selectivity towards DYRK2 than other kinases,
123 including DRYK1A, DRYK1B, DYRK3, Haspin, and MARK3 (IC₅₀ values of 889, 697,
124 121305, 45, and 100 nM, respectively; Table 1). Therefore, compound 6 was chosen as
125 the lead compound for further chemical modification.

126 We subsequently crystallized DYRK2 in complex with compound 6 and determined
127 the structure at a resolution of 2.2 Å (Figure 1A, Figure 1—figure supplement 1C). Not
128 surprisingly, compound 6 binds the ATP-binding site of DYRK2 like LDN192960. A water
129 molecule is located deep inside the binding pocket acting as a bridge in the interactions
130 between LDN192960 and the protein. The newly added amino side chain displays
131 apparent densities and adopts an extended conformation. An in-depth analysis of the
132 crystal structure revealed several additional sites for chemical expansion that may further
133 strengthen its interaction with DYRK2 (Figure 1—figure supplement 2A-B). First, a
134 hydrophilic group can be introduced into the acridine core to functionally replace the
135 aforementioned water molecule and maintain constant contact with DYRK2. Second, a
136 bulky functional group can replace the methoxy groups to mediate other interactions with

137 DYRK2. Finally, the amine side chain can be altered to stabilize its conformation (Figure
138 1—figure supplement 2A-B). To this end, we synthesized 9 new compounds (compounds
139 7-15) and evaluated their inhibitory effects on DYRK2 and related kinases (Figure
140 1—figure supplement 2C-D). We also determined the co-crystallized structures of several
141 of these compounds with DYRK2 to visualize their detailed interactions (Figure 1, Figure
142 1—figure supplement 3). Compound 7, introducing a hydroxymethyl group to the acridine
143 core, inhibits DYRK2 efficiently as compound 6 while displaying better selectivity against
144 other DYRK family members (Table 1). The co-crystallized structure shows that the
145 hydroxymethyl group directly contacts the main chain amide group of Ile367 and indirectly
146 coordinates Glu266 and Phe369 via a water molecule (Figure 1D). Compared to
147 compound 7, compounds 8-10, which contain a carboxyl, aminomethyl, and fluoromethyl
148 group, respectively, instead of a hydroxymethyl group, display reduced inhibition towards
149 DYRK2. Compounds 11-15, designed to replace the methoxy group with a bulkier side
150 chain, showed significantly decreased activity and selectivity and were not further pursued
151 (Table 1).

152 Further chemical modification was carried out based on compound 7. By changing
153 the 6-membered ring to a straight-chain or smaller ring, we synthesized compounds 16-19
154 (Table 1, Figure 1—figure supplement 2E). Among these compounds, C17 with an
155 (S)-3-methylpyrrolidine side-chain exhibited the best potency and selectivity among all the
156 analogs (Table 1). Interestingly, we noticed that compound 18 containing an
157 (R)-3-methylpyrrolidine side chain was not as good as C17, indicating that the chirality of
158 the 3-methylpyrrolidine motif plays an essential role in both potency and selectivity.
159 Further modification of compound 17 (leading to compound 20) to promote further
160 hydrogen bond interactions with DYRK2 failed to improve the inhibitory effect. We also
161 wondered whether acridine was the best aromatic core structure and synthesized two new
162 compounds (compounds 21 and 22) by changing one side of the benzene group to a
163 sulfur-containing thiazole structure (Figure 1—figure supplement 2F), which we thought
164 might facilitate hydrophobic interactions with DYRK2 within the ATP-binding pocket;
165 however, they did not have as effective an inhibitory effect as compound 17 (Table 1).

166

167

Figure 1

168 **Figure 1.** Crystal structures of DYRK2 bound to novel inhibitors. **(A)** Overall structure of
169 DYRK2 (grey) bound to 6 (green), 7 (pink), C17 (orange), and 18 (blue). **(B)** Composite
170 omit maps are contoured at 1.5σ and shown as grey meshes to reveal the presence of
171 compounds 6, 7, 17, and 18 in the respective crystal structures. **(C-F)** Close-up view of
172 the DYRK2 binding pocket with compounds 6, 7, 17, and 18. Hydrogen bonds are shown
173 as dashed lines. Water molecules are indicated with red spheres.

174 **Figure 1—source data 1**

175 Data collection and refinement statistics of crystal structures of DYRK2 with different
176 inhibitors.

177

178 **C17 is a potent and selective DYRK2 inhibitor**

179 We set to comprehensively characterize the inhibitory function of compound 17
180 (Figure 2A), referred to as C17 hereafter. *In vitro*, C17 displays an effect on DYRK2 at a
181 single-digit nanomolar IC_{50} value (9 nM) (Figure 2B, Figure 2—figure supplement 1A). To
182 further evaluate the selectivity of C17, we performed kinome profiling analyses. Among
183 the 468 human kinases tested, C17 targeted only DYRK2, Haspin, and MARK3 at a
184 concentration of 500 nM (Figure 2C). Nonetheless, the *in vitro* IC_{50} values of C17 for
185 Haspin and MARK3 (26 nM and 87 nM, respectively) were 3-10-fold higher than that for
186 DYRK2 (Figure 2B, Figure 2—figure supplement 1B-F). Similarly, C17 also inhibited
187 DYRK3 to a lesser extent (IC_{50} of 68 nM). In contrast, LDN192960 inhibited DYRK3 and
188 Haspin more than it inhibited DYRK2 (Banerjee et al., 2019; Cuny et al., 2010).
189 Significantly, C17 also efficiently suppressed DYRK2 activity in the cell and abolished
190 Rpt3-Thr25 phosphorylation at an inhibitor concentration of less than 1 μ M (Figure 2D).
191 Taken together, these data demonstrate that C17 is a highly potent and selective DYRK2
192 inhibitor both *in vitro* and *in vivo*.

193 Acridine derivatives have traditionally been used as antibacterial, antiparasitic, and
194 anticancer agents since these compounds usually show strong DNA intercalating effects
195 (Chaikuad et al., 2016; Jouanne et al., 2017). Considering the potential toxicity of C17 due
196 to its possible DNA-binding capacity, we also assessed the DNA-binding effect of C17

197 (Figure 2—figure supplement 3). Isothermal titration calorimetry revealed that C17
198 ($K_d=22.9 \mu\text{M}$) binds to DNA with significantly lower affinity than LDN192960 binds to DNA
199 ($K_d=198 \text{ nM}$), possibly because of the introduction of hydroxymethyl group on the acridine
200 core, which is not present in LDN192960.

201

202

Figure 2

203 **Figure 2.** C17 is a potent and selective inhibitor of DYRK2. **(A)** Chemical structure of C17.
204 **(B)** IC_{50} values of C17 against DYRK1A, DYRK1B, DYRK3, Haspin and MARK3. **(C)**
205 Kinome profiling of C17 at 500 nM was carried out using 468 human kinases
206 (<https://www.discoverx.com/>). **(D)** C17 inhibits Rpt3-Thr25 phosphorylation. HEK293T
207 cells stably expressing FLAG-DYRK2 were treated with the indicated concentrations of
208 C17 for 1 h. The cells were lysed, and immunoblotting was carried out with the indicated
209 antibodies.

210 **Figure 2—source data 1**

211 Raw data of C17 Kinome profiling list for Figure 2C.

212 **Figure 2—source data 2**

213 Raw data of Western blot for Figure 2D.

214

215 **DYRK2 substrate profiling by quantitative phosphoproteomic analyses**

216 Quantitative phosphoproteomic approaches have significantly expanded the scope of
217 phosphorylation analysis, enabling the quantification of changes in thousands of
218 phosphorylation sites simultaneously (Alvarez-Salamero et al., 2017). To obtain a
219 comprehensive list of potential DYRK2 targets, we treated the myeloma U266 cells with
220 C17 and carried out quantitative phosphoproteomic analyses (Chen et al., 2018; Högberg
221 et al., 2018). We prepared lysates of U266 cells treated with C17 or the DMSO control and
222 trypsinized them. Phosphorylated peptides were then enriched using Ti^{4+} -immobilized
223 metal ion affinity chromatography (IMAC) tips and analyzed by LC-MS/MS (Figure 3A). A
224 total of 15,755 phosphosites were identified, among which 12,818 (81%) were serine, and
225 2,798 (18%) were threonine. A total of 10,647 (68%) phosphosites were Class I
226 (localization probability >0.75), 2,557 (16%) were Class II ($0.5 <$ localization probability
227 ≤ 0.75), and 2,401 (16%) were Class III ($0.25 <$ localization probability ≤ 0.5) (Figure 3B).

228 This is a very comprehensive phosphoproteomic dataset prepared for DYRK2 substrate
229 profiling by treating the U266 cells with 10 μ M of C17. A good Pearson correlation
230 coefficient of 0.9 was obtained for the phosphosite intensities among the treatment and
231 control samples (Figure 3—figure supplement 1), and the coefficient of variance of the
232 intensities of the majority of the phosphosites was lower than 20% (Figure 3—figure
233 supplement 2), demonstrating the high quantification precision of our label-free
234 phosphoproteomic analysis. Remarkably, C17 treatment led to significant downregulation
235 of 373 phosphosites (Figure 3C), including pThr37 of the eukaryotic translation initiation
236 factor 4E-binding protein 1 (4E-BP1), as well as pSer519 and pSer521 in the stromal
237 interaction molecule 1 (STIM1) (Figure 3D, Figure 3—figure supplement 3). Interestingly,
238 another 445 phosphosites were upregulated (Figure 3C), suggesting that DYRK2 likely
239 inhibited some downstream kinases or activated phosphatases, and suppressing its
240 activity reversed these effects. Together, these data demonstrate that DYRK2 is involved
241 in a network of phosphorylation events and can directly or indirectly regulate the
242 phosphorylation status of many proteins. The top pathways with which DYRK2 may
243 participate were revealed by a global analysis of the significantly up- and down-regulated
244 phosphoproteins (Figure 3E).

245

246 **Figure 3**

247 **Figure 3.** Quantitative phosphoproteomic analysis of U266 cells treated with C17. (A)
248 Workflow of the phosphoproteomic approach. Triplicate samples treated with/without 10
249 μ M C17 for 1 h were separately lysed and digested, and the phosphorylated peptides
250 were enriched by the Ti⁴⁺-IMAC tip and analyzed by LC-MS/MS. (B) Distribution of the
251 assigned amino acid residues and their localization probabilities (Class I >0.75, Class
252 II >0.5 and \leq 0.75, Class III >0.25 and \leq 0.5) for all identified phosphorylation sites. (C)
253 Volcano plot (FDR < 0.05 and S0 = 2) shows the significantly up- and downregulated
254 phosphosites after C17 treatment. (D) MS/MS spectra of the phosphosites of two potential
255 DYRK2 substrates, pT37 of 4E-BP1 and pS519 and pS521 of STIM1. (E) Global
256 canonical pathway analysis of the significantly up- and downregulated phosphoproteins. –
257 Log₁₀ adjusted *p*-values associated with a pathway are presented.

258 **Figure 3—source data 1**

259 Raw data of the significantly up- and down-regulated phosphosites after U266 cells
260 treated with C17 for Figure 3C.

261

262 **4E-BP1 is a direct cellular target of DYRK2**

263 We set out to determine whether some of the 337 downregulated phosphosites are
264 genuine DYRK2 targets. We first examined 4E-BP1 for several reasons. First, C17
265 treatment decreased the pThr37 level in U266 cells (Figure 3C). Second, a previous study
266 showed that Ser65 and Ser101 in 4E-BP1 can be phosphorylated by DYRK2 *in vitro*,
267 indicating that 4E-BP1 is a potential DYRK2 substrate (Wang et al., 2003). And lastly,
268 several phosphosite-specific antibodies for 4E-BP1 are commercially available. 4E-BP1 is
269 a master regulator of protein synthesis. It has been well established that its
270 phosphorylation by other kinases such as mTORC1 leads to its dissociation from
271 eukaryotic initiation factor 4E (eIF4E), allowing mRNA translation (Laplante and Sabatini,
272 2012; Ma et al., 2009).

273 Using an antibody that detects 4E-BP1 only when it is phosphorylated at Thr37 and
274 Thr46, we found that C17 treatment significantly reduced the level of pThr37/pThr46 of
275 endogenous 4E-BP1 in HEK293T cells (Figure 4A), consistent with our mass spec
276 analyses in U266 cells. Further investigations using two other 4E-BP1
277 phosphosite-specific antibodies showed that C17 also decreased the phosphorylation of
278 Ser65 in endogenous 4E-BP1 (Figure 4A) by a previous study (Wang et al., 2003); as well
279 as Thr70. Knockdown of endogenous DYRK2 using a short hairpin RNA (shRNA) also
280 significantly reduced the phosphorylation of these sites (Figure 4B). Successful
281 knockdown is demonstrated by quantitative RT-PCR analysis (Figure 4—figure
282 supplement 1). Similarly, C17 suppressed DYRK2-mediated phosphorylation of 4E-BP1
283 when overexpressed in the HEK293 cells (Figure 4C). To ascertain whether DYRK2 can
284 directly phosphate 4E-BP1, we performed an *in vitro* kinase assay using purified DYRK2
285 and 4E-BP1 proteins. DYRK2 efficiently phosphorylated 4E-BP1 at multiple sites,
286 including Thr37/Thr46, Ser65, and Thr70, whereas the kinase-deficient DYRK2 mutant
287 (D275N) displayed no activity (Figure 4D). C17 suppressed the phosphorylation of these

288 sites in a dose-dependent manner (Figure 4E). These results demonstrate that DYRK2
289 effectively phosphorylated 4E-BP1 on multiple sites *in vivo* and *in vitro*.

290 4E-BP1 is targeted by multiple kinases (Qin et al., 2016). Indeed, C17 or DYRK2
291 shRNA decreased but did not abolish the phosphorylation of 4E-BP1 (Figure 4A, 4B). A
292 previous study showed that combined inhibition of AKT and MEK kinases suppressed
293 4E-BP1 phosphorylation and tumor growth (She et al., 2010). We observed similar results
294 when we treated the HEK293A cells with AKTi (an AKT1/AKT2 inhibitor) and PD0325901
295 (a MEK inhibitor). Significantly, knockdown of DYRK2 in the presence of these
296 compounds further markedly diminished 4E-BP1 phosphorylation (Figure 4B). To assess
297 whether C17 can also elicit a synergistic effect with these kinase inhibitors, we treated
298 HEK293A, HCT116, and U266 cells with these molecules, either alone or in combination,
299 and examined the phosphorylation status of endogenous 4E-BP1 (Figure 4F-H). The
300 presence of C17 potentiated the inhibitory effect of AKTi and PD0325901 in all these cells.
301 Together, these results confirm that 4E-BP1 is a direct cellular target of DYRK2 and
302 suggest the potential use of DYRK2 inhibitors in combination with other kinase inhibitors
303 for cancer therapy.

304

305

Figure 4

306 **Figure 4.** 4E-BP1 is a substrate of DYRK2. (A) C17 treatment for 1 h reduced the
307 phosphorylation of endogenous 4E-BP1 in HEK293T cells. The phosphorylation status of
308 4E-BP1 was analyzed by immunoblotting cell lysates using indicated antibodies. (B)
309 DYRK2 knockdown decreases the phosphorylation of endogenous 4E-BP1 in HEK293T
310 cells. (C) HEK293A cells stably expressing HA-DYRK2 and FLAG-4E-BP1 were treated
311 with indicated concentrations of C17 for 1 h. The cells were lysed, and immunoblotting
312 was carried out with indicated antibodies. (D) DYRK2 directly phosphorylated 4E-BP1 at
313 multiple sites. (E) C17 inhibited DYRK2-mediated 4E-BP1 phosphorylation in a
314 concentration-dependent manner. (F-H) C17 displayed a synergistic effect with AKT and
315 MEK inhibitors to suppress 4E-BP1 phosphorylation in HEK293A (F), HCT116 (G), and
316 U266 cells. (H) The cells were treated with indicated concentrations of PD032590,
317 AKTi-1/2, and C17 alone or in combination for 1 h. Cell lysates were immunoblotted with

318 indicated antibodies.

319 **Figure 4—source data 1**

320 Raw data of Western blot for Figure 4A and B.

321 **Figure 4—source data 2**

322 Raw data of Western blot for Figure 4C and D.

323 **Figure 4—source data 3**

324 Raw data of Western blot for Figure 4E and F.

325 **Figure 4—source data 4**

326 Raw data of Western blot for Figure 4G and H.

327

328

329 **DYRK2 promotes STIM1-ORAI1 interaction to modulate SOCE**

330 In addition to 4E-BP1, another potential target of DYRK2 is STIM1, as the
331 phosphorylation levels of both Ser519 and Ser521 in endogenous STIM1 were
332 significantly reduced upon DYRK2 inhibition in our mass spectrometry analyses (Figure
333 3C). STIM1 is a single-pass transmembrane protein residing in the endoplasmic reticulum
334 (ER) and plays a vital role in the store-operated calcium entry (SOCE) process (Collins et
335 al., 2013). The luminal domain of STIM1 senses calcium depletion in the ER and induces
336 protein oligomerization and puncta formation (Liou et al., 2005; Prakriya and Lewis, 2015;
337 Zheng et al., 2018b). Oligomerized STIM1 then travels to the ER-plasma membrane
338 contact site and activates the ORAI1 calcium channel. The cytosolic region of STIM1
339 contains multiple phosphorylation sites, and it has been shown that the function of STIM1
340 is regulated by several kinases, including ERK1/2 (Pozo-Guisado et al., 2013;
341 Pozo-Guisado and Martin-Romero, 2013).

342 Purified wild-type DYRK2, but not the kinase-dead mutant D275N, induced mobility
343 changes of the cytosolic region of STIM1 (STIM1^{235-END}) in SDS-PAGE gel (Figure 5A). As
344 increasing amounts of DYRK2 lead to greater shifts of STIM1^{235-END}, there are likely
345 multiple DYRK2 phosphorylation sites in STIM1. Consistently, DYRK2 induced a mobility
346 shift of STIM1 when they were co-expressed in the HEK293A cells (Figure 5B). To further
347 pinpoint DYRK2-specific phosphorylation sites, we co-expressed DYRK2, Orai1, and
348 STIM1 in HEK293A cells, treated the cells with C17, isolated STIM1 using Anti-FLAG
349 agarose, and then subjected it to label-free quantitative mass spectrometry analyses. The
350 phosphorylation levels of at least eight phosphosites on four peptides of STIM1 were

351 significantly reduced upon treatment with C17 compared with the untreated sample
352 (Figure 5—figure supplement 1A-B), including Ser519 and Ser521 that were identified in
353 the U266 phosphoproteome analysis (Figure 3C). In a separate mass spec experiment,
354 phosphorylation of Ser608 and Ser616 were also reduced by C17. Together, these results
355 demonstrate that DYRK2 can phosphorylate multiple sites in the cytosolic region of
356 STIM1.

357 STIM1 puncta formation indicates its oligomerization and activation (Liou et al., 2005;
358 Prakriya and Lewis, 2015; Zheng et al., 2018b). To assess the functional outcome of
359 STIM1 phosphorylation by DYRK2, we co-expressed STIM1 and DYRK2 in an
360 Orai-deficient (Orai-KO) cell line, which has all three Orai genes genetically ablated
361 (Zheng et al., 2018a). DYRK2 induced the appearance of STIM1 puncta under resting
362 conditions, indicating that DYRK2 promotes STIM1 oligomerization (Figure 5C). In
363 contrast, the STIM1 puncta were not observed in the presence of C17. DYRK2 also failed
364 to promote the punctate formation of STIM1-10M, a STIM1 variant with all ten potential
365 DYRK2 phosphorylation sites mutated to Ala (Figure 5C, Figure 5—figure supplement
366 1C).

367 To further understand the importance of STIM1 phosphorylation, we examined the
368 interaction between STIM1 and Orai1 using co-immunoprecipitation. Expression of WT
369 DYRK2 significantly increased the interaction between STIM1 and Orai1, whereas
370 expression of DYRK2-KD exerted no such effect (Figure 5D). Treating cells with C17
371 effectively abolished the DYRK2-dependent STIM1-Orai1 interaction. Notably, both
372 STIM1-1-491, a C-terminal truncated STIM1 (Figure 5C, Figure 5—figure supplement 1C),
373 and STIM1-10M displayed significantly reduced interaction with Orai1 even in the
374 presence of WT DYRK2 (Figure 5E), suggesting that DYRK2-mediated phosphorylation is
375 essential to promote the binding between STIM1 and Orai1. C17 also decreased the
376 interaction between STIM1 and Orai1 without exogenously expressing DYRK2 (Figure
377 5F).

378 We examined fluorescence resonance energy transfer (FRET) between STIM1-YFP
379 and CFP-Orai1 to validate the regulatory function of DYRK2 on STIM1-Orai1 interaction.
380 The FRET signals between STIM1-YFP and CFP-Orai1 were significantly increased in

381 HEK293 cells in the presence of WT DYRK2 (Figure 5G). To exclude the influence of
382 endogenous STIM1, we performed further analyses in a STIM1-STIM2 DKO cell line
383 (Zheng et al., 2018a). The FRET signals between STIM1-1-491 and Orai1 were unaltered
384 by DYRK2 (Figure 5H), indicating that the effect of DYRK2 is dependent on the C-terminal
385 region of STIM1. Furthermore, the FRET signals between STIM1-10M and Orai1 were
386 unaffected by DYRK2 (Figure 5I). These results are consistent with the
387 co-immunoprecipitation results and demonstrate that DYRK2 can promote the
388 STIM1-Orai1 interaction via STIM1 phosphorylation.

389 Lastly, to examine the physiological relevance of the STIM1-Orai1 interaction
390 regulated by DYRK2, we performed SOCE analyses in HEK293A cells expressing
391 GCaMP6f, a genetically encoded calcium sensor (Nakai et al., 2001). Treating cells grown
392 in a calcium-free medium containing thapsigargin resulted in a transient increase in
393 GCaMP6f fluorescence due to calcium release from the ER to the cytosol (Figure 5J,
394 black line). Subsequent addition of calcium to the cell culture medium resulted in a
395 marked increase in GCaMP6f signaling, indicating calcium entry into the cells, further
396 augmented by STIM1 overexpression (Figure 5J, blue line). Pre-treating cells with C17 for
397 1 h substantially reduced SOCE in cells with either endogenous (Figure 5J, green line) or
398 overexpressed STIM1 (Figure 5J, red line). Quantifications of these results are present in
399 Figure 5K. Taken together, our results strongly suggest that DYRK2 can directly enhance
400 SOCE by phosphorylating STIM1 and promoting its interaction with ORAI1, which can all
401 be effectively inhibited by C17.

402

403

Figure 5

404 **Figure 5.** Phosphorylation of STIM1 by DYRK2 modulates SOCE. (A) DYRK2 directly
405 phosphorylated STIM1. GST-STIM1^{235-END} was incubated with wild-type or
406 kinase-deficient DYRK2 in the presence of Mn-ATP for 30 minutes. Phosphorylation of
407 GST-STIM1^{235-END} was indicated by the mobility change of STIM1 in SDS-PAGE gel. (B)
408 DYRK2 phosphorylated STIM1 *in vivo*. HEK293A cells were co-transfected with
409 FLAG-STIM1 and DYRK2 for 36 h, then states immunoblotted with the indicated
410 antibodies. (C) Typical confocal microscopy images showing the effects of

411 mCherry-DYRK2 and/or C17 (1 μ M) on the puncta formation of STIM1 in the HEK293
412 Orai1/Orai2/Orai3-TKO cells. The scale bar is 10 μ m. The experiments were repeated, six
413 cells were examined each time. (D) DYRK2 promoted the interaction between STIM1 and
414 Orai1. HEK293A cells were co-transfected with FLAG-STIM1, GFP-Orai1, and DYRK2
415 for 36 h. STIM1 was immunoprecipitated with FLAG agarose, and the associated proteins
416 were analysed using the indicated antibodies. (E) Phosphosites mutations in STIM1
417 disrupt the interaction with Orai1. (F) C17 inhibits the interaction between FLAG-STIM1
418 and GFP-Orai1 without exogenously expressing DYRK2. (G-I) Effects of DYRK2 on the
419 FRET signals between STIM1-YFP and CFP-Orai1. Upper panel, typical traces; lower
420 panel, statistics. (G) HEK293 cells stably expressing STIM1-YFP and CFP-Orai1. (n=3,
421 ****, P<0.0001, unpaired Student's t-test). (H) HEK293 STIM1-STIM2 DKO cells stably
422 expressing Orai1-CFP cells transiently expressing STIM1-1-491-YFP (n=3, unpaired
423 Student's t-test). (I) HEK STIM1-STIM2 DKO cells transiently expressing STIM1-YFP (red)
424 or STIM1-10M (blue). (n=3, ****, P<0.0001, unpaired Student's t-test). (J) C17 inhibited
425 SOCE in HEK293A cells. HEK293A cells were transfected with GCAMP6f or GCAMP6f
426 plus STIM1 for 24 h and then treated with 1 μ M C17 for 1 h. Before thapsigargin treatment,
427 the cell culture medium was switched to a Ca²⁺-free medium containing thapsigargin
428 (1 μ M, solid lines) or DMSO (dashed lines) was added to the cells, and 2 mM Ca²⁺ was
429 added 12 minutes later. The red and green lines correspond to C17-treated cells. Blue
430 and black lines represent untreated cells. GCAMP6f fluorescence was monitored by a
431 Zeiss LSM 700 laser scanning confocal microscope. (K) Quantification of J. The following
432 number of cells were monitored: STIM1, 45 cells on 3 coverslips (blue solid line); STIM1 +
433 C17 (1 μ M), 48 cells on 3 coverslips (red solid line); endogenous, 47 cells on 3 coverslips
434 (black solid line); endogenous + C17 (1 μ M), 42 cells on 3 coverslips (green solid line).
435 STIM1(-Tg), 43 cells on 3 coverslips (blue dashed line). STIM1 + C17 (1 μ M) (-Tg), 43
436 cells on 3 coverslips (red dashed line); endogenous (-Tg), 43 cells on 3 coverslips (black
437 dashed line); and endogenous + C17 (1 μ M) (-Tg), 43 cells on 3 coverslips (green dashed
438 line). Error bars represent the means \pm SEM. (L) A hypothetical model depicts
439 DYRK2-mediated STIM1 activation.

440 **Figure 5—source data 1**

441 Raw data of Coomassie Blue Staining for Figure 5A.

442 **Figure 5—source data 2**

443 Raw data of Western blot and Coomassie Blue Staining for Figure 5B.

444 **Figure 5—source data 3**

445 Raw data of Western blot for Figure 5D and E.

446 **Figure 5—source data 4**

447 Raw data of Western blot for Figure 5F.

448 **Figure 5—source data 5**

449 Raw data of FRET responses between STIM1-YFP and CFP-Orai1 for Figure 5G, FRET

450 responses between STIM1-1-491-YFP and CFP-Orai1 for Figure 5H, FRET responses

451 between STIM1-YFP, STIM1-10M-YFP and CFP-Orai1 for Figure 5I.

452 **Figure 5—source data 6**

453 Raw data of Store-operated Ca^{2+} entry (SOCE) analyses for Figure 5J.

454

455 **Discussion**

456 We used a structure-based approach to design, synthesize and evaluate a series of
457 new analogs based on the acridine core structure and eventually identified C17 as a
458 potent and selective DYRK2 inhibitor. We showed that C17 affects DYRK2 at a single-digit
459 nanomolar IC_{50} and inhibits DYRK2 more potently than closely related kinases such as
460 DYRK3, Haspin, and MARK3. The crystal structure of DYRK2 bound to C17 revealed
461 critical interactions that explain its high selectivity, including a hydrogen bond between the
462 (S)-3-methylpyrrolidine ring and Glu352 in DYRK2.

463 C17 provided us with a unique tool to interrogate the physiological functions of
464 DYRK2. We treated U266 cells with C17 and performed quantitative phosphoproteomic
465 analyses. We found that the cellular phosphorylation pattern is significantly altered by C17,
466 suggesting that DYRK2 likely has multiple cellular targets and is involved in a network of
467 biological processes. We then identified several leading phosphosites that are
468 downregulated and demonstrated that 4E-BP1 and STIM1 are bona fide substrates of
469 DYRK2. We showed that DYRK2 efficiently phosphorylated 4E-BP1 at multiple sites,
470 including Thr37, and combined treatment of C17 with AKT and MEK inhibitors resulted in
471 marked suppression of 4E-BP1 phosphorylation. Therefore, DYRK2 likely functions
472 synergistically with other kinases to regulate protein synthesis.

473 For the first time, we also discovered that DYRK2 could efficiently phosphorylate
474 STIM1, and phosphorylation of STIM1 by DYRK2 substantially increased the interaction
475 between STIM1 and ORAI1. Treating cells with C17 suppressed SOCE, validating the
476 critical role of DYRK2 in regulating calcium entry into cells. These data allow us to present
477 a hypothetical model showing how DYRK2 triggers the activation of STIM1 (Figure 5L).
478 Under resting conditions, the cytosolic portion of STIM1 likely adopts an inactive
479 conformation. DYRK2 can phosphorylate STIM1 and induce its oligomerization, which
480 then interacts with the Orai1 channel and leads to its opening. One inadequacy of our
481 study is the lack of further insight into the regulation mechanism of this process. In
482 particular, what is the upstream signal that triggers DYRK2 activation? Nevertheless, our
483 data offer a valuable model that allows further investigation of the relationship between
484 DYRK2 and SOCE.

485 Recently, Mehnert et al. developed a multilayered proteomic workflow and
486 determined how different pathological-related DYRK2 mutations altered protein
487 conformation, substrates modification, and biological function (Qin et al., 2016). DYRK2 is
488 implicated in regulating multiple cellular processes, and the selective DYRK2 inhibitor we
489 developed here will serve as a valuable tool in dissecting its complex downstream
490 pathways.

491

492 **Materials and methods**

493 **Antibodies and Reagents**

494 Antibodies used in this study were: anti-4E-PB1 (Cell Signaling Technology, RRID:
495 AB_2097841), anti-phosphorylated 4E-BP1 (Thr37/46) (Cell Signaling Technology, RRID:
496 AB_560835), anti-phosphorylated 4E-BP1 (Ser65) (Cell Signaling Technology, RRID:
497 AB_330947), anti-phosphorylated 4E-BP1 (Thr70) (Cell Signaling Technology, RRID:
498 AB_2798206), anti-HA (Cell Signaling Technology, RRID: AB_1549585), anti-Flag (Sigma,
499 RRID: AB_259529), anti-Flag (Abcam, #ab205606), anti-GFP (Proteintech, RRID:
500 AB_11182611), Anti-GFP (Abcam, #ab183734), anti-RPT3 (Thermo Fisher Scientific, RRID:
501 AB_2781512), anti-GAPDH (TransGen Biotech, #HC301-01). Secondary antibodies were
502 horseradish peroxidase (HRP)-conjugated anti-rabbit IgG (H+L) or HRP-conjugated
503 anti-mouse IgG (H+L) purchased from Transgene Biotechnology (#HC101-01, #HC201-01).
504 Rabbit anti-pThr25 polyclonal antibody was generated using the following phospho-peptide as
505 immunogen: LSVSRPQ(pT)GLSFLGP as reported previously (Guo et al., 2016). Reagents
506 used in this study were: AKTi-1/2 (Selleck, #S80837), PD0325901 (Aladdin, #P125494),
507 Thapsigargin (Aladdin, #T135258). Inhibitors were dissolved in dimethyl sulfoxide. All
508 chemical reagents were used as supplied by Sigma-Aldrich, J&K Scientific, Alfa Aesar
509 Chemicals, Energy Chemicals and Bide Pharmatech. DCM, DMF, DMSO were distilled from
510 calcium hydride; tetrahydrofuran was distilled from sodium/benzophenone ketyl prior to use.

511 **Cloning**

512 The GCaMP6f, pEGFP-Orai1, and mCherry-STIM1 plasmids were kindly gifted from the
513 Xiaowei Chen Lab (Peking University, China). The GFP-tagged human DYRK1A, 1B, 2, 3, 4,

514 pLL3.7-DYRK2-shRNA, psPAX2, and pMD2.G plasmids were kindly gifted from the Xing Guo
515 Lab (Zhejiang University, China). DYRK2²⁰⁸⁻⁵⁵² was subcloned into the pQlinkHx vector
516 (Clontech) with an engineered N-terminal His tag. STIM1^{235-END} and full-length 4EBP1 were
517 subcloned into the pQlinkGx vector (Clontech) with an engineered N-terminal GST tag.
518 Full-length STIM1 was subcloned into a pCCF vector (Clontech) with an engineered
519 N-terminal FLAG tag. The HA-mcherry-DYRK2 and HA-mcherry-DYRK2-D275N plasmids
520 were generated by modification of pEGFP-DYRK2 and pEGFP-DYRK2-D275N plasmids.
521 HA-mcherry was PCR amplified from pmCherry-N1 plasmid and replaced EGFP by
522 homologous recombination. All plasmids were verified by DNA sequencing.

523 **Cell culture, transfection and infection**

524 Mammalian cells were all grown in a humidified incubator with 5% CO₂ at 37 °C. HEK293T
525 (RRID:CVCL_0063), HEK293A (Thermo Fisher, R70507), and HEK293 (RRID:CVCL_0045)
526 cells were grown in Dulbecco's Modified Eagle Media (DMEM, Gibco) supplemented with 10%
527 FBS, 4 mM L-glutamine, 100 U/mL penicillin, and 100 mg/mL streptomycin (Gibco). U266
528 (RRID:CVCL_0566) cells were grown in RPMI 1640 (Gibco) supplemented with 10% FBS, 4
529 mM L-glutamine, 100 U/mL penicillin, and 100 mg/mL streptomycin (Gibco). HCT116 cells
530 (China Infrastructure of Cell Line Resources, 1101HUM-PUMC000158) were grown in Iscove's
531 Modified Dulbecco's Medium (IMDM, Gibco) supplemented with 10% FBS, 4 mM L-glutamine,
532 100 U/mL penicillin, and 100 mg/mL streptomycin (Gibco). All cell lines were confirmed by STR
533 (short tandem repeat) profiling and tested negative for mycoplasma contamination. All cell
534 lines are not in the list of commonly misidentified cell lines maintained by the International Cell
535 Line Authentication Committee (version 11). Transient transfection of HEK293T, HEK293A

536 cells were carried out using Lipofectamine 2000 (Thermo Fisher Scientific) or X-tremeGENE 9
537 DNA Transfection reagent (Roche) as recommended by the manufacturer, and transfected
538 cells were used in experiments 24–48 h later. In Lipofectamine transfection, the cells were
539 cultured to ~70-80% confluency in 10-cm dishes, followed by transfection with 10–12 µg
540 plasmid. The cells were changed with fresh DMEM after 12 h and incubated for 36 h before
541 further experiments. In X-tremeGENE 9 DNA transfection, the cells were cultured to ~50
542 confluency in 35-mm glass bottom dishes coated with poly-D-lysine, followed by transfection
543 with 1-3 µg plasmid. The cells were changed with fresh DMEM after 6 h and incubated for
544 24-36 h before further experiments. Lentiviruses were produced using the psPAX2 and
545 pMD2.G packaging vectors. Viral media were passed through a pre-wetted 0.45 µm filter and
546 mixed with 10 µg mL⁻¹ Polybrene (Sigma) before being added to recipient cells. Infected cells
547 were selected with puromycin (1-2 µg mL⁻¹, Life Technologies) to generate stable populations.

548 **DYRK2 protein purification and co-crystallization**

549 DYRK2²⁰⁸⁻⁵⁵² with an N-terminal 6×His affinity tag and TEV protease cleavage site which
550 expressed in *E. coli* BL21 (DE3). Bacterial cultures were grown at 37 °C in LB medium to an
551 OD600 of 0.6-0.8 before induced with 0.5 mM IPTG overnight at 18 °C. Cells were collected by
552 centrifugation and frozen at -80 °C. For protein purification, the cells were suspended in the
553 lysis buffer (50 mM HEPES, pH 7.5, 500 mM NaCl, 20 mM imidazole, 5% glycerol, 5 mM
554 β-mercaptoethanol, and 1 mM phenylmethanesulfonylfluoride) and disrupted by sonication.
555 The insoluble debris was removed by centrifugation. The supernatant was applied to a Ni-NTA
556 column (GE Healthcare). The column was washed extensively with the wash buffer (50 mM
557 HEPES, pH 7.5, 500 mM NaCl, 50 mM imidazole, 5% glycerol, and 5 mM β-mercaptoethanol)

558 and bound DYRK2 protein was eluted using the elution buffer (50 mM HEPES, pH 7.5, 500
559 mM NaCl, 500 mM imidazole, 5% glycerol, and 5 mM β -mercaptoethanol). After cleavage with
560 TEV protease, the protein sample was passed through a second Ni-NTA column to separate
561 untagged DYRK2 from the uncut protein and the protease. Final purification was performed
562 using a Superdex 200 gel filtration column (GE Healthcare), and the protein was eluted using
563 the final buffer (25 mM HEPES, pH 7.5, 400 mM NaCl, 1 mM DTT, and 5% glycerol). Purify the
564 DYRK2-D275N using the same method as shown above. Purified DYRK2 and DYRK2-D275N
565 were concentrated to 10 mg mL⁻¹ and flash-frozen with liquid nitrogen.

566 DYRK2²⁰⁸⁻⁵⁵² was incubated with 200 μ M compounds on ice before crystallization. The
567 protein-compounds mixture was then mixed in a 1:1 ratio with the crystallization solution (0.36
568 M-0.5 M sodium citrate tribasic dihydrate, 0.01 M sodium borate, pH 7.5-9.5) in a final drop
569 size of 2 μ l. The DYRK2-compounds crystals were grown at 18 °C by the sitting-drop vapor
570 diffusion method. Cuboid-shaped crystals appeared after 4-7 days. Crystals were
571 cryoprotected in the crystallization solution supplemented with 35% glycerol before frozen in
572 liquid nitrogen.

573 The X-ray diffraction data were collected at Shanghai Synchrotron Radiation Facility (SSRF)
574 beamline BL17U. The diffraction data were indexed, integrated, and scaled using HKL-2000
575 (HKL Research). The structure was determined by molecular replacement using the published
576 DYRK2 structure (PDB ID: 3K2L) (Soundararajan et al., 2013) as the search model using the
577 Phaser program (McCoy et al., 2007). Chembiodraw (version 13.0) was used to generated
578 the .cif files for compounds, and then compounds were fitted using the LigandFit program in
579 Phenix (Adams et al., 2010). The structural model was further adjusted in Coot (Emsley et al.,

580 2010) and refined using Phenix. The quality of the structural model was checked using the
581 MolProbity program in Phenix. The crystallographic data and refinement statistics are
582 summarized in Figure 1-source data 1.

583 **IC₅₀ determination**

584 IC₅₀ determination was carried out using the ADP-GloTM kinase assay system (Promega,
585 Madison, WI). Active DYRK1A, DYRK1B, DYRK2, DYRK3, Haspin and MARK3 were purified
586 as reported previously. C17 IC₅₀ measurements were carried out against the kinases with final
587 concentrations between 0.01 nM to 100 μ M *in vitro* (C17 was added to the kinase reaction
588 prior to ATP master mix). The values were expressed as a percentage of the DMSO control.
589 DYRK isoforms (1 ng/ μ L diluted in 50 mM Tris-HCl pH7.5, 2 mM DTT) were assayed against
590 Woodtide (KKISGRLSPIMTEQ) in a final volume of 5 μ L containing 50 mM Tris pH 7.5, 150
591 μ M substrate peptide, 5 mM MgCl₂ and 10-50 μ M ATP (10 μ M for DYRK2 and DYRK3, 25 μ M
592 for DYRK1A and 50 μ M for DYRK1B) and incubated for 60 min at room temperature. Haspin
593 (0.2 ng/ μ L diluted in 50 mM Tris-HCl pH7.5, 2 mM DTT) was assayed against a substrate
594 peptide H3(1-21) (ARTKQTARKSTGGKAPRKQLA) in a final volume of 5 μ L containing 50 mM
595 Tris pH 7.5, 200 μ M substrate peptide, 5 mM MgCl₂ and 200 μ M ATP and incubated for 120
596 min at room temperature. MARK3 (1 ng/ μ L diluted in 50 mM Tris-HCl pH7.5, 2 mM DTT) was
597 assayed against Cdc25C peptide (KKKVSRSGLYRSPSPENLNRPR) in a final volume of 5
598 μ L 50 mM Tris pH 7.5, 200 μ M substrate peptide, 10 mM MgCl₂ and 5 μ M ATP and incubated
599 for 120 min at room temperature. After incubation, the ADP-GloTM kinase assay system was
600 used to determine kinase activity following the manufacturer's protocol. IC₅₀ curves were

601 developed as % of DMSO control and IC₅₀ values were calculated using GraphPad Prism
602 8.4.0 software. Results are means ± SD for triplicate reactions with similar results obtained in
603 at least one other experiment.

604 **KINOMEScan® kinase profiling**

605 The KINOMEScan® kinase profiling assay was carried out at The Largest Kinase Assay Panel
606 in the world for Protein Kinase Profiling (<https://www.discoverx.com>). C17 kinase selectivity
607 was determined against a panel of 468 protein kinases. Results are presented as a
608 percentage of kinase activity in DMSO control reactions. Protein kinases were assayed *in vitro*
609 with 500 nM final concentration of C17 and the results are presented as an average of
610 triplicate reactions ± SD or in the form of comparative histograms.

611 **Quantitative phosphoproteomic analysis**

612 Triplicate U266 cells treated with/without C17 were lysed by the lysis buffer containing 1% (v/v)
613 Triton X-100, 7M Urea, 50 mM Tris-HCl, pH 8.5, 1 mM pervanadate, protease inhibitor mixture
614 (Roche), and phosphatase inhibitor mixtures (Roche). The cell lysates were firstly digested
615 with trypsin (Promega, USA) by the in-solution digestion method (Chen et al., 2018). After
616 desalting, the Ti⁴⁺-IMAC tip was used to purify the phosphopeptides. The phosphopeptides
617 were desalted by the C18 StageTip prior to the LC MS/MS analysis(Chen et al., 2018). An
618 Easy-nLC 1200 system coupled with the Q-Exactive HF-X mass spectrometer (Thermo Fisher
619 Scientific, USA) was used to analyze the phosphopeptide samples with 1 h LC gradient. The
620 raw files were searched against Human fasta database (71772 protein entries, downloaded

621 from Uniprot on March 27, 2018) by MaxQuant (version 1.5.5.1). The oxidation (M),
622 deamidation (NQ), and Phospho (STY) were selected as the variable modifications for the
623 phosphopeptide identification, while the carbamidomethyl was set as the fixed modification.
624 The false discovery rate (FDR) was set to 0.01 on PTM site, peptide, and protein level.
625 Label-free quantification (LFQ) and match between runs were set for the triplicate analysis
626 data. The MaxQuant searching file "Phospho (STY)Sites.txt" was loaded into the Perseus
627 software (version 1.5.5.3) to make volcano plots using student's t-test and cutoff of "FDR<
628 0.05 and S0=2". The pathway analysis was performed using the Kyoto Encyclopedia of Genes
629 and Genomes (KEGG) database with cutoff of adjusted p-value < 0.05.

630 **Quantitative RT-PCR**

631 Total RNA from cells was extracted using the RNeasy Mini Kit (Qiagen) and
632 reverse-transcribed with the PrimeScript Real Time reagent Kit (with genomic DNA Eraser,
633 TAKARA). The product of reverse transcription was diluted five times then subjected to
634 quantitative rtPCR reaction in Applied Biosystems ViATM7 Real-Time PCR System (Applied
635 Biosystems). The 20 µl quantitative rtPCR reaction contained 2 µl of the reverse-transcription
636 reaction mixture, 2× Hieff quantitative rtPCR SYBR Green Master Mix (Yeasen), 0.2 µM
637 quantitative rtPCR forward primer, 0.2 µM quantitative rtPCR reverse primer (Figure 4—figure
638 supplement 2) and ddH₂O. The quantitative rtPCR reaction condition was as follows: 95 °C, 5
639 min; (95 °C. 10 s; 60 °C, 30 s) ×40 cycles; 95 °C, 15 s; 60 °C, 1 min; 95 °C. 15 s (collect
640 fluorescence at a ramping rate of 0.05 °C s⁻¹); 4 °C, hold. Data analysis was performed by
641 QuantStudio™ Real-Time PCR Software v.1.3.

642 **STIM1 and 4EBP1 protein purification**

643 The cytosolic domain of STIM1 (bases 235-END) with an N-terminal GST-tag and TEV
644 protease cleavage site which expressed in E. coli BL21 (DE3). Bacterial cultures were grown
645 at 37 °C in LB medium to an OD600 of 0.6-0.8 before induced with 0.5 mM IPTG overnight at
646 18 °C. Cells were collected by centrifugation and frozen at -80 °C. For protein purification, the
647 cells were suspended in the lysis buffer 50 mM Tris-HCl (pH 7.5), 500 mM NaCl, 5 mM
648 β-mercaptoethanol, and 1 mM phenylmethanesulfonylfluoride and disrupted by sonication.
649 The insoluble debris was removed by centrifugation. The supernatant was applied to a
650 glutathione-Sepharose column (GE Healthcare) and eluted in lysis buffer containing 20 mM
651 glutathione. Purify the GST-4EBP1 using the same method as shown above. Purified STIM1
652 and 4EBP1 were flash-frozen with liquid nitrogen.

653 ***In vitro* kinase assays**

654 DYRK2 kinase assays were performed in 50 mM HEPES, pH 7.5, 100 mM NaCl, 10 mM MnCl₂,
655 10 mM ATP using STIM1 or 4EBP1 as substrate. The kinase reactions were initiated by the
656 addition of DYRK2 with indicated concentration. Assays (25 μl volume) were carried out at
657 30 °C for 30 minutes, and terminated by addition of SDS-PAGE buffer containing 20 mM EDTA
658 and then boiled. The reaction mixtures were then separated by SDS-PAGE and visualized by
659 Coomassie Blue staining or analyzed by immuno-blot using primary antibodies as indicated
660 throughout.

661 **Co-immunoprecipitation and western blotting**

662 HEK293A cells were cultured and transfected as described above. After transfection, the cells
663 were washed three times with Ca²⁺-free buffer containing 10 mM HEPES, 10 mM D-glucose,

664 150 mM NaCl, 4 mM KCl, 3 mM MgCl₂ and 0.1 mM EGTA (pH 7.4). Treatment of DMEM
665 containing 1 μM of C17 at 37°C were used for DYRK2 inhibition. Ca²⁺-store depletion was
666 triggered by incubating cells with 2 μM thapsigargin for 20 min. The cells were then lysed with
667 lysis buffer consisting of 50 mM Tris-HCl (pH 7.5), 1 mM EGTA, 1 mM EDTA, 1% (v/v) Nonidet
668 P40 (substitute), 1 mM sodium orthovanadate, 50 mM sodium fluoride, 5 mM sodium
669 pyrophosphate, 0.27 M sucrose, 2 mM dithiothreitol (DTT), 1 mM benzamidine, 0.1 mM PMSF
670 (added before lysis), 1% (v/v) protease inhibitor cocktail (Roche) and 1% (v/v) Phosphatase
671 Inhibitor Cocktail (Roche). Protein concentrations were determined with the BCA protein assay
672 kit Pierce (Thermo-Pierce). For immunoprecipitations, lysates containing equal protein
673 amounts were incubated with FLAG-beads 2 h at 4°C. FLAG-beads were washed three times
674 with lysis buffer containing 0.15 M NaCl. Proteins were eluted from the FLAG-beads by
675 addition of 300 ug FLAG peptides (Smart Lifesciences). Eluted proteins were reduced by
676 addition of loading buffer with 4 mM DTT followed by heating at 95 °C for 10 minutes. For
677 western blotting, samples were electrophoresed in 10% or 12% gels and transferred to PVDF
678 membranes. All antibody dilutions and washes were carried out in Tris-buffered saline (TBS;
679 137 mM NaCl, 19 mM Tris HCl and 2.7 mM KCl, at pH 7.4) containing 0.1% Tween-20 (TBS-T).
680 Membranes were blocked in 5% non-fat milk solution in TBS-T for 1 h at room temperature,
681 incubated with indicated primary antibodies overnight at 4 °C, and incubated with secondary
682 antibodies (horseradish peroxidase-linked anti-mouse or anti-rabbit) for 1 h at room
683 temperature. Blots were developed with AMERSHAM ImageQuant 800 (GE Healthcare) and
684 exposed to film.

685 **Quantitative analysis of phosphorylation sites on STIM1**

686 Triplicate HEK293A cells co-transfected with GFP-ORAI1, FLAG-DRYK2 and FLAG-STIM1 for
687 36 h was treated with 1 μ M and 10 μ M C17 respectively for 1 h. After collected, cells were
688 washed with the Ca^{2+} -free buffer to remove excess Ca^{2+} and then lysed by the lysis buffer. For
689 immunoprecipitations, lysates containing equal protein amounts were incubated with FLAG-
690 beads for 1 h at 4 °C, which were washed three times with the lysis buffer afterwards. The
691 proteins were eluted from the FLAG-beads by addition of 500 ug FLAG peptides (Smart
692 Lifesciences). Then the eluted proteins were digested with trypsin by the FASP digestion
693 method(Wisniewski et al., 2009). The peptides were analyzed on a Q Exactive Plus mass
694 spectrometer (Thermo Fisher Scientific) with 1 h LC gradient. The raw files were searched
695 against Human fasta database (downloaded from Uniprot) by MaxQuant (version 1.6.3.4). The
696 oxidation (M), deamidation (NQ), and Phospho (STY) were selected as the variable
697 modifications for the phosphopeptide identification, while the carbamidomethyl was set as the
698 fixed modification. The false discovery rate (FDR) was set to 0.01 on PTM site, peptide, and
699 protein level. Label-free quantification (LFQ) and match between runs were set for the
700 triplicate analysis data.

701 **Confocal microscopy**

702 Confocal imaging were carried out with a ZEISS LSM880 imaging system equipped with 65 \times
703 oil objective (NA=1.45, Zeiss), 488- and 543-nm laser, controlled by Zen 2.3 SP1 software.
704 YFP (505 \pm 35) and mCherry (640 \pm 50) emission were collected with CaAsP PMT (Optical
705 section, 1.1 μ m). Image analysis was performed using Image J Fiji (NIH) (Zheng et al., 2018a).
706 Each repeat contains data from at least 6 cells.

707 **Fluorescence imaging**

708 Fluorescence signals were recorded using a ZEISS obersever-7 microscope equipped with an
709 X-Cite 120-Q (Lumen dynamics), brightline filter sets (Semrock Inc.), a 40×oil objective (NA =
710 1.30), and a Prime 95B Scientific CMOS (sCMOS) camera (Teledyne Imaging). This system
711 was controlled by Slide book6 software (3i). For fluorescence resonance energy transfer
712 (FRET) measurements, three-channel-corrected FRET include cyan fluorescent protein (CFP),
713 yellow fluorescent protein(YFP) and FRET raw were collected with corresponding filters, F_{CFP}
714 ($438\pm 12E_x/483\pm 16E_m$), F_{YFP} ($510\pm 10E_x/542\pm 13.5E_m$) and $FRET_{raw}$ ($438\pm 12E_x/542\pm 13.5E_m$),
715 every 10 sec. Calibration of bleed through from FRET donor or acceptor to FRET channel
716 (0.20, and 0.36, correspondingly), as well as the system-dependent factor, G (2.473) were
717 done as described earlier (Ma et al., 2015). These parameters were then used to generate
718 calculate FRET efficiency (E_{app}) values from raw fluorescent signals, similar to those
719 previously described (Ma et al., 2017). At least 16 cells were collected for each repeat.
720 Corresponding results were calculated with Matlab 2014a software and plotted with GraphPad
721 Prism 8.4.0 software. Representative traces of at least three independent experiments are
722 shown as mean \pm SEM.

723 **Confocal imaging and intracellular Ca^{2+} measurement**

724 Intracellular Ca^{2+} measurement was performed on a Zeiss LSM 700 laser scanning confocal
725 microscope equipped with a 63× oil immersion objective lens (N.A. = 1.4) controlled by ZEN
726 software. GCaMP6f fluorescence was excited using a 488-nm line of solid-state laser and
727 fluorescence emission was collected with a 490- to 555-nm band-pass filter; mCherry

728 fluorescence was excited using a 555-nm line of solid-state laser and fluorescence emission
729 was collected with a 580-nm long-pass filter. Two high-sensitivity PMTs were used for
730 detection. Cells were imaged at 10 s intervals for up to 20 mins. All live cell imaging
731 experiments were performed at room temperature. Data were processed and analyzed using
732 Zen and ImageJ software.

733 For intracellular Ca^{2+} measurement, HEK293A cells were plated on glass-bottom 35-mm
734 dishes and transfected as described above. Cells were washed with Ca^{2+} free buffer 3 times
735 24 h after transfection. For DYRK2 inhibition, cells were treated with DMEM containing 1 μM of
736 C17 at 37°C for 1 h before Ca^{2+} free buffer rinse. Depletion of Ca^{2+} -stores was triggered by
737 incubating cells with 1 μM thapsigargin in Ca^{2+} -free buffer, and Store-operated Ca^{2+} entry
738 (SOCE) was induced by addition of 2 mM CaCl_2 to thapsigargin containing buffer. 1 μM C17
739 was added for DYRK2 inhibition assay. The intracellular free calcium concentration was
740 measured by monitoring the fold change of GCaMP6f fluorescence, the data were shown as
741 the mean \pm SEM.

742 **Statistics and data presentation**

743 Most experiments were repeated 3 times with multiple technical replicates to be eligible for the
744 indicated statistical analyses, and representative image has been shown. All results are
745 presented as mean \pm SD unless otherwise mentioned. Data were analysed using Graphpad
746 Prism 8.4.0 statistical package.

747 **Data availability**

748 The structural coordinates of DYRK2 in complex with compounds 5, 6, 7, 8, 10, 13, 14, 17, 18,
749 19, and 20 have been deposited in the Protein Data Bank with accession codes 7DH3, 7DG4,
750 7DH9, 7DHV, 7DHC, 7DHK, 7DHO, 7DJO, 7DL6, 7DHH, and 7DHN, respectively.

751 All the raw mass spectrometry data as well as the identified and significantly regulated
752 phosphosites tables have been deposited in the public proteomics repository MassIVE and are
753 accessible at <ftp://massive.ucsd.edu/MSV000087106/>

754

755

756 **Figure 1—figure supplement 1.** Chemical compounds derived from LDN192960. (A)
757 Structure of amino side chain change analogues 1-6 based on LDN192960. (B) HEK293T
758 cells stably expressing FLAG-DYRK2 were treated with the indicated concentrations of
759 compound 6 in 1h. Cells were lysed and immunoblotting was carried out with the indicated
760 antibodies. (C) Structure of DYRK2 in complex with compound 6. DYRK2 is shown as ribbons
761 and colored in blue white. The 2Fo-Fc difference electron density map (1.5σ which reveals the
762 presence of 6 and water is shown as a gray mesh. The 6 and water are omitted to calculate
763 the map).

764 **Figure 1—figure supplement 1-source data 1.**

765 Raw data of Western blot for Figure 1—figure supplement 1B.

766

767 **Figure 1—figure supplement 2.** Structure-guided engineering of DYRK2 inhibitors based on
768 compound 6. (A) The possible sites for further expansion based on the co-crystal structure of
769 6 and DYRK2. (B) Overview of modification of compound 6. (C) Modifications for inner space 1.
770 (D) Modifications for cavity around ATP-binding pocket. (E) Modifications of amine side chain
771 based on compound 7. (F) Modifications based on compound 17.

772

773 **Figure 1—figure supplement 3.** The 2Fo-Fc composite omit maps (1.5σ surrounding
774 compounds 5, 10, 13, 14, 19 and 20 are shown in the co-crystal structures with DYRK2
775 respectively).

776

777 **Figure 2—figure supplement 1.** IC_{50} of C17 on DYRK2 and its main off targets. (A-E) IC_{50} of
778 C17 on DYRK2, DYRK1A, DYRK1B, DYRK3, Haspin and MARK3. The IC_{50} graph was plotted

779 using GraphPad Prism 8.4.0 software. The results are presented as the percentage of kinase
780 activity relative to the DMSO-treated control. Results are means \pm SD for triplicate reactions
781 with similar results obtained in at least one other experiment.

782

783 **Figure 2—figure supplement 2.** Binding strength of LDN192960 and C17 with calf thymus
784 DNA. **(A)** Binding strength of LDN192960 with calf thymus DNA tested by Isothermal titration
785 calorimetry. **(B)** Binding strength of C17 with calf thymus DNA tested by Isothermal titration
786 calorimetry.

787

788 **Figure 3—figure supplement 1.** Correlation of the intensities of phosphosites between any
789 two samples in phosphoproteomic analysis of U266 cells treated with/without C17.

790 **Figure 3—figure supplement 1-source data 1.**

791 Raw data of the intensities of phosphosites in phosphoproteomic analysis of U266 cells
792 treated with/without C17.

793

794 **Figure 3—figure supplement 2.** Coefficient of variance of the intensities of phosphosites in
795 phosphoproteomic analysis of U266 cells treated with/without C17.

796 **Figure 3—figure supplement 2-source data 1.**

797 Raw data of the intensities of phosphosites in phosphoproteomic analysis of U266 cells
798 treated with/without C17.

799

800 **Figure 3—figure supplement 3.** The intensities for pT37 phosphosite of EIF4E-BP1 and
801 pS519, pS521 phosphosites of STIM1. Data was presented as mean values \pm SD (error bars).

802 **Figure 3—figure supplement 3-source data 1.**

803 Raw data of the intensities for pT37 phosphosite of 4E-BP1 and pS519, pS521 phosphosites
804 of STIM1 for Figure 3—figure supplement 1-source data 1.

805

806 **Figure 4—figure supplement 1.** Knockdown efficiency of DYRK2-expression in wild-type
807 HEK293T stably expressed DYRK2 shRNA was measured by qPCR. GAPDH was used as an
808 internal standard, and fold change was calculated by comparing expression levels relative to
809 those of pLL3.7-shRNA-scramble (negative control). Data are presented as the means \pm SD
810 (n=3 biological replicates per condition, ***, P=0.0001, unpaired Student's t-test).

811 **Figure 4—figure supplement 1-source data 1.**

812 Raw qPCR data of knockdown efficiency of DYRK2-expression in wild-type HEK293T for
813 Figure 4—figure supplement 1-source data 1.

814

815 **Figure 4—figure supplement 2.** All primer sequences for qRT-PCR, shRNA targeting
816 sequences are listed.

817

818 **Figure 5—figure supplement 1. (A)** Quantitative analysis of phosphorylation sites on STIM1.
819 Workflow for the identification of phosphosites influenced by C17 on STIM1. Triplicate
820 HEK293A cells co-transfected with FLAG-STIM1 were treated with 10 μ M C17 for 1 h,
821 enriched by FLAG-beads, digested by FASP (Filter-Aided Sample Preparation) and quantified
822 by label-free proteomics. **(B)** The changed phosphorylation levels on peptides of STIM1. The

823 phosphorylation of eight phosphosites (shown in red) on four peptides of STIM1 was
824 significantly reduced upon treatment with C17 compared with the control group. (C) STIM1
825 constructs used.

826 **Figure 5—figure supplement 1-source data 1.**

827 Raw data of quantitative analysis of phosphorylation sites on STIM1 by DYRK2 upon C17
828 treatment for Figure 5—figure supplement 1-source data 1.

829

830 **References:**

- 831 Adams, P.D., Afonine, P.V., Bunkoczi, G., Chen, V.B., Davis, I.W., Echols, N., Headd, J.J.,
832 Hung, L.W., Kapral, G.J., Grosse-Kunstleve, R.W., *et al.* (2010). PHENIX: a comprehensive
833 Python-based system for macromolecular structure solution. *Acta crystallographica Section D,*
834 *Biological crystallography* 66, 213-221.
- 835 Alvarez-Salamero, C., Castillo-Gonzalez, R., and Navarro, M.N. (2017). Lighting Up T
836 Lymphocyte Signaling with Quantitative Phosphoproteomics. *Front Immunol* 8, 938.
- 837 Aranda, S., Laguna, A., and de la Luna, S. (2011). DYRK family of protein kinases:
838 evolutionary relationships, biochemical properties, and functional roles. *FASEB J* 25, 449-462.
- 839 Banerjee, S., Ji, C., Mayfield, J.E., Goel, A., Xiao, J., Dixon, J.E., and Guo, X. (2018). Ancient
840 drug curcumin impedes 26S proteasome activity by direct inhibition of dual-specificity
841 tyrosine-regulated kinase 2. *Proc Natl Acad Sci U S A* 115, 8155-8160.
- 842 Banerjee, S., Wei, T., Wang, J., Lee, J.J., Gutierrez, H.L., Chapman, O., Wiley, S.E., Mayfield,
843 J.E., Tandon, V., Juarez, E.F., *et al.* (2019). Inhibition of dual-specificity tyrosine
844 phosphorylation-regulated kinase 2 perturbs 26S proteasome-addicted neoplastic progression.
845 *Proc Natl Acad Sci U S A* 116, 24881-24891.
- 846 Becker, W., and Joost, H.G. (1999). Structural and functional characteristics of Dyrk, a novel
847 subfamily of protein kinases with dual specificity. *Prog Nucleic Acid Res Mol Biol* 62, 1-17.
- 848 Becker, W., and Sippl, W. (2011). Activation, regulation, and inhibition of DYRK1A. *FEBS J* 278,
849 246-256.
- 850 Chaikuad, A., Diharce, J., Schroder, M., Foucourt, A., Leblond, B., Casagrande, A.S., Desire,
851 L., Bonnet, P., Knapp, S., and Besson, T. (2016). An Unusual Binding Model of the Methyl
852 9-Anilinothiazolo[5,4-f]quinazoline-2-carbimidates (EHT 1610 and EHT 5372) Confers High
853 Selectivity for Dual-Specificity Tyrosine Phosphorylation-Regulated Kinases. *Journal of*
854 *Medicinal Chemistry* 59, 10315-10321.
- 855 Chen, W., Chen, L., and Tian, R. (2018). An integrated strategy for highly sensitive
856 phosphoproteome analysis from low micrograms of protein samples. *Analyst* 143, 3693-3701.
- 857 Collins, G.A., and Goldberg, A.L. (2017). The Logic of the 26S Proteasome. *Cell* 169, 792-806.
- 858 Collins, H.E., Zhu-Mauldin, X., Marchase, R.B., and Chatham, J.C. (2013).
859 STIM1/Orai1-mediated SOCE: current perspectives and potential roles in cardiac function and

860 pathology. *Am J Physiol-Heart C* 305, H446-H458.

861 Coux, O., Tanaka, K., and Goldberg, A.L. (1996). Structure and functions of the 20S and 26S
862 proteasomes. *Annu Rev Biochem* 65, 801-847.

863 Cuny, G.D., Robin, M., Ulyanova, N.P., Patnaik, D., Pique, V., Casano, G., Liu, J.F., Lin, X.J.,
864 Xian, J., Glicksman, M.A., *et al.* (2010). Structure-activity relationship study of acridine analogs
865 as haspin and DYRK2 kinase inhibitors. *Bioorganic & Medicinal Chemistry Letters* 20,
866 3491-3494.

867 Cuny, G.D., Ulyanova, N.P., Patnaik, D., Liu, J.F., Lin, X.J., Auerbach, K., Ray, S.S., Xian, J.,
868 Glicksman, M.A., Stein, R.L., *et al.* (2012). Structure-activity relationship study of
869 beta-carboline derivatives as haspin kinase inhibitors. *Bioorganic & Medicinal Chemistry*
870 *Letters* 22, 2015-2019.

871 Emsley, P., Lohkamp, B., Scott, W.G., and Cowtan, K. (2010). Features and development of
872 Coot. *Acta crystallographica Section D, Biological crystallography* 66, 486-501.

873 Guo, X., Huang, X., and Chen, M.J. (2017). Reversible phosphorylation of the 26S
874 proteasome. *Protein Cell* 8, 255-272.

875 Guo, X., Wang, X., Wang, Z., Banerjee, S., Yang, J., Huang, L., and Dixon, J.E. (2016).
876 Site-specific proteasome phosphorylation controls cell proliferation and tumorigenesis. *Nature*
877 *cell biology* 18, 202-212.

878 Högberg, A., von Stechow, L., Bekker-Jensen, D.B., Weinert, B.T., Kelstrup, C.D., and Olsen,
879 J.V. (2018). Benchmarking common quantification strategies for large-scale
880 phosphoproteomics. *Nat Commun* 9, 1045.

881 Jouanne, M., Rault, S., and Voisin-Chiret, A.S. (2017). Tau protein aggregation in Alzheimer's
882 disease: An attractive target for the development of novel therapeutic agents. *European*
883 *Journal of Medicinal Chemistry* 139, 153-167.

884 Laplante, M., and Sabatini, D.M. (2012). mTOR signaling in growth control and disease. *Cell*
885 149, 274-293.

886 Liou, J., Kim, M.L., Heo, W.D., Jones, J.T., Myers, J.W., Ferrell, J.E., Jr., and Meyer, T. (2005).
887 STIM is a Ca²⁺ sensor essential for Ca²⁺-store-depletion-triggered Ca²⁺ influx. *Curr Biol* 15,
888 1235-1241.

889 Liu, X., Xiao, W., Zhang, Y., Wiley, S.E., Zuo, T., Zheng, Y., Chen, N., Chen, L., Wang, X.,
890 Zheng, Y., *et al.* (2020). Reversible phosphorylation of Rpn1 regulates 26S proteasome
891 assembly and function. *Proc Natl Acad Sci U S A* 117, 328-336.

892 Lochhead, P.A., Sibbet, G., Morrice, N., and Cleghon, V. (2005). Activation-loop
893 autophosphorylation is mediated by a novel transitional intermediate form of DYRKs. *Cell* 121,
894 925-936.

895 Ma, G., Wei, M., He, L., Liu, C., Wu, B., Zhang, S.L., Jing, J., Liang, X., Senes, A., Tan, P., *et al.*
896 (2015). Inside-out Ca²⁺ signalling prompted by STIM1 conformational switch. *Nat Commun*
897 6, 7826.

898 Ma, G., Zheng, S., Ke, Y., Zhou, L., He, L., Huang, Y., Wang, Y., and Zhou, Y. (2017).
899 Molecular Determinants for STIM1 Activation During Store- Operated Ca²⁺ Entry. *Curr Mol*
900 *Med* 17, 60-69.

901 Ma, S., Bhattacharjee, R.B., and Bag, J. (2009). Expression of poly(A)-binding protein is
902 upregulated during recovery from heat shock in HeLa cells. *FEBS J* 276, 552-570.

903 Manning, G., Whyte, D.B., Martinez, R., Hunter, T., and Sudarsanam, S. (2002). The protein

904 kinase complement of the human genome. *Science* 298, 1912-1934.

905 McCoy, A.J., Grosse-Kunstleve, R.W., Adams, P.D., Winn, M.D., Storoni, L.C., and Read, R.J.

906 (2007). Phaser crystallographic software. *Journal of applied crystallography* 40, 658-674.

907 Nakai, J., Ohkura, M., and Imoto, K. (2001). A high signal-to-noise Ca²⁺ probe composed of

908 a single green fluorescent protein. *Nat Biotechnol* 19, 137-141.

909 Pozo-Guisado, E., Casas-Rua, V., Tomas-Martin, P., Lopez-Guerrero, A.M.,

910 Alvarez-Barrientos, A., and Martin-Romero, F.J. (2013). Phosphorylation of STIM1 at ERK1/2

911 target sites regulates interaction with the microtubule plus-end binding protein EB1. *J Cell Sci*

912 126, 3170-3180.

913 Pozo-Guisado, E., and Martin-Romero, F.J. (2013). The regulation of STIM1 by

914 phosphorylation. *Commun Integr Biol* 6, e26283.

915 Prakriya, M., and Lewis, R.S. (2015). Store-Operated Calcium Channels. *Physiol Rev* 95,

916 1383-1436.

917 Qin, X., Jiang, B., and Zhang, Y. (2016). 4E-BP1, a multifactor regulated multifunctional protein.

918 *Cell Cycle* 15, 781-786.

919 Rai, A.K., Chen, J.X., Selbach, M., and Pelkmans, L. (2018). Kinase-controlled phase

920 transition of membraneless organelles in mitosis. *Nature* 559, 211-216.

921 She, Q.B., Halilovic, E., Ye, Q., Zhen, W., Shirasawa, S., Sasazuki, T., Solit, D.B., and Rosen,

922 N. (2010). 4E-BP1 is a key effector of the oncogenic activation of the AKT and ERK signaling

923 pathways that integrates their function in tumors. *Cancer Cell* 18, 39-51.

924 Soundararajan, M., Roos, A.K., Savitsky, P., Filippakopoulos, P., Kettenbach, A.N., Olsen, J.V.,

925 Gerber, S.A., Eswaran, J., Knapp, S., and Elkins, J.M. (2013). Structures of Down syndrome

926 kinases, DYRKs, reveal mechanisms of kinase activation and substrate recognition. *Structure*

927 (London, England : 1993) 21, 986-996.

928 Wang, X., Li, W., Parra, J.L., Beugnet, A., and Proud, C.G. (2003). The C terminus of initiation

929 factor 4E-binding protein 1 contains multiple regulatory features that influence its function and

930 phosphorylation. *Mol Cell Biol* 23, 1546-1557.

931 Wegiel, J., Gong, C.X., and Hwang, Y.W. (2011). The role of DYRK1A in neurodegenerative

932 diseases. *FEBS J* 278, 236-245.

933 Wippich, F., Bodenmiller, B., Trajkovska, M.G., Wanka, S., Aebersold, R., and Pelkmans, L.

934 (2013). Dual specificity kinase DYRK3 couples stress granule condensation/dissolution to

935 mTORC1 signaling. *Cell* 152, 791-805.

936 Wisniewski, J.R., Zougman, A., Nagaraj, N., and Mann, M. (2009). Universal sample

937 preparation method for proteome analysis. *Nat Methods* 6, 359-362.

938 Zheng, S., Zhou, L., Ma, G., Zhang, T., Liu, J., Li, J., Nguyen, N.T., Zhang, X., Li, W.,

939 Nwokonko, R., *et al.* (2018a). Calcium store refilling and STIM activation in STIM- and

940 Orai-deficient cell lines. *Pflugers Arch* 470, 1555-1567.

941 Zheng, S., Zhou, L., Ma, G., Zhang, T., Liu, J., Li, J., Nguyen, N.T., Zhang, X., Li, W.,

942 Nwokonko, R., *et al.* (2018b). Calcium store refilling and STIM activation in STIM- and

943 Orai-deficient cell lines. *Pflugers Arch* 470, 1555-1567.

944 Schindelin, J., Arganda-Carreras, I., Frise, E., Kaynig, V., Longair, M., Pietzsch, T., Preibisch,

945 S., Rueden, C., Saalfeld, S., Schmid, B., *et al.* (2012). Fiji: an open-source platform for

946 biological-image analysis. *Nat Methods* 9, 676-682.

947

949 **Acknowledgements:** We thank the National Center for Protein Sciences at Peking
950 University for assistance with crystal screening, and Shanghai Synchrotron Radiation Facility
951 and KEK Photon Factory for assistance with X-ray data collection. This work is supported by
952 National Key Research & Development Plan (2017YFA0505200 to X.L. and J.X.,
953 2019YFA0802104 to Y.W., and 2020YFE0202200 to R. T.), the National Natural Science
954 Foundation of China (91853202, 21625201, 21961142010, 21661140001, and 21521003 to
955 X.L., 31822014 to J.X., 31700088 to W. C., 91954205 to Y.W., and 91953118 to R.T.), and the
956 Beijing Outstanding Young Scientist Program (BJJWZYJH01201910001001 to X.L.).

1 Appendix 1

2 General information for chemical synthesis

3 NMR spectra were recorded on a Varian 400 MHz spectrometer, Bruker 400 MHz NMR
4 spectrometer (ARX400), Bruker 400 MHz NMR spectrometer (AVANCE III), Bruker-500M Hz
5 NMR spectrometer (500M) and Bruker-600M Hz NMR spectrometer (600M) at ambient
6 temperature with CDCl₃ as the solvent unless otherwise stated. Chemical shifts are reported in
7 parts per million relative to CDCl₃ (1H, δ 7.26; 13C, δ 77.16) and MeOD (1H, δ 3.31; 13C, δ
8 49.00). Data for 1H NMR are reported as follows: chemical shift, integration, multiplicity (s =
9 singlet, d = doublet, t = triplet, q = quartet, quint = quintet, sext = sextet, m = multiplet) and
10 coupling constants. High-resolution mass spectra were obtained at Peking University Mass
11 Spectrometry Laboratory using a Bruker APEX Flash chromatography. The samples were
12 analyzed by UPLC/MS on a Waters Auto Purification LC/MS system (Waters C18 5 μm 150 X
13 4.6 mm SunFire separation column) or prepared by HPLC/MS on a Waters Auto Purification
14 LC/MS system (ACQUITY UPLC® BEH C18 17 μm 2.1X50 mm column). Analytical thin layer
15 chromatography was performed using 0.25 mm silica gel 60-F plates, using 250 nm UV light
16 as the visualizing agent and a solution of phosphomolybdic acid and heat as developing
17 agents. Flash chromatography was performed using 200-400 mesh silica gel. Yields refer to
18 chromatographically pure materials, unless otherwise stated. All reactions were carried out in
19 oven-dried glassware under an argon atmosphere unless otherwise noted.

20

21 Synthetic Procedures:

22 **Appendix 1-scheme 1.** Synthesis route of C1-C4.

23 **5-methoxy-2-((4-methoxyphenyl)amino) benzoic acid (1a).** 2-bromo-5-methoxybenzoic
24 acid (9.26 g, 40 mmol), 4-methoxyaniline (6.90 g, 56 mmol), copper (0.73 g, 11 mmol), cuprous
25 oxide (0.82 g, 5.7 mmol) and potassium carbonate (7.74 g, 56 mmol) were added to 100 mL
26 DMF, the mixture was stirred at 80 °C overnight. The resulting slurry was cooled to room
27 temperature, and 2M HCl was added into the mixture until the system became acidic and a
28 large amount of solid was precipitated. After filtration, the precipitate was washed with water
29 and dried to give compound **1a** (4.02 g, 37%) as a dark green solid. **1a** was used in next step
30 without further purification.

31 **9-chloro-2,7-dimethoxyacridine (1b).** Compound **1a** (2.58 g, 9.45 mmol) was added in a
32 sealed tube, and 30 mL of phosphorus oxychloride was added under argon atmosphere. The
33 reaction was heated at 130 °C for 8 h. The resulting slurry was poured onto ice with vigorous
34 stirring, and a large amount of a yellow solid was precipitated. After filtration, the precipitate

35 was washed with water and dried to give compound **1b** (2.58 g, quant.) as an orange solid. **1b**
36 was used in next step without further purification.

37 **tert-butyl (3-((2,7-dimethoxyacridin-9-yl)thio)propyl)carbamate (1)**. To a solution of **1b** (50
38 mg, 0.183 mmol) in 5 mL of anhydrous DMF, sodium hydrosulfide hydrate powder (67% 22.9
39 mg, 0.274 mmol) was added under argon atmosphere, and the reaction was stirred at 50 °C
40 for 2 h until full conversion of **1b**. *N*-Boc-3-aminopropyl bromide (60.9 mg, 0.274 mmol) and
41 potassium carbonate (50.5 mg, 0.365 mmol) were added into the slurry and the reaction was
42 allowed to react at room temperature overnight. The solvent was then evaporated and the
43 residue was dissolved with dichloromethane and washed with water. The combined organic
44 extracts were dried over anhydrous Na₂SO₄ and concentrated *in vacuo*. The residue was
45 purified by chromatography on a silica gel column to give compound **1** as a light yellow solid
46 (47.4 mg, 61%). ¹H NMR (400 MHz, CDCl₃) δ 8.10 (d, *J* = 9.3 Hz, 2H), 7.94 (s, 2H), 7.42 (d, *J* =
47 9.3 Hz, 2H), 4.04 (s, 6H), 3.20 (d, *J* = 5.9 Hz, 2H), 2.95 (t, *J* = 7.2 Hz, 2H), 1.70 - 1.61 (m, 2H),
48 1.39 (s, 9H). ¹³C NMR (151 MHz, CDCl₃) δ 158.5, 156.0, 144.3, 136.0, 132.1, 130.7, 124.1,
49 102.2, 79.5, 55.8, 39.6, 33.6, 30.8, 28.5. HRMS(ESI) [M + H]⁺ calculated for C₂₃H₂₉N₂O₄S:
50 429.1843, found: 429.1831.

51

52 **Compounds 2-4**. By employment of the above-described procedure, starting from **1b** and
53 using suitable bromides, compounds 2-4 were prepared.

54 ***N*-(3-((2,7-dimethoxyacridin-9-yl)thio)propyl)acetamide (2)**. Yield 58%. ¹H NMR (400 MHz,
55 CDCl₃) δ 8.10 (d, *J* = 9.4 Hz, 2H), 7.94 (d, *J* = 2.7 Hz, 2H), 7.42 (dd, *J* = 9.4, 2.8 Hz, 2H), 4.04
56 (s, 6H), 3.30 (dd, *J* = 13.2, 6.7 Hz, 2H), 2.96 (t, *J* = 7.3 Hz, 2H), 1.88 (s, 3H), 1.69 - 1.59 (m,
57 2H). ¹³C NMR (151 MHz, CDCl₃) δ 170.2, 158.6, 144.3, 135.8, 132.2, 130.7, 124.1, 102.2, 55.8,
58 38.7, 33.6, 30.4, 23.4. HRMS(ESI) [M + H]⁺ calculated for C₂₀H₂₃N₂O₃S: 371.1424, found:
59 371.1428.

60 ***N*-(4-((2,7-dimethoxyacridin-9-yl)thio)butyl)acetamide (3)**. Yield 57%. ¹H NMR (400 MHz,
61 CDCl₃) δ 8.10 (d, *J* = 9.3 Hz, 2H), 7.95 (d, *J* = 2.7 Hz, 2H), 7.42 (dd, *J* = 9.3, 2.7 Hz, 2H), 4.04
62 (s, 6H), 3.15 (dd, *J* = 13.1, 6.7 Hz, 2H), 2.94 (t, *J* = 7.1 Hz, 2H), 1.86 (s, 3H), 1.59 (m, 2H), 1.49
63 (m, 2H). ¹³C NMR (101 MHz, CDCl₃) δ 170.1, 158.4, 144.2, 136.2, 132.0, 130.7, 124.0, 102.2,
64 55.8, 39.0, 35.9, 28.9, 27.5, 23.3. HRMS(ESI) [M + H]⁺ calculated for C₂₁H₂₅N₂O₃S: 385.1580,
65 found: 385.1572.

66 **4-((2,7-dimethoxyacridin-9-yl)thio)butanenitrile (4)**. Yield 52%. ¹H NMR (400 MHz, CDCl₃)
67 δ 8.11 (d, *J* = 9.4 Hz, 2H), 7.89 (d, *J* = 2.7 Hz, 2H), 7.43 (dd, *J* = 9.4, 2.8 Hz, 2H), 4.04 (s, 6H),
68 3.07 (t, *J* = 7.0 Hz, 2H), 2.47 (t, *J* = 7.0 Hz, 2H), 1.82 - 1.72 (m, 2H). ¹³C NMR (101 MHz, CDCl₃)

69 δ 158.7, 144.3, 134.4, 132.3, 130.6, 124.2, 118.8, 101.7, 55.8, 34.4, 25.8, 16.4. HRMS(ESI) [M
70 + H]⁺ calculated for C₁₉H₁₉N₂O₂S: 339.1162, found: 339.1159.

71

72

Appendix 1-scheme 2. Synthesis route of C5-C6.

73

74 **tert-butyl 4-((2,7-dimethoxyacridin-9-yl)thio)piperidine-1-carboxylate (5a).** To a solution of
75 **1b** (50 mg, 0.183 mmol) in 5 mL of anhydrous DMF, sodium hydrosulfide hydrate powder (67%
76 22.9 mg, 0.274 mmol) was added under argon atmosphere, and the reaction was stirred at
77 50 °C for 2 h until full conversion of **1b**. 4-bromopiperidine-1-carboxylic acid tert-butyl ester
78 (72.4mg, 0.274mmol) and potassium carbonate (50.5 mg, 0.365 mmol) were added into the
79 slurry and the reaction was allowed to react at room temperature overnight. The solvent was
80 then evaporated and the residue was dissolved with dichloromethane and washed with water.
81 The combined organic extracts were dried over anhydrous Na₂SO₄ and concentrated *in vacuo*.
82 The residue was purified by chromatography on a silica gel column to give compound **5a** as a
83 light yellow solid (45.4mg, 55%). ¹H NMR: (400 MHz, CDCl₃) δ 8.08 (d, *J* = 9.3 Hz, 2H), 7.93 (d,
84 *J* = 2.7 Hz, 2H), 7.40 (dd, *J* = 9.3, 2.8 Hz, 2H), 4.01 (s, 6H), 3.98-3.84 (m, 2H), 3.25 - 3.17 (m,
85 1H), 2.81 (ddd, *J* = 13.5, 10.5, 3.0 Hz, 2H), 1.86-1.72 (m, 2H), 1.72-1.58 (m, 2H), 1.42 (s, 9H).
86 ¹³C NMR (101 MHz, CDCl₃) δ 158.4, 154.7, 144.3, 134.8, 132.0, 131.1, 124.0, 102.4, 79.8,
87 55.7, 46.9, 43.2, 33.1, 28.5. HRMS(ESI) [M + H]⁺ calculated for C₂₅H₃₁N₂O₄S: 455.1999, found:
88 455.1995.

89 **Compounds 6a.** By employment of the above-described procedure, starting from **1b** and
90 using suitable bromide, compound **6a** were prepared.

91 **tert-butyl 4-(((2,7-dimethoxyacridin-9-yl)thio)methyl)piperidine-1-carboxylate (6a).** Yield
92 **79%**. ¹H NMR (400 MHz, CDCl₃) δ 8.10 (d, *J* = 9.4 Hz, 2H), 7.94 (d, *J* = 2.7 Hz, 2H), 7.42 (dd, *J*
93 = 9.4, 2.8 Hz, 2H), 4.03 (d, *J* = 48.7 Hz, 6H), 4.15 - 3.98 (overlapped, m, 2H), 2.82 (d, *J* = 6.8
94 Hz, 2H), 2.59 (t, *J* = 12.1 Hz, 2H), 1.86 (br s, 2H), 1.53 - 1.46 (m, 1H), 1.43 (s, 9H), 1.23-1.14
95 (m, *J* = 10.9 Hz, 2H). ¹³C NMR (101 MHz, CDCl₃) δ 158.4, 154.8, 144.2, 136.7, 132.0, 130.4,
96 123.9, 102.0, 79.5, 55.6, 43.6, 42.9, 36.8, 28.5. HRMS(ESI) [M + H]⁺ calculated for
97 C₂₆H₃₆N₂O₄S: 469.2156, found: 469.2153.

98 **2,7-dimethoxy-9-(piperidin-4-ylthio)acridine (5).** Compound **5a** (45.4mg, 0.100 mmol) was
99 dissolved in a 5% trifluoroacetic acid dichloromethane solution and the mixture was allowed to
100 react at room temperature for 2h. The solvent was then evaporated and the residue was
101 dissolved with methanol, then purified by HPLC/MS on a Waters Auto Purification LC/MS
102 system (ACQUITY UPLC ® BEH C18 17 μ m 2.1X50 mm column) to afford **5** as a dark red

103 solid (35.2mg, 75%). ¹H NMR (400 MHz, MeOD) δ 8.05 (d, *J* = 9.4 Hz, 2H), 8.00 (d, *J* = 2.7 Hz,
104 2H), 7.49 (dd, *J* = 9.4, 2.8 Hz, 2H), 4.05 (s, 6H), 3.36-3.33 (m, 1H), 2.99 (d, *J* = 6.8 Hz, 2H),
105 2.85 (td, *J* = 12.8, 2.9 Hz, 2H), 2.13 (d, *J* = 16.5 Hz, 2H), 1.70-1.65 (m, 2H). ¹³C NMR (151
106 MHz, MeOD) δ 160.9, 144.0, 138.6, 132.9, 129.7, 126.7, 104.0, 56.0, 45.5, 44.4, 30.9.
107 HRMS(ESI) [M + H]⁺ calculated for C₂₀H₂₃N₂O₂S: 355.1475, found: 355.1467.

108 **Compounds 6.** By employment of the above-described procedure, starting from **6a**,
109 compounds **6** was prepared.

110 **2,7-dimethoxy-9-((piperidin-4-ylmethyl)thio)acridine (6).** Yield 56%. ¹H NMR (400 MHz,
111 MeOD) δ 8.24 (d, *J* = 9.4 Hz, 2H), 8.17 (d, *J* = 2.3 Hz, 2H), 7.85 (dd, *J* = 9.4, 2.4 Hz, 2H), 4.14
112 (s, 6H), 3.75-3.68 (m, 1H), 3.39 (d, *J* = 13.3 Hz, 2H), 3.01 (t, *J* = 10.9 Hz, 2H), 2.18 - 2.09 (m,
113 2H), 2.05 - 2.01 (m, 2H), 1.37 - 1.32 (m, 2H). ¹³C NMR (101 MHz, MeOD) δ 61.0, 151.0, 135.6,
114 131.8, 131.1, 124.0, 104.0, 56.8, 44.7, 44.2, 35.9, 29.1. HRMS(ESI) [M + H]⁺ calculated for
115 C₂₁H₂₅N₂O₂S: 369.1631, found: 369.1638.

116

117 **Appendix 1-scheme 3.** General procedure of C7, C16-C19 synthesis.

118

119 **6,6'-azanediylbis-3-methoxybenzoic acid (1a').** 2-amino-5-methoxybenzoic acid (2.00 g,
120 8.66 mmol), 2-bromo-5-methoxybenzoic acid (0.11 g, 1.73 mmol), copper (0.11 g, 1.73 mmol),
121 cuprous oxide (0.12 g, 0.87 mmol) and potassium carbonate (7.74 g, 56 mmol) were added to
122 15 mL DMF, the mixture was stirred at 80 °C overnight. The resulting slurry was cooled to
123 room temperature, and 2 M HCl was added into the mixture until the system became acidic
124 and a large amount of solid was precipitated. After filtration, the precipitate was washed with
125 water and dried to give compound **1a'** (2.00 g, 73%) as a green solid. **1a'** was used in next
126 step without further purification.

127 **9-chloro-2,7-dimethoxyacridine-4-carboxylic acid (1b').** Compound **1a'** (1.00 g, 3.16 mmol)
128 was added in a sealed tube, and 10 mL of phosphorus oxychloride was added under argon
129 atmosphere. The reaction was heated at 130 °C for 8 h. The resulting slurry was poured onto
130 ice with vigorous stirring, and a large amount of a yellow solid was precipitated. After filtration,
131 the precipitate was washed with water and dried to give compound **1b** (1.00 g, 95%) as an
132 orange solid. **1b'** was used in next step without further purification.

133 **methyl 9-chloro-2,7-dimethoxyacridine-4-carboxylate (1c).** To a suspension of **1b'** (0.89 g,
134 2.67 mmol) in 10 mL of dry dichloromethane, 0.40 mL of oxalyl chloride was added followed by
135 one drop of DMF, and a large amount of bubbles was generated. The mixture was allowed to
136 react at room temperature for 0.5 h until the system became a brownish black solution. Then

137 the reaction was quenched by dry menthol at room temperature for 2 h, followed by the
138 addition of triethylamine until the mixture became neutral. The system was diluted with
139 dichloromethane, washed twice with brine, dried over anhydrous Na₂SO₄ and concentrated *in*
140 *vacuo*. The residue was purified by chromatography on a silica gel column (dichloromethane /
141 ethyl acetate = 95/5) to give compound **1c** as a yellow solid (0.74 g, 80%). ¹H NMR (400 MHz,
142 CDCl₃) δ 8.12 (d, *J* = 9.3 Hz, 1H), 7.70 (s, 1H), 7.64 (s, 1H), 7.46 (s, 1H), 7.42 (d, *J* = 9.4 Hz,
143 1H), 4.09 (s, 3H), 4.03 (s, 6H). ¹³C NMR (101 MHz, CDCl₃) δ 167.9, 159.0, 157.1, 144.8, 141.3,
144 135.9, 134.1, 132.6, 125.8, 125.7, 125.0, 124.9, 103.0, 99.6, 56.0, 55.8, 52.3. HRMS(ESI) [*M*
145 + H]⁺ calculated for C₁₇H₁₅ClNO₄: 332.0684, found: 332.0680.

146

147 **Appendix 1-scheme 4** Synthesis route of C7.

148

149 **methyl-9-(((1-(tert-butoxycarbonyl)piperidin-4-yl)methyl)thio)-2,7-dimethoxyacridine-4-c**
150 **arboxylate (7a)**. To a solution of **1c** (0.38 g, 1.16 mmol) in 10 mL of anhydrous DMF, sodium
151 hydrosulfide hydrate powder (70%, 0.10 g, 1.21 mmol) was added under argon atmosphere,
152 and the reaction was stirred at 50 °C for 2 h until full conversion of **1c**.
153 1-Boc-4-bromomethylpiperidine (0.64 g, 2.31 mmol) and potassium carbonate (0.40 g, 2.89
154 mmol) were added into the slurry and the reaction was allowed to react at room temperature
155 overnight. The solvent was then evaporated and the residue was dissolved with
156 dichloromethane and washed with water. The combined organic extracts were dried over
157 anhydrous Na₂SO₄ and concentrated *in vacuo*. The residue was purified by chromatography
158 on a silica gel column (dichloromethane / ethyl acetate = 95/5) to give compound **7a** as a
159 yellow solid (0.38g, 63%). ¹H NMR (400 MHz, CDCl₃) δ 8.13 (d, *J* = 9.4 Hz, 1H), 8.08 (d, *J* =
160 2.0 Hz, 1H), 7.89 (s, 1H), 7.68 (d, *J* = 1.9 Hz, 1H), 7.41 (dd, *J* = 9.4, 1.9 Hz, 1H), 4.09 (s, 3H),
161 4.02 (s, 6H), 2.78 (d, *J* = 6.7 Hz, 2H), 2.55 (t, *J* = 12.2 Hz, 2H), 1.82 (br s, 2H), 1.45-1.35(m,
162 3H), 1.43 (s, 9H), 1.20-1.09 (m, 2H). ¹³C NMR (101 MHz, CDCl₃) δ 168.2, 158.9, 157.0, 154.8,
163 144.7, 141.2, 137.0, 134.6, 133.0, 130.7, 130.5, 124.4, 124.3, 105.11, 101.74, 79.6, 56.0, 55.7,
164 52.8, 43.8, 43.1 (br s), 36.8, 31.8, 28.5. HRMS(ESI) [*M* + H]⁺ calculated for C₂₈H₃₅N₂O₆S:
165 527.2210, found: 527.2212.

166 **Compounds 16a-19a**. By employment of the above-described procedure, starting from **1c**'
167 and using suitable bromides, compounds **16a-19a** were prepared.

168 **methyl**

169 **9-((3-(((tert-butoxycarbonyl)amino)propyl)thio)-2,7-dimethoxyacridine-4-carboxylate**
170 **(16a)**. Yield 76%. ¹H NMR (400 MHz, CDCl₃) δ 8.12 (d, *J* = 9.4 Hz, 1H), 8.09 (d, *J* = 2.8 Hz,

171 1H), 7.89 (d, $J = 2.8$ Hz, 1H), 7.68 (dd, $J = 2.9, 0.8$ Hz, 1H), 7.41 (dd, $J = 9.3, 2.8$ Hz, 1H), 4.40
172 (br s, 1H), 4.09 (s, 3H), 4.04 (s, 3H), 4.03 (s, 3H), 3.17 (q, $J = 6.6$ Hz, 2H), 2.92 (t, $J = 7.3$ Hz,
173 2H), 1.61-1.59 (m, 2H), 1.39 (s, 9H). ^{13}C NMR (101 MHz, CDCl_3) δ 168.2, 158.8, 157.0, 155.9,
174 144.57, 141.08, 136.2, 134.5, 132.9, 130.8, 130.6, 124.3, 124.3, 105.1, 101.8, 55.9, 55.7, 52.8,
175 39.5, 33.7, 30.7, 28.4. HRMS(ESI) $[\text{M} + \text{H}]^+$ calculated for $\text{C}_{25}\text{H}_{31}\text{N}_2\text{O}_6\text{S}$: 487.1889, found:
176 487.1897.

177 **methyl-(S)-9-(((1-(tert-butoxycarbonyl)pyrrolidin-3-yl)methyl)thio)-2,7-dimethoxyacridin**
178 **e-4-carboxylate (17a). Yield 76%.** ^1H NMR (400 MHz, CDCl_3) δ 8.13 (d, $J = 9.4$ Hz, 1H), 8.08
179 (d, $J = 2.4$ Hz, 1H), 7.88 (d, $J = 2.6$ Hz, 1H), 7.68 (d, $J = 2.7$ Hz, 1H), 7.42 (dd, $J = 9.4, 2.6$ Hz,
180 1H), 4.10 (s, 3H), 4.05 (s, 3H), 4.04 (s, 3H), 3.61-3.14 (m, 2H), 3.27-2.1 (m, 4H), 2.10-2.01 (m,
181 1H), 1.90-1.85 (m, 1H), 1.68-1.59 (m, 1H), 1.43 (s, 9H). ^{13}C NMR (101 MHz, CDCl_3) δ 168.2,
182 159.0, 157.1, 154.5, 144.6, 141.1, 135.9, 134.7, 133.1, 130.7, 130.5, 124.4, 124.3, 104.9,
183 101.6, 79.4, 55.9 (d, $J = 96$ Hz), 52.8, 51.0 (d, $J = 104$ Hz), 45.2 (d, $J = 104$ Hz), 39.6-39.3 (m),
184 38.4, 31.3, 30.7, 28.6. HRMS(ESI) $[\text{M} + \text{H}]^+$ calculated for $\text{C}_{27}\text{H}_{33}\text{N}_2\text{O}_6\text{S}$: 513.2052, found:
185 513.2054.

186 **methyl-(R)-9-(((1-(tert-butoxycarbonyl)pyrrolidin-3-yl)methyl)thio)-2,7-dimethoxyacridin**
187 **e-4-carboxylate (18a). Yield 84%.** ^1H NMR (400 MHz, CDCl_3) δ 8.13 (d, $J = 9.4$ Hz, 1H), 8.07
188 (s, 1H), 7.88 (s, 1H), 7.68 (s, 1H), 7.41 (d, $J = 8.8$ Hz, 1H), 4.09 (s, 3H), 4.04 (s, 6H), 3.62-3.31
189 (m, 2H), 3.26-3.18 (m, 1H), 3.10-2.79 (m, 3H), 2.11-1.99 (m, 1H), 1.97-1.86 (m, 1H), 1.65-1.56
190 (m, 1H), 1.43 (s, 9H). ^{13}C NMR (126 MHz, CDCl_3) δ 168.2, 159.1, 157.2, 154.5, 144.7, 141.3,
191 135.9, 134.8, 133.2, 130.8, 130.6, 124.4, 124.3, 105.0, 101.7, 79.4, 55.9 (d, $J = 105$ Hz), 52.8,
192 51.1 (d, $J = 115$ Hz), 45.2 (d, $J = 135$ Hz), 39.7-39.4 (m), 38.5, 31.4, 30.7, 28.6. HRMS(ESI) $[\text{M}$
193 $+ \text{H}]^+$ calculated for $\text{C}_{27}\text{H}_{33}\text{N}_2\text{O}_6\text{S}$: 513.2052, found: 513.2054.

194 **methyl-9-(((1-(tert-butoxycarbonyl)azetidid-3-yl)methyl)thio)-2,7-dimethoxyacridine-4-ca**
195 **rboxylate (19a). Yield 75%.** ^1H NMR (400 MHz, CDCl_3) δ 8.14 (d, $J = 9.4$ Hz, 1H), 8.03 (s, 1H),
196 7.84 (s, 1H), 7.68 (d, $J = 1.6$ Hz, 1H), 7.42 (d, $J = 9.4$ Hz, 1H), 4.10 (s, 3H), 4.04 (s, 6H), 3.85 (t,
197 $J = 8.3$ Hz, 2H), 3.60 (s, 2H), 3.10 (d, $J = 7.8$ Hz, 2H), 2.26-2.16 (m, 1H), 1.40 (s, 9H). ^{13}C NMR
198 (126 MHz, CDCl_3) δ 168.2, 159.2, 157.3, 156.3, 144.7, 141.2, 134.9, 134.8, 133.2, 130.9,
199 130.7, 124.5, 124.3, 104.9, 101.6, 79.7, 56.0, 55.8, 54.0 (br s), 52.8, 39.9, 29.0, 28.5.
200 HRMS(ESI) $[\text{M} + \text{H}]^+$ calculated for $\text{C}_{26}\text{H}_{31}\text{N}_2\text{O}_6\text{S}$: 499.1897, found: 499.1895.

201 **tert-butyl-4-(((4-(hydroxymethyl)-2,7-dimethoxyacridin-9-yl)thio)methyl)piperidine-1-car**
202 **boxylate (7b).** 3.1 mL of 1.5 M DIBAL-H solution in toluene was added to a solution of **7a** (348
203 mg, 0.661 mmol) in 10 mL of dry dichloromethane at 0 °C, and the reaction was stirred at room
204 temperature for 4 h. The reaction was quenched by adding saturated potassium hydrogen

205 tartrate solution, diluted with dichloromethane, washed twice with brine, dried over anhydrous
206 Na₂SO₄ and concentrated *in vacuo*. The residue was purified by chromatography on a silica
207 gel column (dichloromethane / ethyl acetate = 90/10) to give compound **7b** (180 mg, 55%) as
208 yellow foam. ¹H NMR (400 MHz, CDCl₃) δ 8.03 (d, *J* = 9.3 Hz, 1H), 7.88 (s, 1H), 7.81 (s, 1H),
209 7.39 (d, *J* = 9.3 Hz, 1H), 7.27 (s, 1H), 5.41 (s, 1H), 5.21 (s, 2H), 4.02 (s, 3H), 4.00 (s, 3H) 2.79
210 (d, *J* = 6.7 Hz, 2H), 2.57 (t, *J* = 11.7 Hz, 2H), 1.84 (br s, 2H), 1.47-1.25 (m, 3H), 1.43 (s, 9H),
211 1.20-1.09 (m, 2H). ¹³C NMR (101 MHz, CDCl₃) δ 158.5, 157.9, 154.8, 143.3, 142.7, 140.4,
212 137.6, 131.9, 131.1, 130.5, 124.1, 122.1, 102.0, 101.4, 79.6, 65.0, 55.7, 55.7, 43.6, 43.1, 36.8,
213 31.8, 28.5. HRMS(ESI) [M + H]⁺ calculated for C₂₇H₃₅N₂O₅S: 499.2258, found: 499.2261.

214 **Compounds 16b-19b.** By employment of the above-described procedure, starting from
215 **16a-19a**, compounds **16b-19b** were prepared.

216 **tert-butyl (3-((4-(hydroxymethyl)-2,7-dimethoxyacridin-9-yl)thio)propyl)carbamate (16b).**
217 **Yield 68%.** ¹H NMR (400 MHz, CDCl₃) δ 8.04 (d, *J* = 9.3 Hz, 1H), 7.92 (d, *J* = 2.8 Hz, 1H), 7.85
218 (d, *J* = 2.8 Hz, 1H), 7.41 (dd, *J* = 9.3, 2.8 Hz, 1H), 7.27 (d, *J* = 2.7 Hz, 1H), 5.42 (br s, 1H), 5.21
219 (s, 2H), 4.43 (br s, 1H), 4.04 (s, 5H), 4.01 (s, 5H), 3.19 (d, *J* = 6.7 Hz, 2H), 2.93 (t, *J* = 7.3 Hz,
220 2H), 1.62 (t, *J* = 7.0 Hz, 3H), 1.39 (s, 9H). ¹³C NMR (101 MHz, CDCl₃) δ 158.6, 158.0, 156.0,
221 143.4, 142.7, 132.0, 131.3, 130.8, 124.2, 122.2, 102.1, 101.6, 65.1, 55.8, 55.8, 39.6, 33.7,
222 30.8, 28.5. HRMS(ESI) [M + H]⁺ calculated for C₂₄H₃₁N₂O₅S: 459.1948, found: 459.1950.

223 **tert-butyl-(S)-3-(((4-(hydroxymethyl)-2,7-dimethoxyacridin-9-yl)thio)methyl)pyrrolidine-1**
224 **-carboxylate (17b). 68%.** ¹H NMR (400 MHz, CDCl₃) δ 8.06 (d, *J* = 9.3 Hz, 1H), 7.92 (d, *J* =
225 2.6 Hz, 1H), 7.85 (d, *J* = 2.3 Hz, 1H), 7.42 (dd, *J* = 9.3, 2.5 Hz, 1H), 7.29 (s, 1H), 5.36 (br s, 1H),
226 5.21 (s, 2H), 4.05 (s, 3H), 4.02 (s, 3H), 3.62-3.32 (m, 2H), 3.27 - 2.84 (m, 4H), 2.15-2.05 (d, *J* =
227 6.4 Hz, 1H), 2.01 - 1.92 (m, 1H), 1.70-1.60 (m, 1H), 1.43 (d, *J* = 4.8 Hz, 9H). ¹³C NMR (126
228 MHz, CDCl₃) δ 158.6, 158.0, 154.4, 143.4, 142.7, 140.5, 136.5, 131.9, 131.1, 130.5, 124.1,
229 122.1, 101.9, 101.3, 79.3, 64.9, 55.7, 51.1 (d, *J* = 115 Hz), 45.1 (d, *J* = 135 Hz), 39.4, 38.4,
230 31.2, 30.6, 28.5. HRMS(ESI) [M + H]⁺ calculated for C₂₆H₃₃N₂O₅S: 485.2105, found: 485.2110.

231 **tert-butyl-(R)-3-(((4-(hydroxymethyl)-2,7-dimethoxyacridin-9-yl)thio)methyl)pyrrolidine-1**
232 **-carboxylate (18b). 64%.** ¹H NMR (400 MHz, CDCl₃) δ 8.05 (d, *J* = 9.4 Hz, 1H), 7.90 (d, *J* =
233 2.7 Hz, 1H), 7.83 (d, *J* = 2.6 Hz, 1H), 7.41 (dd, *J* = 9.3, 2.7 Hz, 1H), 7.28 (s, 1H), 5.38 (br s, 1H),
234 5.21 (s, 2H), 4.04 (s, 3H), 4.02 (s, 3H), 3.64 - 3.20 (m, 4H), 3.08 - 2.87 (m, 2H), 2.14 - 2.03 (m,
235 1H), 1.99-1.90 (m, 1H), 1.68 - 1.57 (m, 1H), 1.42 (d, *J* = 5.2 Hz, 9H). ¹³C NMR (126 MHz,
236 CDCl₃) δ 158.6, 158.0, 154.4, 143.3, 142.7, 140.5, 136.4, 131.9, 131.1, 130.5, 124.1, 122.0,
237 101.9, 101.3, 79.3, 64.9, 55.7, 50.9 (d, *J* = 115 Hz), 45.1 (d, *J* = 140 Hz), 39.4, 38.4, 31.2, 30.6,
238 28.5. HRMS(ESI) [M + H]⁺ calculated for C₂₆H₃₃N₂O₅S: 485.2105, found: 485.2102.

239 **tert-butyl-3-(((4-(hydroxymethyl)-2,7-dimethoxyacridin-9-yl)thio)methyl)azetidone-1-carb**
240 **oxylate (19b). 50%.** ¹H NMR (400 MHz, CDCl₃) δ 8.08 (d, *J* = 9.3 Hz, 1H), 7.87 (d, *J* = 2.7 Hz,
241 1H), 7.80 (d, *J* = 2.7 Hz, 1H), 7.43 (dd, *J* = 9.3, 2.7 Hz, 1H), 7.30 (d, *J* = 2.6 Hz, 1H), 5.22 (s,
242 2H), 4.04 (s, 3H), 4.02 (s, 3H), 3.85 (t, *J* = 8.4 Hz, 2H), 3.59 (dd, *J* = 8.8, 5.2 Hz, 2H), 3.12 (d, *J*
243 = 7.9 Hz, 2H), 2.24 (td, *J* = 7.9, 4.1 Hz, 1H), 1.39 (s, 9H). ¹³C NMR (126 MHz, CDCl₃) δ 158.7,
244 158.1, 156.2, 143.0, 142.5, 140.5, 135.6, 131.8, 131.2, 130.7, 124.3, 122.3, 101.8, 101.2, 79.6,
245 64.8, 55.7, 55.7, 39.7, 29.0, 28.3. HRMS(ESI) [M + H]⁺ calculated for C₂₅H₃₁N₂O₅S: 471.1948,
246 found: 471.1939.

247 **(2,7-dimethoxy-9-((piperidin-4-ylmethyl)thio)acridin-4-yl)methanol (7).** Compound **7b**
248 (24.2 mg, 0.048 mmol) was dissolved in 2 mL of 5% trifluoroacetic acid dichloromethane
249 solution and the mixture was allowed to react at room temperature for 2 h. The solvent was
250 then evaporated and the residue was dissolved with methanol, then purified by HPLC/MS on a
251 Waters Auto Purification LC/MS system (ACQUITY UPLC ® BEH C18 17 μm 2.1X50 mm
252 column) to afford **7** (11.2 mg, 45%) as a dark red solid. ¹H NMR (400 MHz, MeOD) δ 8.09 (d, *J*
253 = 9.4 Hz, 1H), 7.76 (d, *J* = 2.2 Hz, 1H), 7.71 (d, *J* = 2.2 Hz, 1H), 7.54 (d, *J* = 1.1 Hz, 1H), 7.50
254 (dd, *J* = 9.4, 2.5 Hz, 1H), 5.23 (s, 2H), 4.04 (s, 3H), 4.03 (s, 3H), 3.33 - 3.30 (m, 2H), 2.95 (d, *J*
255 = 6.7 Hz, 2H), 2.83 (td, *J* = 12.8, 1.6 Hz, 2H), 2.07-1.99 (m, 2H), 1.66 - 1.55 (m, 1H), 1.51 -
256 1.40 (m, 2H). ¹³C NMR (126 MHz, MeOD) δ 160.0, 159.8, 144.0, 143.1, 143.0, 137.7, 132.9,
257 131.7, 131.4, 124.9, 121.8, 102.8, 101.7, 62.2, 56.2, 56.1, 44.8, 42.9, 35.7, 29.4. HRMS(ESI)
258 [M + H]⁺ calculated for C₂₂H₂₇N₂O₃S: 399.1737, found: 399.1732.

259 **Compounds 16-19.** By employment of the above-described procedure, starting from **16b-19b**,
260 compounds **16-19** were prepared.

261 **(9-((3-aminopropyl)thio)-2,7-dimethoxyacridin-4-yl)methanol (16).** Yield 88%. ¹H NMR
262 (400 MHz, MeOD) δ 8.13 (d, *J* = 9.4 Hz, 1H), 7.94 (d, *J* = 26.6 Hz, 2H), 7.58 - 7.54 (m, 1H),
263 7.50 (dd, *J* = 9.4, 2.7 Hz, 1H), 5.31 (s, 2H), 4.05 (s, 3H), 4.05 (s, 3H), 3.09 (t, *J* = 7.4 Hz, 2H),
264 2.95 - 2.88 (t, *J* = 7.4 Hz, 2H), 1.79 - 1.70 (m, 2H). ¹³C NMR (151 MHz, MeOD) δ 160.3, 160.0,
265 141.4, 140.9, 140.6, 139.8, 132.1, 131.7, 129.9, 127.0, 124.3, 103.2, 102.3, 62.1, 56.4, 56.3,
266 39.5, 34.1, 29.4. HRMS(ESI) [M + H]⁺ calculated for C₁₉H₂₃N₂O₃S: 359.1424, found: 359.1428.

267 **(S)-(2,7-dimethoxy-9-((pyrrolidin-3-ylmethyl)thio)acridin-4-yl)methanol (17).** Yield 93%.
268 ¹H NMR (400 MHz, MeOD) δ 8.11 (d, *J* = 9.4 Hz, 1H), 7.81 (s, 1H), 7.75 (s, 1H), 7.57 (s, 1H),
269 7.51 (d, *J* = 9.4 Hz, 1H), 5.27 (s, 2H), 4.07 (s, 3H), 4.07 (s, 3H), 3.36 - 3.27 (m, 2H), 3.19 - 3.05
270 (m, 3H), 2.96 (dd, *J* = 11.4, 8.3 Hz, 1H), 2.25 (hept, *J* = 7.6 Hz, 1H), 2.17 - 2.05 (m, 1H), 1.80 -
271 1.70 (m, 1H). ¹³C NMR (126 MHz, MeOD) δ 160.3, 160.1, 141.8, 141.4, 140.7, 139.9, 131.8,

272 131.4, 130.8, 126.4, 123.6, 103.0, 102.0, 62.1, 56.3, 56.2, 50.7, 46.2, 40.0, 39.5, 30.9.
273 HRMS(ESI) [M + H]⁺ calculated for C₂₁H₂₅N₂O₃S: 385.1580, found: 385.1580.
274 **(R)-(2,7-dimethoxy-9-((pyrrolidin-3-ylmethyl)thio)acridin-4-yl)methanol (18). Yield 64%.**
275 ¹H NMR (400 MHz, MeOD) δ 8.14 (d, *J* = 9.3 Hz, 1H), 7.96 (s, 1H), 7.89 (s, 1H), 7.58 (s, 1H),
276 7.53 - 7.48 (m, 1H), 5.32 (s, 2H), 4.06 (s, 6H), 3.35 - 3.26 (m, 2H), 3.20 - 3.08 (m, 3H), 2.97 -
277 2.92 (m, 1H), 2.26 (hept, *J* = 7.6 Hz, 1H), 2.17 - 2.07 (m, 1H), 1.80 - 1.71 (m, 1H). ¹³C NMR
278 (126 MHz, MeOD) δ 160.2, 160.0, 141.4, 141.1, 140.3, 140.2, 131.7, 131.3, 130.5, 126.5,
279 123.7, 103.0, 102.0, 62.1, 56.3, 56.2, 50.6, 46.1, 39.9, 39.6, 30.9. HRMS(ESI) [M + H]⁺
280 calculated for C₂₁H₂₅N₂O₃S: 385.1580, found: 385.1579.

281 **(9-((azetidin-3-ylmethyl)thio)-2,7-dimethoxyacridin-4-yl)methanol (19). Yield 56%. ¹H**
282 **NMR (400 MHz, MeOD) δ 8.07 (d, *J* = 9.4 Hz, 1H), 7.80 (d, *J* = 2.2 Hz, 1H), 7.73 (d, *J* = 2.1 Hz,**
283 **1H), 7.53 (s, 1H), 7.46 (dd, *J* = 9.3, 2.2 Hz, 1H), 5.28 (s, 2H), 4.04 (s, 3H), 4.03 (s, 3H), 3.82 (t,**
284 ***J* = 9.7 Hz, 2H), 3.69 - 3.62 (m, 2H), 3.26 (d, *J* = 7.9 Hz, 2H), 2.71 - 2.58 (m, 1H). ¹³C NMR**
285 **(101 MHz, MeOD) δ 160.4, 160.2, 142.4, 142.0, 141.3, 138.0, 132.0, 131.7, 131.5, 126.2,**
286 **123.2, 102.7, 101.6, 62.0, 56.3, 56.2, 51.9, 38.9, 33.9. HRMS(ESI) [M + H]⁺ calculated for**
287 **C₂₀H₂₃N₂O₃S: 371.1424, found: 371.1431.**

288

289

Appendix 1-scheme 5. Synthesis route of C8.

290 **2,7-dimethoxy-9-((piperidin-4-ylmethyl)thio)acridine-4-carboxylic acid (8).** 0.4 mL of
291 aqueous 1.0 M lithium hydroxide solution of was added into a solution of compound **7a** (42 mg,
292 0.080 mmol) 2 mL of tetrahydrofuran, and the mixture was reacted at 40 ° C for 20 h. After
293 cooling to room temperature, 5 mL of a 10% solution of trifluoroacetic acid in dichloromethane
294 was added to the system, and the mixture was reacted at room temperature for 6 h. The
295 solvent was then evaporated and the residue was dissolved with methanol, then purified by
296 HPLC/MS on a Waters Auto Purification LC/MS system (ACQUITY UPLC ® BEH C18 17 µm
297 2.1X50 mm column) to afford **8** (21.6 mg, 51%) as a dark red foam. ¹H NMR (600 MHz, MeOD)
298 δ 8.39 (d, *J* = 2.8 Hz, 1H), 8.23 (d, *J* = 2.7 Hz, 1H), 8.12 (d, *J* = 9.3 Hz, 1H), 7.97 (d, *J* = 2.5 Hz,
299 1H), 7.62 (dd, *J* = 9.3, 2.6 Hz, 1H), 4.09 (s, 3H), 4.07 (s, 3H), 3.36-3.33 (m, 2H), 3.02 (d, *J* =
300 6.8 Hz, 2H), 2.89 - 2.82 (m, 2H), 2.11 (d, *J* = 14.0 Hz, 2H), 1.70 - 1.64 (m, 1H), 1.50 - 1.41 (m,
301 2H). ¹³C NMR (126 MHz, MeOD) δ 168.7, 160.7, 158.9, 141.9, 141.4, 140.9, 131.6, 131.5,
302 130.7, 130.5, 128.0, 126.7, 108.6, 103.1, 56.6, 56.5, 44.8, 43.4, 35.7, 29.4. HRMS(ESI) [M +
303 H]⁺ calculated for C₂₂H₂₅N₂O₄S: 413.1530, found: 413.1526.

304

305

Appendix 1-scheme 6. Synthesis route of C9.

306

307 **tert-butyl 4-(((4-formyl-2,7-dimethoxyacridin-9-yl)thio)methyl)piperidine-1-carboxylate**
308 **(9a)**. 20.4 μL of oxalyl chloride was dissolved in 1 mL of dry tetrahydrofuran and the mixture
309 was cooled to -78°C . 25.6 μL of dimethyl sulfoxide was slowly added to the system, the
310 reaction was stirred at -78°C for 30 min, followed by addition of a solution of compound **7b**
311 (60 mg, 0.12 mmol) in 1 mL of tetrahydrofuran solution, and the reaction was continued at -78°C
312 for 1 h. 0.10 mL of triethylamine was then added, and the reaction was allowed to return to
313 room temperature for 2 h. The solvent was then evaporated and the residue was purified by
314 chromatography on a silica gel column (dichloromethane / ethyl acetate = 95/5) to give
315 compound **9a** (56 mg, 94%) as a light yellow solid. ^1H NMR (400 MHz, CDCl_3) δ 11.54 (s, 1H),
316 8.19 (d, $J = 2.9$ Hz, 1H), 8.09 (d, $J = 9.3$ Hz, 1H), 7.98 (d, $J = 2.9$ Hz, 1H), 7.86 (d, $J = 2.6$ Hz,
317 1H), 7.44 (dd, $J = 9.4, 2.7$ Hz, 1H), 4.10-3.98 (m, 2H), 4.04 (s, 3H), 4.03 (s, 3H), 2.80 (d, $J =$
318 6.8 Hz, 2H), 2.58 (t, $J = 12.2$ Hz, 2H), 1.83 (m, 2H), 1.52 - 1.44 (m, 1H), 1.43 (s, 9H), 1.23-1.08
319 (m, 2H). ^{13}C NMR (101 MHz, CDCl_3) δ 192.8, 158.9, 157.6, 154.8, 144.5, 142.9, 137.3, 133.5,
320 132.5, 130.7, 130.7, 125.0, 123.0, 109.0, 101.9, 79.7, 56.0, 55.8, 43.8 (br s), 43.2, 36.9, 31.8,
321 28.5. HRMS(ESI) $[\text{M} + \text{H}]^+$ calculated for $\text{C}_{27}\text{H}_{33}\text{N}_2\text{O}_5\text{S}$: 497.2105, found: 497.2101.

322 **tert-butyl 4-(((4-(aminomethyl)-2,7-dimethoxyacridin-9-yl)thio)methyl)piperidine-1-carbo-**
323 **xylate (9b)**. Under argon atmosphere, compound **9a** (55 mg, 0.11 mmol), ammonium acetate
324 (85 mg, 1.11 mmol), sodium cyanoborohydride (6.9 mg, 0.11 mmol), 4 mg of 4A molecular
325 sieves was dissolved in 3 mL of dry methanol at -5°C , then the reaction was stirred at the
326 same temperature overnight. After the removal of solid by filtration, the solvent was diluted
327 with methylene chloride, washed with brine, and then evaporated under vacuum. The residue
328 was purified by chromatography on a silica gel column (dichloromethane /methanol = 95/5) to
329 give compound **9b** (25 mg, 46%) as a light yellow solid. ^1H NMR (400 MHz, CDCl_3) δ 7.54 (d,
330 $J = 2.6$ Hz, 1H), 7.52 (d, $J = 2.5$ Hz, 1H), 7.30 (d, $J = 9.3$ Hz, 1H), 7.08 (d, $J = 2.3$ Hz, 1H), 6.90
331 (dd, $J = 9.3, 2.6$ Hz, 1H), 4.86 (s, 2H), 4.06 - 3.95 (m, 2H), 4.04 (s, 3H), 3.96 (s, 3H), 2.62 (d, J
332 = 6.7 Hz, 2H), 2.52 (t, $J = 12.0$ Hz, 2H), 1.85-1.70 (m, 2H), 1.41 (s, 9H), 1.35-1.30 (m, 1H),
333 1.18-1.04 (m, 2H). ^{13}C NMR (151 MHz, CDCl_3) δ 158.7, 157.2, 154.8, 142.5, 140.9, 137.2,
334 131.2 (overlapped), 130.0, 129.6, 126.0, 124.0, 103.2, 101.5, 79.7, 55.7 (overlapped), 50.4,
335 43.6 (br s), 43.1, 36.8, 31.8, 28.5. HRMS(ESI) $[\text{M} + \text{H}]^+$ calculated for $\text{C}_{27}\text{H}_{36}\text{N}_3\text{O}_4\text{S}$: 498.2421,
336 found: 498.2420.

337 **(2,7-dimethoxy-9-((piperidin-4-ylmethyl)thio)acridin-4-yl)methanamine (9)**. Compound **9b**
338 (13.5 mg, 0.027 mmol) was dissolved in 2 mL of 5% trifluoroacetic acid dichloromethane
339 solution and the mixture was allowed to react at room temperature for 2 h. The solvent was

340 then evaporated and the residue was dissolved with methanol, then purified by HPLC/MS on a
341 Waters Auto Purification LC/MS system (ACQUITY UPLC ® BEH C18 17 µm 2.1X50 mm
342 column) to afford **9** (6.3 mg, 45%) as a dark red foam. ¹H NMR (400 MHz, MeOD) δ 7.55 (dd, *J*
343 = 18.2, 2.6 Hz, 2H), 7.47 (d, *J* = 9.3 Hz, 1H), 7.17 (d, *J* = 2.5 Hz, 1H), 6.95 (dd, *J* = 9.3, 2.7 Hz,
344 1H), 4.14 - 4.07 (m, 3H), 4.02 (s, 3H), 2.86 - 2.72 (m, 4H), 2.07 - 1.98 (m, 3H), 1.57 - 1.31 (m,
345 4H). ¹³C NMR (151 MHz, MeOD) δ 160.2, 158.7, 143.5, 141.6, 137.9, 132.0, 131.7, 130.9,
346 130.4, 127.6, 125.2, 104.1, 102.5, 56.3, 56.2, 50.7, 44.8, 42.9, 35.6, 29.4. HRMS(ESI) [M + H]⁺
347 calculated for C₂₂H₂₈N₃O₂S: 398.1897, found: 398.1896.

348

349 **Appendix 1-scheme 7.** Synthesis route of C10.

350

351 **(9-chloro-2,7-dimethoxyacridin-4-yl)methanol (10a).** 0.28 mL of 1.0 M DIBAL-H solution in
352 toluene was added to a solution of **1c** (40 mg, 0.12 mmol) in 5 mL of dry dichloromethane at
353 -70 °C, then the reaction was stilled at the same temperature overnight. The reaction was
354 quenched by adding saturated potassium hydrogen tartrate solution, diluted with
355 dichloromethane, washed twice with brine, dried over anhydrous Na₂SO₄ and concentrated *in*
356 *vacuo*. The residue was purified by chromatography on a silica gel column (dichloromethane /
357 ethyl acetate = 90/10) to give compound **10a** (180 mg, 55%) as a light yellow solid. ¹H NMR
358 (400 MHz, CDCl₃) δ 8.00 (d, *J* = 9.3 Hz, 1H), 7.44 - 7.34 (m, 3H), 7.27 (s, 1H), 5.28 (br s, 1H),
359 5.19 (s, 2H), 4.02 (s, 3H), 4.00 (s, 3H). ¹³C NMR (101 MHz, CDCl₃) δ 158.6, 158.0, 143.4,
360 142.9, 140.1, 136.3, 131.5, 126.0, 125.6, 124.7, 122.5, 99.8, 99.2, 64.8, 55.8, 55.8. HRMS(ESI)
361 [M + H]⁺ calculated for C₁₆H₁₅ClNO₃: 304.0735, found: 304.0732.

362 **9-chloro-4-(difluoromethyl)-2,7-dimethoxyacridine (10b).** To a solution of compound **10a**
363 (30 mg, 0.10 mmol) in 3 mL of dichloromethane, Dess-Martin oxidant (60 mg, 0.14 mmol) was
364 added and the reaction was allowed to stir at room temperature for 2 h. The solution was
365 diluted with dichloromethane, washed twice with brine, dried over anhydrous Na₂SO₄ and
366 concentrated *in vacuo*. Under argon atmosphere, the crude product was dissolved in 2 mL of
367 dry dichloromethane, 0.1 mL of diethylaminosulfur trifluoride was added, and the mixture was
368 reacted at room temperature overnight. The reaction was quenched by sodium bicarbonate
369 aqueous solution, then diluted with dichloromethane, washed twice with brine, dried over
370 anhydrous Na₂SO₄ and concentrated *in vacuo*. The residue was purified by chromatography
371 on a silica gel column (petroleum ether / ethyl acetate = 5/1) to afford **10b** (7.4mg, 23%) as
372 white solid. ¹H NMR (400 MHz, CDCl₃) δ 8.08 (d, *J* = 9.3 Hz, 1H), 7.91 (t, *J* = 55.4 Hz, 1H),
373 7.76 - 7.73 (m, 1H), 7.59 (d, *J* = 2.6 Hz, 1H), 7.48 - 7.41 (m, 2H), 4.05 (s, 3H), 4.03 (s, 3H). ¹³C

374 NMR (151 MHz, CDCl₃) δ 158.9, 157.6, 144.3, 141.2 (t, *J* = 19Hz), 135.9, 133.8 (t, *J* = 85 Hz),
375 132.2, 125.9, 125.6, 125.0, 121.8 (t, *J* = 27 Hz), 112.1 (t, *J* = 942 Hz), 102.4, 99.7, 56.0, 55.9.
376 HRMS(ESI) [M + H]⁺ calculated for C₁₆H₁₃ClF₂NO₂: 324.0597, found: 324.0597.

377 **tert-butyl**

378 **4-(((4-(difluoromethyl)-2,7-dimethoxyacridin-9-yl)thio)methyl)piperidine-1-carboxylate**
379 **(10c)**. To a solution of **10b** (7.4 mg, 0.023 mmol) in 2 mL of anhydrous DMF, sodium
380 hydrosulfide hydrate powder (70%, 1.9 mg, 0.034 mmol) was added under argon atmosphere,
381 and the reaction was stirred at 60 °C overnight. 1-Boc-4-bromomethylpiperidine (12.7 mg,
382 0.0461 mmol) and potassium carbonate (15.8 mg, 0.114 mmol) were added into the slurry and
383 the reaction was allowed to react at room temperature overnight. The solvent was then
384 evaporated and the residue was dissolved with dichloromethane and washed with water. The
385 combined organic extracts were dried over anhydrous Na₂SO₄ and concentrated *in vacuo*. The
386 residue was purified by flash chromatography on a silica gel column (Petroleum ether / ethyl
387 acetate = 3/1) to give compound **10c** as a yellow solid (5.3 mg, 45%) and used for next step.

388 **4-(difluoromethyl)-2,7-dimethoxy-9-((piperidin-4-ylmethyl)thio)acridine (10)**. Compound
389 **10c** (5.3 mg, 0.010 mmol) was dissolved in 2 mL of 5% trifluoroacetic acid dichloromethane
390 solution and the mixture was allowed to react at room temperature for 2 h. The solvent was
391 then evaporated and the residue was dissolved with methanol, then purified by HPLC/MS on a
392 Waters Auto Purification LC/MS system (ACQUITY UPLC ® BEH C18 17 μm 2.1X50 mm
393 column) to afford **10** (3.8 mg, 70%) as a yellow solid. ¹H NMR (400 MHz, MeOD) δ 8.08 (d, *J* =
394 6.3 Hz, 1H), 7.93 (d, *J* = 2.8 Hz, 1H), 7.89 (t, *J* = 59.6Hz, 1H) 7.89 (d, *J* = 4.1 Hz, 1H), 7.68 (dd,
395 *J* = 2.8, 1.4 Hz, 1H), 7.47 (dd, *J* = 9.4, 2.8 Hz, 1H), 4.09-4.05(overlapped, m, 2H), 4.06 (s, 3H),
396 4.04 (s, 3H), 2.96 (d, *J* = 6.7 Hz, 2H), 2.90 - 2.78 (m, 2H), 2.11 (d, *J* = 14.4 Hz, 2H), 1.68 - 58
397 (m, 1H), 1.52 - 1.43 (m, 2H). ¹³C NMR (151 MHz, MeOD) δ 160.4, 158.9, 145.1, 142.0, 137.7,
398 135.5 (t, *J* = 85 Hz), 133.4, 131.7, 131.4, 125.6, 122.0 (t, *J* = 27 Hz), 113.3 (t, *J* = 937 Hz),
399 105.3, 102.7, 56.4, 56.2, 44.8, 43.0, 35.7, 29.5. HRMS(ESI) [M + H]⁺ calculated for
400 C₂₂H₂₅F₂N₂O₂S: 419.1599, found: 419.1587.

401

402 **Appendix 1-scheme 8.** General procedure of C11-C14 synthesis.

403

404 General procedures of synthesizing **1c'**/**1d**; To a suspension of compound **1b** (1.65 g, 6.05
405 mmol) in 200 mL of dry dichloromethane was slowly added 30 mL of boron tribromide, and the
406 mixture was reacted at 0 ° C for 2 h. Methanol was added to the reaction system to quench the
407 reaction, and the solvent was removed under reduced pressure. The crude product was
408 separated and purified with a silica gel column (dichloromethane / methanol = 92/8) to obtain

409 **1c'** (0.22 g, 14%) and the reported compound **1d** (0.80 g, 56%), with 0.70 g of the starting
410 material recovered. **1c'**: ¹H NMR (400 MHz, MeOD) δ 8.08 (dd, *J* = 9.4, 4.8 Hz, 2H), 7.64 (dd,
411 *J* = 7.6, 4.4 Hz, 4H), 4.07 (s, 3H). ¹³C NMR (151 MHz, MeOD) δ 160.8, 159.2, 129.2, 127.8,
412 127.2, 104.6, 101.3, 56.6. HRMS(ESI) [M + H]⁺ calculated for C₁₄H₁₁ClNO₂: 260.0473, found:
413 260.0471.

414

415 General procedures of synthesizing **11a,12a**: To a solution of **1c'** (94.5 mg, 0.364 mmol, 100
416 mol%) in 10 mL of anhydrous DMF, potassium carbonate (75.4 mg, 0.546 mmol, 150 mol%)
417 silver oxide (126.5 mg, 0.546 mmol, 150 mol%) and suitable bromides (0.546 mmol, 150 mol%)
418 was added. The reaction was allowed to react at 40 °C until full conversion. The reaction
419 solution was spin-dried under reduced pressure, and water / dichloromethane was separated.
420 The solvent was then evaporated and the residue was dissolved with dichloromethane and
421 washed with water. The combined organic extracts were dried over anhydrous Na₂SO₄ and
422 concentrated *in vacuo*. The residue was purified by chromatography on a silica gel column
423 (Petroleum ether / ethyl acetate = 9/1) to give the desired compound.

424 **2-(benzyloxy)-9-chloro-7-methoxyacridine (11a). Yield 100%**. ¹H NMR (400 MHz, CDCl₃) δ
425 8.08 (dd, *J* = 9.3, 7.6 Hz, 2H), 7.60 (d, *J* = 2.6 Hz, 1H), 7.56 - 7.35 (m, 8H), 5.27 (s, 2H), 4.02 (s,
426 3H). ¹³C NMR (101 MHz, CDCl₃) δ 158.4, 157.5, 144.4, 144.3, 136.2, 135.7, 131.6, 131.5,
427 128.3, 127.9, 128.0, 125.6, 125.6, 124.7, 124.6, 101.2, 99.9, 70.6, 55.8. HRMS(ESI) [M + H]⁺
428 calculated for C₂₁H₁₇ClNO₂: 350.0942, found: 350.0941.

429 **9-chloro-2-isopropoxy-7-methoxyacridine (12a). Yield 78%**. ¹H NMR (400 MHz, CDCl₃) δ
430 8.08 (dd, *J* = 9.4, 2.2 Hz, 2H), 7.51 (dd, *J* = 13.1, 2.7 Hz, 2H), 7.41 (ddd, *J* = 9.3, 7.5, 2.7 Hz,
431 2H), 4.85 (p, *J* = 6.0 Hz, 1H), 4.03 (s, 3H), 1.48 (d, *J* = 6.0 Hz, 6H). ¹³C NMR (151 MHz, CDCl₃)
432 δ 158.5, 156.7, 144.4, 144.3, 135.5, 131.7, 131.7, 125.8, 125.6, 125.5, 124.5, 101.8, 99.9,
433 70.5, 55.8, 22.0. HRMS(ESI) [M + H]⁺ calculated for C₁₇H₁₇ClNO₂: 302.0942, found: 302.0942.

434

435 General procedures of synthesizing **11-14**: To a solution of suitable acridine chloride (100
436 mol%) in 2 mL of anhydrous DMF, sodium hydrosulfide hydrate powder (150 mol%) was added
437 under argon atmosphere, and the reaction was stirred at 50 °C for 3 h. Suitable bromides (200
438 mol%) and potassium carbonate (500 mol%) were added into the slurry and the reaction was
439 allowed to react at room temperature overnight. The solvent was then evaporated and the
440 residue was dissolved with dichloromethane and washed with water. The combined organic
441 extracts were dried over anhydrous Na₂SO₄ and concentrated *in vacuo*. The residue was
442 dissolved in 2 mL of 5% trifluoroacetic acid dichloromethane solution and the mixture was

443 allowed to react at room temperature for 2h. The solvent was then evaporated and the residue
444 was dissolved with methanol, then purified by HPLC/MS on a Waters Auto Purification LC/MS
445 system (ACQUITY UPLC © BEH C18 17 µm 2.1X50 mm column) to afford desired product.

446 **3-((2-(benzyloxy)-7-methoxyacridin-9-yl)thio)propan-1-amine (11). Yield 9.6%. ¹H NMR**
447 (400 MHz, MeOD) δ 8.13 (dd, *J* = 12.1, 9.4 Hz, 2H), 8.01 (dd, *J* = 8.5, 2.6 Hz, 2H), 7.81 (dd, *J*
448 = 9.4, 2.7 Hz, 1H), 7.72 (dd, *J* = 9.4, 2.7 Hz, 1H), 7.60-7.34 (m, 5H), 5.42 (s, 2H), 4.08 (s, 3H),
449 3.00 (t, *J* = 7.6Hz, 2H), 2.85(t, *J* = 7.6Hz, 2H), 1.70 (quint, *J* = 7.6Hz, 2H). ¹³C NMR (151 MHz,
450 MeOD) δ 160.9, 159.6, 146.7, 138.5, 138.4, 137.6, 132.4, 132.0, 130.0, 129.9, 129.8, 129.4,
451 128.7, 126.4, 126.2, 105.7, 103.8, 71.8, 56.7, 39.4, 34.6, 29.4. HRMS(ESI) [M + H]⁺ calculated
452 for C₂₄H₂₅N₂O₂S: 405.1631, found: 405.1630.

453 **2-(benzyloxy)-7-methoxy-9-(piperidin-4-ylthio)acridine (12). 24%. ¹H NMR (400 MHz,**
454 MeOD) δ 7.99 (dd, *J* = 14.3, 9.4 Hz, 2H), 7.89 (d, *J* = 2.4 Hz, 2H), 7.58-7.50 (m, 3H), 7.47-7.40
455 (m, 3H), 7.39-7.33 (m, 1H), 5.36 (s, 2H), 4.01 (s, 3H), 3.26 (d, *J* = 13.1 Hz, 2H), 3.19 - 3.10 (m,
456 1H), 2.81 (t, *J* = 10.8 Hz, 2H), 1.86 (d, *J* = 11.5 Hz, 2H), 1.70 (td, *J* = 14.4, 3.7 Hz, 2H). ¹³C
457 NMR (101 MHz, MeOD) δ 159.9, 158.7, 144.7, 144.6, 138.3, 135.9, 132.6, 132.2, 131.8, 131.7,
458 129.8, 129.1, 128.3, 125.8, 125.6, 105.0, 103.3, 71.2, 56.2, 45.5, 45.1, 32.0. HRMS(ESI) [M +
459 H]⁺ calculated for C₂₆H₂₇N₂O₂S: 431.1788, found: 431.1781.

460 **2-(benzyloxy)-7-methoxy-9-((piperidin-4-ylmethyl)thio)acridine (13). 19%. ¹H NMR (400**
461 MHz, MeOD) δ 8.01 - 7.89 (m, 2H), 7.86-7.75 (m, 2H), 7.58 - 7.31 (m, 7H), 5.32 (s, 2H), 3.99 (s,
462 3H), 3.27 (d, *J* = 13.1Hz, 2H), 2.75 (t, *J* = 12.5 Hz, 2H), 2.68 (d, *J* = 6.4 Hz, 2H), 1.94 (d, *J* =
463 13.2 Hz, 2H), 1.44 - 1.28 (m, 3H). ¹³C NMR (151 MHz, MeOD) δ 160.0, 158.7, 144.7, 144.7,
464 138.6, 138.3, 132.0, 131.9, 131.7, 131.3, 129.8, 129.2, 125.8, 125.6, 104.9, 103.0, 71.4, 56.2,
465 45.1, 43.0, 36.0, 30.0. HRMS(ESI) [M + H]⁺ calculated for C₂₇H₂₉N₂O₂S: 445.1944, found:
466 445.1945.

467 **2-isopropoxy-7-methoxy-9-((piperidin-4-ylmethyl)thio)acridine (14). 26%. ¹H NMR (400**
468 MHz, MeOD) δ 8.15 (dd, *J* = 9.4, 3.6 Hz, 2H), 8.06 (t, *J* = 3.0 Hz, 2H), 7.71 (td, *J* = 9.3, 2.6 Hz,
469 2H), 4.98 - 4.92 (m, 1H), 4.09 (s, 3H), 3.36 (d, *J* = 12.9 Hz, 2H), 3.11 (d, *J* = 6.8 Hz, 2H), 2.88 (t,
470 *J* = 11.9 Hz, 2H), 2.12 (d, *J* = 14.0 Hz, 2H), 1.79 - 1.69 (m, 1H), 1.54-1.41 (overlapped, m, 2H),
471 1.51 (s, 3H), 1.49 (s, 3H). ¹³C NMR (151 MHz, MeOD) δ 160.8, 158.9, 139.5, 139.3, 132.1,
472 129.9, 129.0, 127.4, 127.3, 105.6, 103.7, 72.2, 56.6, 44.8, 43.8, 36.0, 29.4, 22.0. HRMS(ESI)
473 [M + H]⁺ calculated for C₂₃H₂₉N₂O₂S: 397.1944, found: 397.1943.

474

475

Appendix 1-scheme 9. Synthesis route of C15.

476

477 **2,7-bis(benzyloxy)-9-chloroacridine (15a)**. To a solution of 1d (94.5 mg, 0.364 mmol) in 10
478 mL of anhydrous DMF, potassium carbonate (150.8 mg, 1.092 mmol) silver oxide (253.0 mg,
479 1.092 mmol) and benzyl bromide (100 μ l) was added. The reaction was allowed to react at 40
480 $^{\circ}$ C until full conversion. The reaction solution was spin-dried under reduced pressure, and
481 water / dichloromethane was separated. The solvent was then evaporated and the residue
482 was dissolved with dichloromethane and washed with water. The combined organic extracts
483 were dried over anhydrous Na_2SO_4 and concentrated in vacuo. The residue was purified by
484 chromatography on a silica gel column (Petroleum ether / ethyl acetate = 9/1) to give 15a
485 (163.9 mg, quant.) as a yellow solid. ^1H NMR (400 MHz, CDCl_3) δ 8.10 (d, J = 9.4 Hz, 2H),
486 7.62 (d, J = 2.7 Hz, 2H), 7.57 - 7.36 (m, 12H), 5.28 (s, 4H). ^{13}C NMR (101 MHz, CDCl_3) δ 157.6,
487 144.5, 136.3, 135.9, 131.8, 128.9, 128.5, 128.0, 125.6, 124.8, 101.2, 70.6. HRMS(ESI) [$\text{M} +$
488 H] $^+$ calculated for $\text{C}_{27}\text{H}_{21}\text{ClNO}_2$: 426.1255, found: 426.1255.

489 **2,7-bis(benzyloxy)-9-((piperidin-4-ylmethyl)thio)acridine (15)**. To a solution of **15a** (20 mg,
490 0.047 mmol) in 2 mL of anhydrous DMF, sodium hydrosulfide hydrate powder (70%, 5.6 mg,
491 0.070 mmol) was added under argon atmosphere, and the reaction was stirred at 50 $^{\circ}$ C for 3 h.
492 *tert*-butyl 4-(bromomethyl)piperidine-1-carboxylate (26.1 mg, 0.094 mmol) and potassium
493 carbonate (32.4 mg, 0.235 mol) were added into the slurry and the reaction was allowed to
494 react at room temperature overnight. The solvent was then evaporated and the residue was
495 dissolved with dichloromethane and washed with water. The combined organic extracts were
496 dried over anhydrous Na_2SO_4 and concentrated *in vacuo*. The residue was dissolved in 2 mL
497 of 5% trifluoroacetic acid dichloromethane solution and the mixture was allowed to react at
498 room temperature for 2h. The solvent was then evaporated and the residue was dissolved with
499 methanol, then purified by HPLC/MS on a Waters Auto Purification LC/MS system (ACQUITY
500 UPLC C_{18} BEH C_{18} 17 μm 2.1X50 mm column) to afford **15** (10.8 mg, 36%). ^1H NMR (400 MHz,
501 MeOD) δ 8.09 (d, J = 9.4 Hz, 2H), 7.85 (d, J = 2.5 Hz, 2H), 7.73 (dd, J = 9.4, 2.6 Hz, 2H), 7.43
502 (ddd, J = 28.6, 28.0, 7.3 Hz, 10H), 5.37 (s, 4H), 3.22 (d, J = 12.8 Hz, 2H), 2.73 - 2.62 (m, 4H),
503 1.75 (d, J = 13.6 Hz, 2H), 1.41 - 1.31 (m, 1H), 1.30 - 1.16 (m, 2H). ^{13}C NMR (101 MHz, MeOD)
504 δ 159.4, 137.6, 137.6, 131.5, 130.3, 129.9, 129.4, 128.5, 125.8, 105.5, 71.8, 44.6, 43.6, 35.8,
505 29.1. HRMS(ESI) [$\text{M} + \text{H}$] $^+$ calculated for $\text{C}_{33}\text{H}_{33}\text{N}_2\text{O}_2\text{S}$: 521.2257, found: 521.2258.

506

507 **Appendix 1-scheme 10**. Synthesis route of C20.

508

509 ***tert*-butyl-(S)-3-(((4-(bromomethyl)-2,7-dimethoxyacridin-9-yl)thio)methyl)pyrrolidine-1-c**
510 **arboxylate (20a)**. **17b** (13 mg, 0.027mmol), Triphenylphosphine (10.6 mg, 0.040 mmol),

511 N-bromosuccinimide (7.2 mg, 0.040 mmol) was dissolved in 1 mL of anhydrous
512 tetrahydrofuran and the reaction was stirred at room temperature for 30 min. The reaction was
513 concentrated *in vacuo* and the residue was purified by chromatography on a silica gel column
514 (pure dichloromethane) to give compound **20a** (9.6 mg, 65%) as a yellow solid. ¹H NMR (400
515 MHz, CDCl₃) δ 8.16 (d, *J* = 9.3 Hz, 1H), 7.94 (s, 1H), 7.91 (s, 1H), 7.59 (s, 1H), 7.43 (d, *J* = 9.2
516 Hz, 1H), 5.31 (d, *J* = 8.9 Hz, 2H), 4.05 (s, 3H), 4.03 (s, 3H), 3.64 - 3.33 (m, 2H), 3.30 - 2.84 (m,
517 4H), 2.12 (br s, 1H), 2.01 - 1.92 (m, 1H), 1.67-1.60 (m, 1H), 1.43 (s, 9H). ¹³C NMR (101 MHz,
518 CDCl₃) δ 158.8, 157.8, 154.6, 143.8, 141.7, 138.8, 135.8, 132.9, 130.8, 130.7, 124.7, 124.1,
519 102.9, 101.8, 79.4, 55.8, 51.0 (d, *J* = 108Hz), 50.9, 45.2 (d, *J* = 112Hz), 39.5, 31.4, 30.7, 29.7,
520 28.6. HRMS(ESI) [M + H]⁺ calculated for C₂₆H₃₂BrN₂O₄S: 547.1261, found: 547.1255.

521 **(S)-2-((2,7-dimethoxy-9-((pyrrolidin-3-ylmethyl)thio)acridin-4-yl)methyl)guanidine (20).**

522 Under argon atmosphere, N, N'-di-Boc-guanidine (3.1 mg, 12.1 μmol) and potassium
523 carbonate (1.7 mg, 12.1 μmol) was added into the solution of **20a** (5.5 mg, 10.0 μmol) in 1 mL
524 of anhydrous DMF. The reaction was performed at 50 °C for 2.5 h. The reaction was
525 concentrated *in vacuo* and the residue was dissolved in 4 mL of dichloromethane containing 5%
526 trifluoroacetic acid and reacted at room temperature for 2 h. The solvent was then evaporated
527 and the residue was dissolved with methanol, then purified by HPLC/MS on a Waters Auto
528 Purification LC/MS system (ACQUITY UPLC® BEH C18 17 μm 2.1X50 mm column) to give
529 compound **20** (2.0 mg, 27%). ¹H NMR (400 MHz, MeOD) δ 8.11 (d, *J* = 9.4 Hz, 1H), 7.96 (d, *J*
530 = 2.7 Hz, 1H), 7.94 (d, *J* = 2.7 Hz, 1H), 7.52 - 7.48 (m, 2H), 5.04 (s, 2H), 4.07 (s, 3H), 4.06 (s,
531 3H), 3.39 - 3.32 (m, 2H), 3.19 - 2.98 (m, 4H), 2.28 (hept, *J* = 7.6 Hz, 1H), 2.20 - 2.09 (m, 1H),
532 1.83 - 1.73 (m, 1H). ¹³C NMR (151 MHz, MeOD) δ 160.5, 159.6, 159.0, 144.3, 142.9, 138.5,
533 137.4, 132.8, 132.1, 131.8, 125.7, 125.1, 103.2, 102.8, 56.3, 50.8, 46.2, 43.1, 40.0, 39.4, 31.0.
534 HRMS(ESI) [M + H]⁺ calculated for C₂₂H₂₈N₅O₂S: 426.1958, found: 426.1946.

535
536

Appendix 1-scheme 11. Synthesis route of C21.

537 **ethyl 5-((4-methoxyphenyl)amino)-2-(methylthio)thiazole-4-carboxylate (21a).** Under
538 argon atmosphere, a solution of a known compound 23 (1.04 g, 5.02 mmol) in 4 mL of
539 anhydrous tetrahydrofuran was added dropwise to a solution of potassium tert-butoxide (0.79
540 g, 7.02 mmol) in THF at -78 °C, followed by a solution of compound 24 (0.83 g, 5.02 mmol) in 4
541 mL of anhydrous tetrahydrofuran. The reaction was performed at -78 °C for 0.5 h and then
542 slowly warmed up to room temperature and reacted overnight. The reaction was quenched by
543 adding saturated ammonium chloride, diluted with dichloromethane, washed twice with brine,
544 dried over anhydrous Na₂SO₄ and concentrated *in vacuo*. The residue was purified by
545 chromatography on a silica gel column (pure dichloromethane) to give compound **21a** (0.29 g,

546 18%) as a light yellow solid. ¹H NMR (400 MHz, CDCl₃) δ 9.39 (s, 1H), 7.17 - 7.11 (m, 2H),
547 6.91 - 6.83 (m, 2H), 4.38 (q, *J* = 7.1 Hz, 2H), 3.77 (s, 3H), 2.57 (s, 3H), 1.39(t, *J* = 7.1 Hz, 3H).
548 ¹³C NMR (101 MHz, CDCl₃) δ 164.7, 158.5, 156.8, 145.4, 134.2, 121.9, 121.5, 114.9, 60.8,
549 55.5, 17.7, 14.6. HRMS(ESI) [M + H]⁺ calculated for C₁₄H₁₇N₂O₃S₂: 325.0675, found:
550 325.0673.

551 **9-chloro-7-methoxy-2-(methylthio)thiazolo[5,4-b]quinolone (21b)**. Compound **21a** (198
552 mg, 0.61 mmol) was added in a sealed tube, and 5 mL of phosphorus oxychloride was added
553 under argon atmosphere. The reaction was heated at 130 °C overnight. The resulting slurry
554 was poured onto ice with vigorous stirring to make full quenching. The mixture was diluted with
555 dichloromethane, washed twice with brine, dried over anhydrous Na₂SO₄ and concentrated *in*
556 *vacuo*. The residue was purified by chromatography on a silica gel column (pure
557 dichloromethane) to give compound **21b** (74 mg, 41%) as a light yellow solid. ¹H NMR (400
558 MHz, CDCl₃) δ 7.97 (d, *J* = 9.2 Hz, 1H), 7.55 (d, *J* = 2.8 Hz, 1H), 7.40 (dd, *J* = 9.2, 2.8 Hz, 1H),
559 4.01 (s, 3H), 2.88 (s, 3H). ¹³C NMR (101 MHz, CDCl₃) δ 172.1, 158.5, 157.6, 142.6, 142.4,
560 130.2, 129.5, 126.2, 123.1, 101.8, 55.8, 15.5. HRMS(ESI) [M + H]⁺ calculated for
561 C₁₂H₁₀ClN₂OS₂: 296.9918, found: 296.9917.

562 **tert-butyl-4-(((7-methoxy-2-(methylthio)thiazolo[5,4-b]quinolin-9-yl)thio)methyl)piperidin**
563 **e-1-carboxylate (21c)**. To a solution of **21b** (0.020 g, 0.067 mmol) in 5 mL of anhydrous DMF,
564 sodium hydrosulfide hydrate powder (70%, 10.8 mg, 0.135 mmol) was added under argon
565 atmosphere and the reaction was stirred at 50 °C for 2 h until full conversion.
566 1-Boc-4-bromomethylpiperidine (37.5 mg, 0.135 mmol) and potassium carbonate (27.9 mg,
567 0.202 mmol) were added into the slurry and the reaction was allowed to react at room
568 temperature overnight. The solvent was then evaporated and the residue was dissolved with
569 dichloromethane and washed with water. The combined organic extracts were dried over
570 anhydrous Na₂SO₄ and concentrated *in vacuo*. The residue was purified by chromatography
571 on a silica gel column (dichloromethane / ethyl acetate = 95/5) to give compound **21c** (14.9 mg,
572 45%) as a light yellow solid. ¹H NMR (400 MHz, CDCl₃) δ 7.94 (d, *J* = 9.2 Hz, 1H), 7.85 (d, *J* =
573 2.8 Hz, 1H), 7.38 (dd, *J* = 9.2, 2.8 Hz, 1H), 4.12 - 4.01 (m, 2H), 4.00 (s, 3H), 3.47 (d, *J* = 6.9 Hz,
574 2H), 2.84 (s, 3H), 2.61 (t, *J* = 12.7 Hz, 2H), 1.86 (d, *J* = 13.1 Hz, 2H), 1.65 - 1.57 (m, 1H), 1.44
575 (s, 9H), 1.23 - 1.14 (m, 2H). ¹³C NMR (101 MHz, CDCl₃) δ 169.9, 158.1, 158.0, 154.9, 145.1,
576 141.7, 132.9, 130.3, 128.7, 122.4, 103.5, 79.6, 55.8, 43.9 (br s), 41.1, 36.9, 31.7, 28.6, 15.5.
577 HRMS(ESI) [M + H]⁺ calculated for C₂₃H₃₀N₃O₃S₃: 492.1444, found: 492.1435.

578 **7-methoxy-2-(methylthio)-9-((piperidin-4-ylmethyl)thio)thiazolo[5,4-b]quinolone (21)**.
579 **21c** (14.9 mg, 0.030 mmol) was dissolved in 2 mL of 5% trifluoroacetic acid dichloromethane

580 solution and the mixture was allowed to react at room temperature for 2 h. The solvent was
581 then evaporated and the residue was dissolved with methanol, then purified by HPLC/MS on a
582 Waters Auto Purification LC/MS system (ACQUITY UPLC ® BEH C18 17 µm 2.1X50 mm
583 column) to afford **21** (14.7 mg, 96%). ¹H NMR (400 MHz, MeOD) δ 7.85 (d, *J* = 9.2 Hz, 1H),
584 7.81 (d, *J* = 2.7 Hz, 1H), 7.40 (dd, *J* = 9.2, 2.8 Hz, 1H), 3.98 (s, 3H), 3.62 (d, *J* = 6.9 Hz, 2H),
585 3.37 - 3.32 (m, 2H), 2.88 (s, 3H), 2.91 - 2.83 (overlapped, m, 2H), 2.12 (d, *J* = 13.8 Hz, 2H),
586 1.82-1.70 (m, 1H), 1.55-1.42 (m, 2H). ¹³C NMR (151 MHz, MeOD) δ 172.0, 159.6, 158.8,
587 146.1, 142.4, 133.9, 130.7, 129.6, 123.5, 104.3, 97.5, 56.2, 44.9, 40.7, 35.7, 29.3, 15.7.
588 HRMS(ESI) [M + H]⁺ calculated for C₁₈H₂₂N₃OS₃: 392.0920, found: 392.0920.

589

590

Appendix 1-scheme 12. Synthesis route of C22.

591

592 **Ethyl-5-((4-methoxy-2-(methoxycarbonyl)phenyl)amino)-2-(methylthio)thiazole-4-carbox**
593 **ylate (22a).** Under argon atmosphere, a solution of a known compound 23 (150 mg, 0.73
594 mmol) in 1 mL of anhydrous tetrahydrofuran was added dropwise to a solution of potassium
595 tert-butoxide (112 mg, 0.92 mmol) in 8 mL of anhydrous tetrahydrofuran at -60 °C, followed by
596 a solution of known compound 24' (150 mg, 0.66 mmol) in 1 mL of anhydrous tetrahydrofuran.
597 The reaction was performed at -60 °C for 1.5 h and then slowly warmed up to room
598 temperature and reacted overnight. The reaction was quenched by adding saturated
599 ammonium chloride, diluted with dichloromethane, washed twice with brine, dried over
600 anhydrous Na₂SO₄ and concentrated *in vacuo*. The residue was purified by chromatography
601 on a silica gel column (pure dichloromethane) to give compound **22a** (69.2 mg, 28%) as a
602 yellow solid. ¹H NMR (400 MHz, CDCl₃) δ 11.61 (s, 1H), 7.58 - 7.50 (m, 2H), 7.11 (dd, *J* = 9.0,
603 3.2 Hz, 1H), 4.49 (q, *J* = 7.1 Hz, 2H), 3.97 (s, 3H), 3.83 (s, 3H), 2.64 (s, 3H), 1.42 (t, *J* = 7.1 Hz,
604 3H). ¹³C NMR (101 MHz, CDCl₃) δ 167.1, 163.9, 154.3, 153.6, 147.0, 137.0, 125.6, 121.0,
605 117.9, 117.4, 115.8, 61.1, 55.9, 52.7, 17.7, 14.7. HRMS(ESI) [M + H]⁺ calculated for
606 C₁₆H₁₉N₂O₅S₂: 383.0730, found: 383.0729.

607 **Methyl-9-chloro-7-methoxy-2-(methylthio)thiazolo[5,4-b]quinoline-5-carboxylate (22b).**

608 Compound **22a** (50 mg, 0.14 mmol) was added in a sealed tube, and 1 mL of phosphorus
609 oxychloride was added under argon atmosphere. The reaction was heated at 130 °C overnight.
610 The resulting slurry was poured onto ice with vigorous stirring to make full quenching. The
611 mixture was diluted with dichloromethane, washed twice with brine, dried over anhydrous
612 Na₂SO₄ and concentrated *in vacuo*. The residue was purified by chromatography on a silica
613 gel column (pure dichloromethane) to give compound **22b** (15 mg, 32%) as a light yellow solid.

614 ¹H NMR (400 MHz, CDCl₃) δ 7.69 (s, 2H), 4.05 (s, 3H), 4.02 (s, 3H), 2.88 (s, 3H). ¹³C NMR
615 (101 MHz, CDCl₃) δ 173.4, 167.5, 157.2, 142.6, 139.3, 132.7, 129.4, 126.6, 123.5, 105.1, 56.1,
616 53.0, 15.5. HRMS(ESI) [M + H]⁺ calculated for C₁₄H₁₂ClN₂O₃S₂: 354.9972, found: 354.9973.

617 **Methyl-9-(((1-(tert-butoxycarbonyl)piperidin-4-yl)methyl)thio)-7-methoxy-2-(methylthio)t**
618 **hiazolo[5,4-b]quinoline-5-carboxylate (22c)**. To a solution of **22b** (15 mg, 0.042 mmol) in 2
619 mL of anhydrous DMF, sodium hydrosulfide hydrate powder (70%, 6.7 mg, 0.084 mmol) was
620 added under argon atmosphere, and the reaction was stirred at 50 °C for 2 h until full
621 conversion of **1c**. 1-Boc-4-bromomethylpiperidine (29.3 mg, 0.105 mmol) and potassium
622 carbonate (17.4 mg, 0.126 mmol) were added into the slurry and the reaction was allowed to
623 react at room temperature overnight. The solvent was then evaporated and the residue was
624 dissolved with dichloromethane and washed with water. The combined organic extracts were
625 dried over anhydrous Na₂SO₄ and concentrated *in vacuo*. The residue was purified by
626 chromatography on a silica gel column (dichloromethane / ethyl acetate = 95/5) to give
627 compound **22c** (16.2 mg, 70%) as a light yellow solid. ¹H NMR (400 MHz, CDCl₃) δ 8.02 (d, *J* =
628 2.9 Hz, 1H), 7.65 (d, *J* = 2.8 Hz, 1H), 4.12-3.96 (overlapped, m, 2H), 4.04 (s, 3H), 4.00 (s, 3H),
629 3.44 (d, *J* = 6.9 Hz, 2H), 2.84 (s, 3H), 2.58 (t, *J* = 12.6 Hz, 2H), 1.82 (d, *J* = 12.9 Hz, 2H), 1.61 -
630 1.52 (m, 1H), 1.44 (s, 9H), 1.23 - 1.13 (m, 2H). ¹³C NMR (151 MHz, CDCl₃) δ 171.2, 167.8,
631 158.8, 156.6, 154.8, 145.2, 138.5, 132.7, 132.6, 129.1, 122.5, 106.7, 79.4, 55.9, 52.8,
632 44.3-43.2 (m), 41.1, 36.7, 31.5, 28.4, 15.4. HRMS(ESI) [M + H]⁺ calculated for C₂₅H₃₂N₃O₅S₃:
633 550.1499, found: 550.1492.

634 **(7-methoxy-2-(methylthio)-9-((piperidin-4-ylmethyl)thio)thiazolo[5,4-b]quinolin-5-yl)met**
635 **haol (22)**. 87 μl of 1.0 M DIBAL-H solution in toluene was added to a solution of **22c** (16.0 mg,
636 0.029 mmol) in 1 mL of dry dichloromethane at -60 °C, and the reaction was slowly warmed to
637 room temperature and reacted overnight. The reaction was quenched by adding saturated
638 potassium hydrogen tartrate solution, diluted with dichloromethane, washed twice with brine,
639 dried over anhydrous Na₂SO₄ and concentrated *in vacuo*. The residue was dissolved in 4 mL
640 of 5% trifluoroacetic acid dichloromethane solution and the mixture was allowed to react at
641 room temperature for 2 h. The solvent was then evaporated and the residue was dissolved
642 with methanol, then purified by HPLC/MS on a Waters Auto Purification LC/MS system
643 (ACQUITY UPLC ® BEH C18 17 μm 2.1X50 mm column) to afford **22** (5.3 mg, 34%). ¹H NMR
644 (400 MHz, MeOD) δ 7.78 (d, *J* = 2.8 Hz, 1H), 7.52 (d, *J* = 2.7 Hz, 1H), 5.20 (s, 2H), 3.98 (s, 3H),
645 3.58 (d, *J* = 6.9 Hz, 2H), 3.37-3.32 (m, 2H), 2.88 (s, 3H), 2.88 - 2.81 (m, 2H), 2.15 - 2.08 (m,
646 2H), 1.78 - 1.69 (m, 1H), 1.55 - 1.41 (m, 2H). ¹³C NMR (151 MHz, MeOD) δ 172.2, 159.5,
647 157.9, 146.2, 142.2, 140.4, 133.5, 129.8, 120.6, 102.9, 61.7, 56.0, 44.9, 40.8, 35.7, 29.3, 15.6.

648 HRMS(ESI) $[M + H]^+$ calculated for $C_{19}H_{24}N_3O_2S_3$: 422.1025, found: 422.1013.
649
650
651
652

Key Resources Table				
Reagent type (species) or resource	Designation	Source or reference	Identifiers	Additional information
cell line (<i>Homo-sapiens</i>)	HEK293T	American Type Culture Collection	Cat#: CRL-3216, RRID: CVCL_0063	
cell line (<i>Homo-sapiens</i>)	HEK293A	Thermo Fisher	Cat#: R70507	
cell line (<i>Homo-sapiens</i>)	HEK293	American Type Culture Collection	Cat#: CRL-1573, RRID: CVCL_0045	
cell line (<i>Homo-sapiens</i>)	U266	American Type Culture Collection	Cat#: TIB-196, RRID: CVCL_0566	
cell line (<i>Homo-sapiens</i>)	HCT116	China Infrastructure of Cell Line Resources	Cat#: 1101HUM-PU MC000158	
antibody	anti-4EPB1(Rabbit polyclonal)	Cell Signaling Technology	Cat#: 9644, RRID: AB_2097841	WB (1:1000)
antibody	anti-phosphorylated 4E-BP1 (Thr37/46) (Rabbit monoclonal)	Cell Signaling Technology	Cat#: 2855, RRID: AB_560835	WB (1:1000)

antibody	anti-phosphorylated 4E-BP1 (Ser65) (Rabbit monoclonal)	Cell Signaling Technology	Cat#: 9451, RRID: AB_330947	WB (1:1000)
antibody	anti-phosphorylated 4E-BP1 (Thr70) (Rabbit monoclonal)	Cell Signaling Technology	Cat#: 13396, RRID: AB_2798206	WB (1:1000)
antibody	anti-HA (Rabbit monoclonal)	Cell Signaling Technology	Cat#: 3724, RRID: AB_1549585	WB (1:1000)
antibody	anti-FLAG (Mouse monoclonal)	Sigma-Aldrich	Cat#: F3165, RRID: AB_259529	WB (1:5000)
antibody	anti-FLAG (Rabbit monoclonal)	Abcam	Cat#: ab205606	WB (1:5000)
antibody	anti-GFP (Rabbit monoclonal)	Abcam	Cat#: ab183734	WB (1:5000)
antibody	anti-GFP (Mouse monoclonal)	Proteintech	Cat#: 66002-1-Ig, RRID: AB_11182611	WB (1:5000)
antibody	anti-RPT3 (Rabbit polyclonal)	Thermo Fisher Scientific	Cat#: A303-849A-M, RRID: AB_2781512	WB (1:1000)
antibody	anti-pThr25 (Rabbit polyclonal)	(Guo et al., 2016)	N/A	WB (1:500)
antibody	anti-GAPDH (Mouse monoclonal)	Transgene Biotechnology	Cat#: HC301-01	WB (1:5000)

antibody	anti-mouse-IgG -HRP (Goat monoclonal)	Transgene Biotechnolo gy	Cat#: HS201-01	WB (1:5000)
antibody	anti-rabbit-IgG- HRP (Goat monoclonal)	Transgene Biotechnolo gy	Cat#: HS101-01	WB (1:5000)
recombinant DNA reagent	GCaMP6f (plasmid)	Xiaowei Chen Lab (Peking University, China)	N/A	
recombinant DNA reagent	pEGFP-Orai1 (plasmid)	Xiaowei Chen Lab (Peking University, China)	N/A	
recombinant DNA reagent	mCherry-STIM 1 (plasmid)	Xiaowei Chen Lab (Peking University, China)	N/A	
recombinant DNA reagent	pLL3.7-DYRK2 -shRNA (plasmid)	Xing Guo Lab (Zhejiang University, China)	(Guo et al., 2016)	
recombinant DNA reagent	Flag-STIM1 (plasmid)	This paper	N/A	This plasmid was generated by modification of mCherry-STI M1 plasmid.
recombinant DNA reagent	pQlinkHx- DYRK2 ²⁰⁸⁻⁵⁵² (plasmid)	This paper	N/A	This plasmid was generated by modification of pEGFP-DYR

				K2 plasmid.
recombinant DNA reagent	pQlinkGx-STIM1 ^{235-END} (plasmid)	This paper	N/A	This plasmid was generated by modification of mCherry-STIM1 plasmid.
recombinant DNA reagent	HA-mcherry-DYRK2 (plasmid)	This paper	N/A	This plasmid was generated by modification of pEGFP-DYRK2 plasmid.
recombinant DNA reagent	HA-mcherry-DYRK2-D275N (plasmid)	This paper	N/A	This plasmid was generated by modification of pEGFP-DYRK2-D275N plasmid.
peptide, recombinant protein	Flag peptide: DYKDDDDK	Smart Lifesciences	Cat#: SLR01002	
peptide, recombinant protein	GST-MARK3 protein	Carna Biosciences	Cat#: 02-122	
peptide, recombinant protein	GST-Haspin protein	Carna Biosciences	Cat#: 05-111	
strain, strain background (<i>Escherichia coli</i>)	BL21(DE3)	Sigma-Aldrich	Cat#: CMC0016	Electrocompetent cells

chemical compound, drug	AKTi-1/2	Selleck	Cat#: S80837	
chemical compound, drug	PD0325901	Aladdin	Cat#: P125494	
chemical compound, drug	Thapsigargin	Aladdin	Cat#: T135258	
chemical compound, drug	X-tremeGENE 9 DNA Transfection Reagent	Roche	Cat#: 19129300	
chemical compound, drug	Lipofectamine 2000	Thermo Fisher Scientific	Cat#: 11668019	
chemical compound, drug	protease inhibitor mixture	Roche	Cat#: 11697498001	
chemical compound, drug	phosphatase inhibitor mixtures	Roche	Cat#: 04906837001	
chemical compound, drug	Ionomycin	Sigma-Aldrich	CAS: 56092-81-0	
chemical compound, drug	2-Bromo-5-methoxybenzoic acid	J&K Scientific	CAS: 22921-68-2	
chemical compound, drug	2-Amino-5-Methoxybenzoic acid	Energy Chemicals	CAS: 6705-03-9	
chemical compound, drug	p-Anisidine	J&K Scientific	CAS: 104-94-9	

chemical compound, drug	1-Boc-4-Bromomethylpiperidine	Bide Pharmatech	CAS: 158407-04-6	
chemical compound, drug	(S)-1-Boc-3-(Bromomethyl)pyrrolidine	Bide Pharmatech	CAS: 1067230-64-1	
chemical compound, drug	(R)-1-Boc-3-(Bromomethyl)pyrrolidine	Bide Pharmatech Ltd	CAS: 1067230-65-2	
chemical compound, drug	4-Methoxyphenyl isothiocyanate	Energy Chemicals	CAS: 2284-20-0	
chemical compound, drug	tert-butyl 4-bromopiperidine-1-carboxylate	J&K Scientific	CAS: 180695-79-8	
chemical compound, drug	DIBAL-H	Alfa Aesar Chemicals	CAS: 1191-15-7	
chemical compound, drug	Dess-Martin	Alfa Aesar Chemicals	CAS: 87413-09-0	
chemical compound, drug	Boron Tribromide	Sigma-Aldrich	CAS: 10294-33-4	
chemical compound, drug	Urea	Sigma-Aldrich	CAS: 57-13-6	
chemical compound, drug	2-Amino-2-(hydroxymethyl)-1,3-propanediol	Sigma-Aldrich	CAS: 77-86-1	
chemical compound, drug	Sodium orthovanadate	NEW ENGLAND BioLabs	Cat#: P0758S	

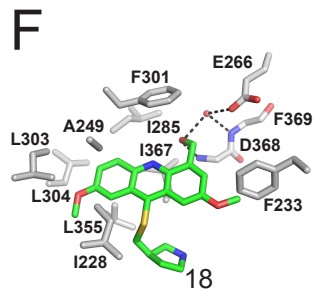
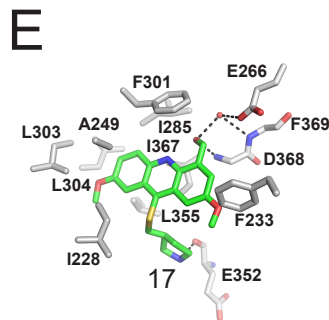
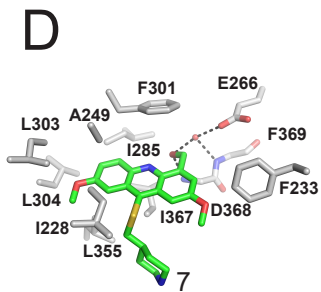
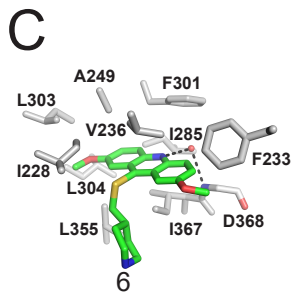
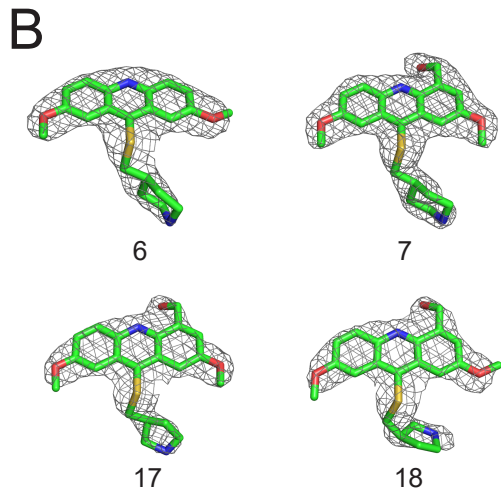
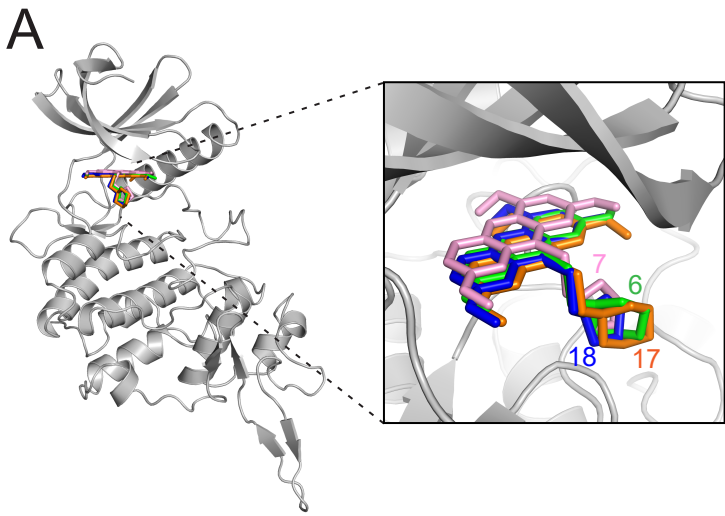
commercial assay or kit	Ni Sepharose 6 Fast Flow	GE healthcare	Cat#: 17531803	
commercial assay or kit	Glutathione Sepharose 4B beads	GE healthcare	Cat#: 17-0756-05	
commercial assay or kit	ANTI-FLAG [®] M2 Affinity Gel	Sigma-Aldrich	Cat#: A2220	
commercial assay or kit	Superdex 200 Increase 10/300 GL	GE healthcare	Cat#: 28990944	
commercial assay or kit	BCA Protein Assay Kit Pierce	Thermo-Pierce	Cat#: 23227	
commercial assay or kit	ADP-Glo [™] kinase assay	Promega	Cat#: V9102	
software, algorithm	Chembiodraw	http://www.perkinelmer.co.uk/category/chemdraw	RRID:SCR_016768	v13
software, algorithm	GraphPad Prism	GraphPad Software	RRID:SCR_002798	v8.4.0
software, algorithm	ImageJ (Fiji)	(Schindelin et al., 2012)	RRID:SCR_003070	
software, algorithm	Matlab	https://ww2.mathworks.com/products/matlab.html	N/A	v2014a
software, algorithm	HKL-2000	HKL Research	RRID:SCR_015547	

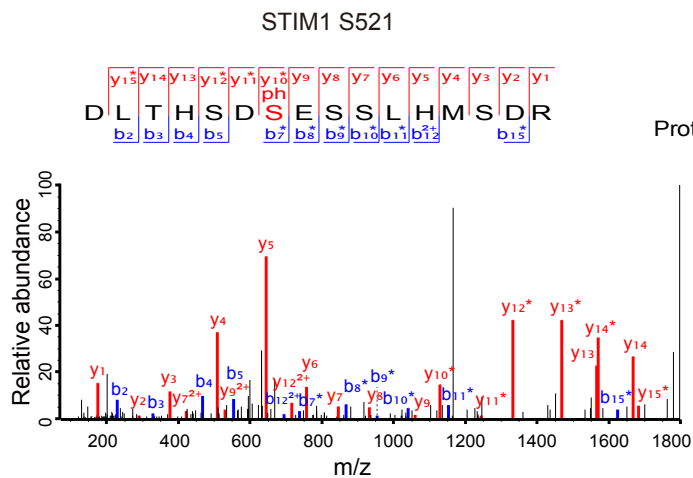
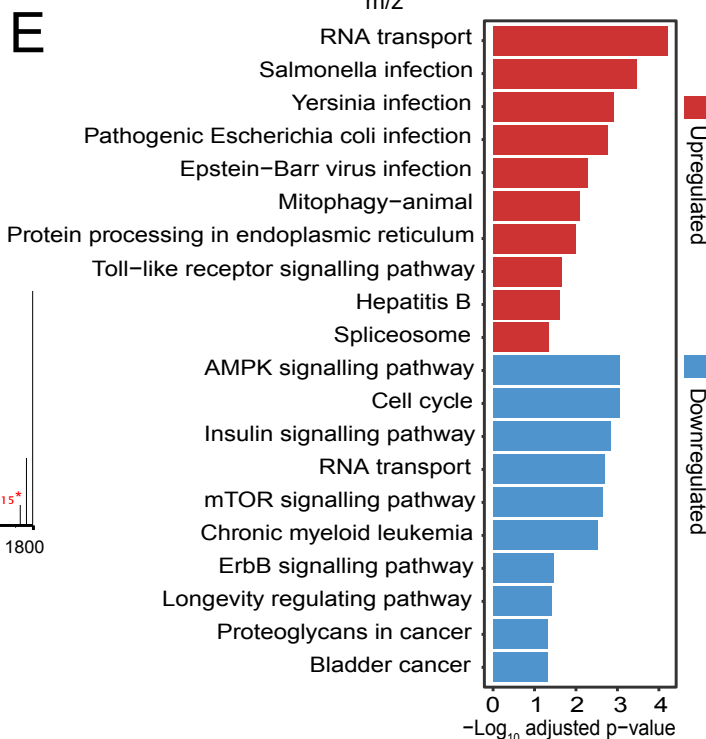
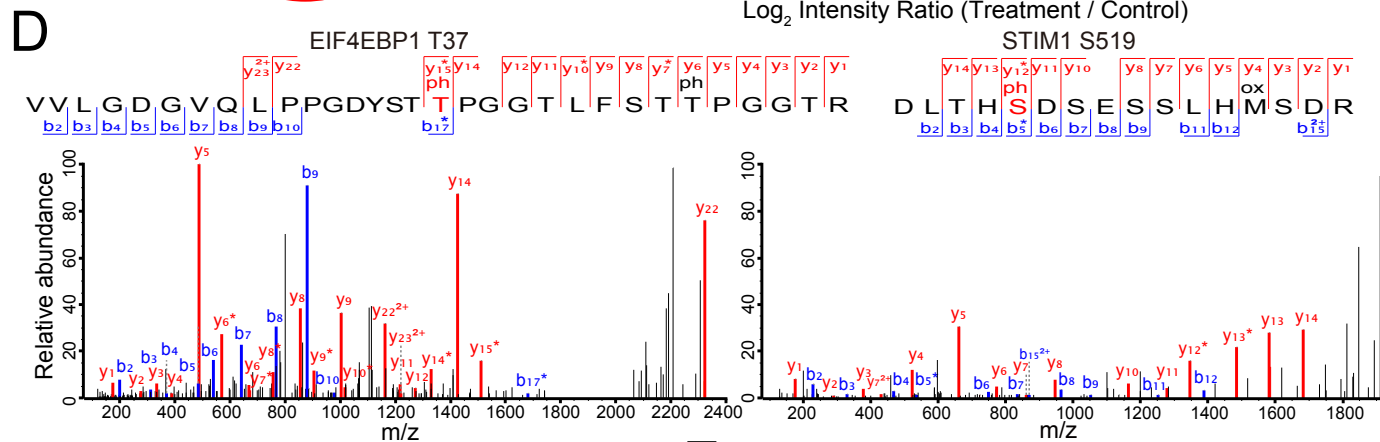
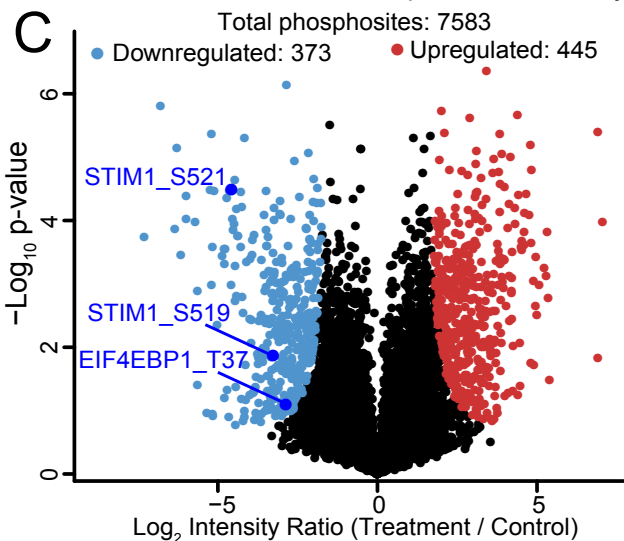
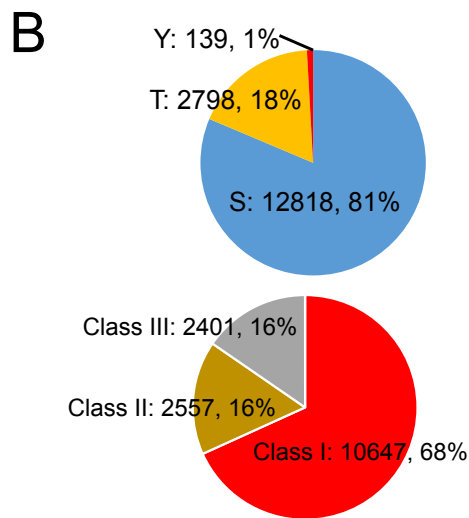
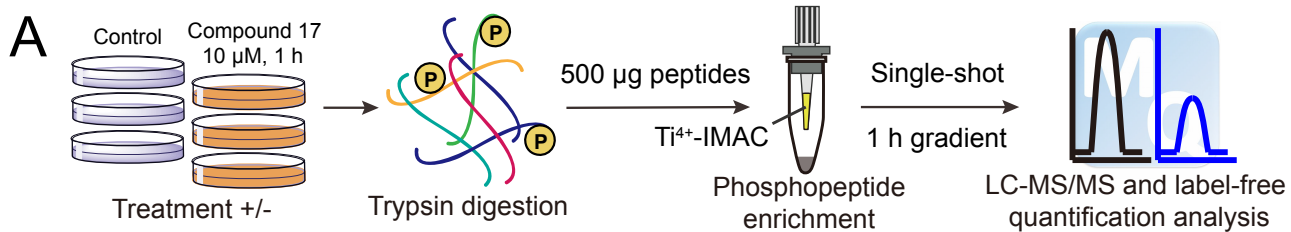
software, algorithm	Phenix	https://www.phenix-online.org/	RRID:SCR_014224	v1.19.2
software, algorithm	Coot	http://www2.mrc-lmb.cam.ac.uk/personal/pemsley/coot/	RRID:SCR_014222	v0.9
software, algorithm	Maxquant	http://www.biochem.mpg.de/5111795/maxquant	RRID:SCR_014485	v1.5.5.1
software, algorithm	Perseus	http://coxdocs.org/doku.php?id=perseus:start	RRID:SCR_015753	v1.5.5.3
software, algorithm	Thermo Xcalibur	https://www.thermofisher.cn/order/catalog/product/OPTON-30965	RRID:SCR_014593	v4.1.50

654

655

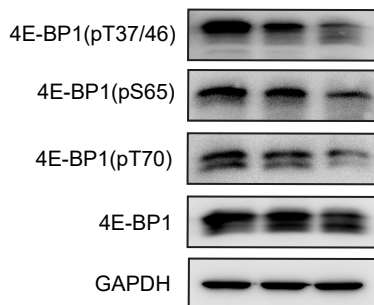
656



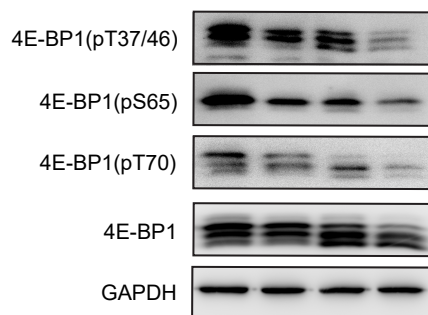


A

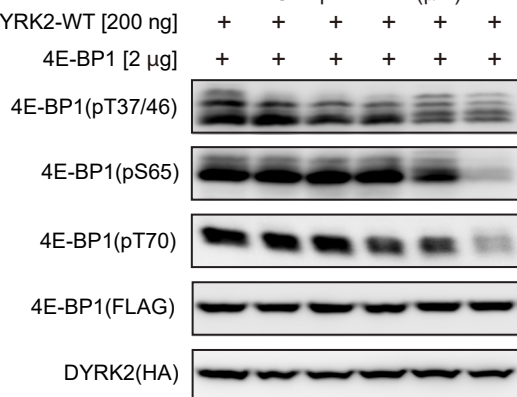
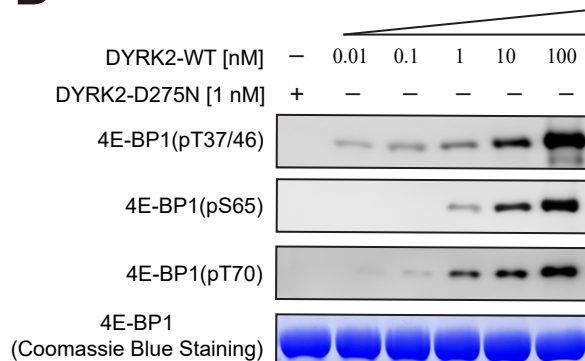
Compound 17 [1 μ M]	-	+	-
Compound 17 [10 μ M]	-	-	+

**B**

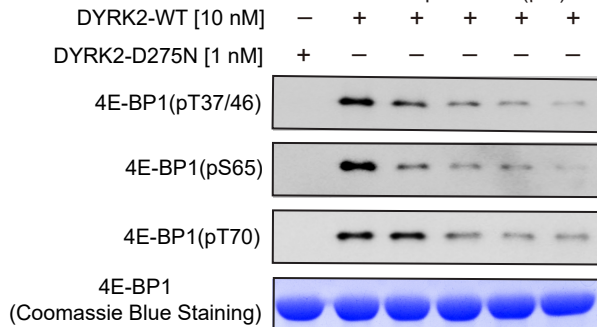
AKTi-1/2 [1 μ M]	-	-	+	+
PD0325901 [50 nM]	-	-	+	+
DYRK2 shRNA	-	+	-	+

**C**

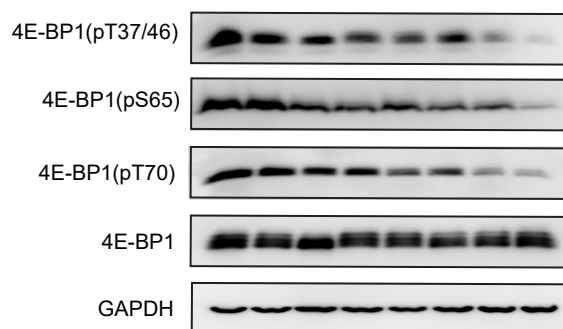
	0	0.1	0.3	1	3	10
DYRK2-WT [200 ng]	+	+	+	+	+	+
4E-BP1 [2 μ g]	+	+	+	+	+	+

**D****E**

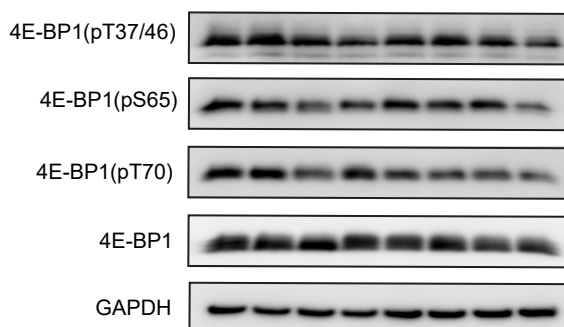
	0	0.3	1	3	10
DYRK2-WT [10 nM]	-	+	+	+	+
DYRK2-D275N [1 nM]	+	-	-	-	-

**F**

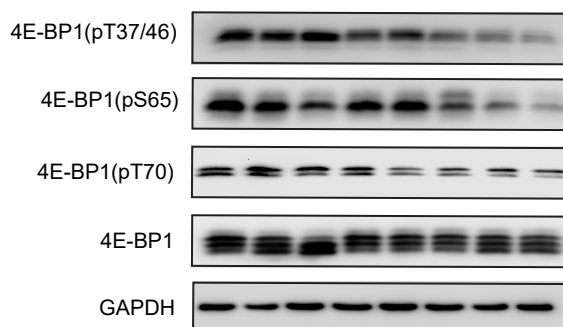
AKTi-1/2 [1 μ M]	-	+	-	-	-	-	+	+
AKTi-1/2 [10 μ M]	-	-	+	-	-	-	-	-
PD0325901 [50 nM]	-	-	-	+	-	-	+	+
PD0325901 [1 μ M]	-	-	-	-	+	-	-	-
Compound 17 [1 μ M]	-	-	-	-	-	+	-	+

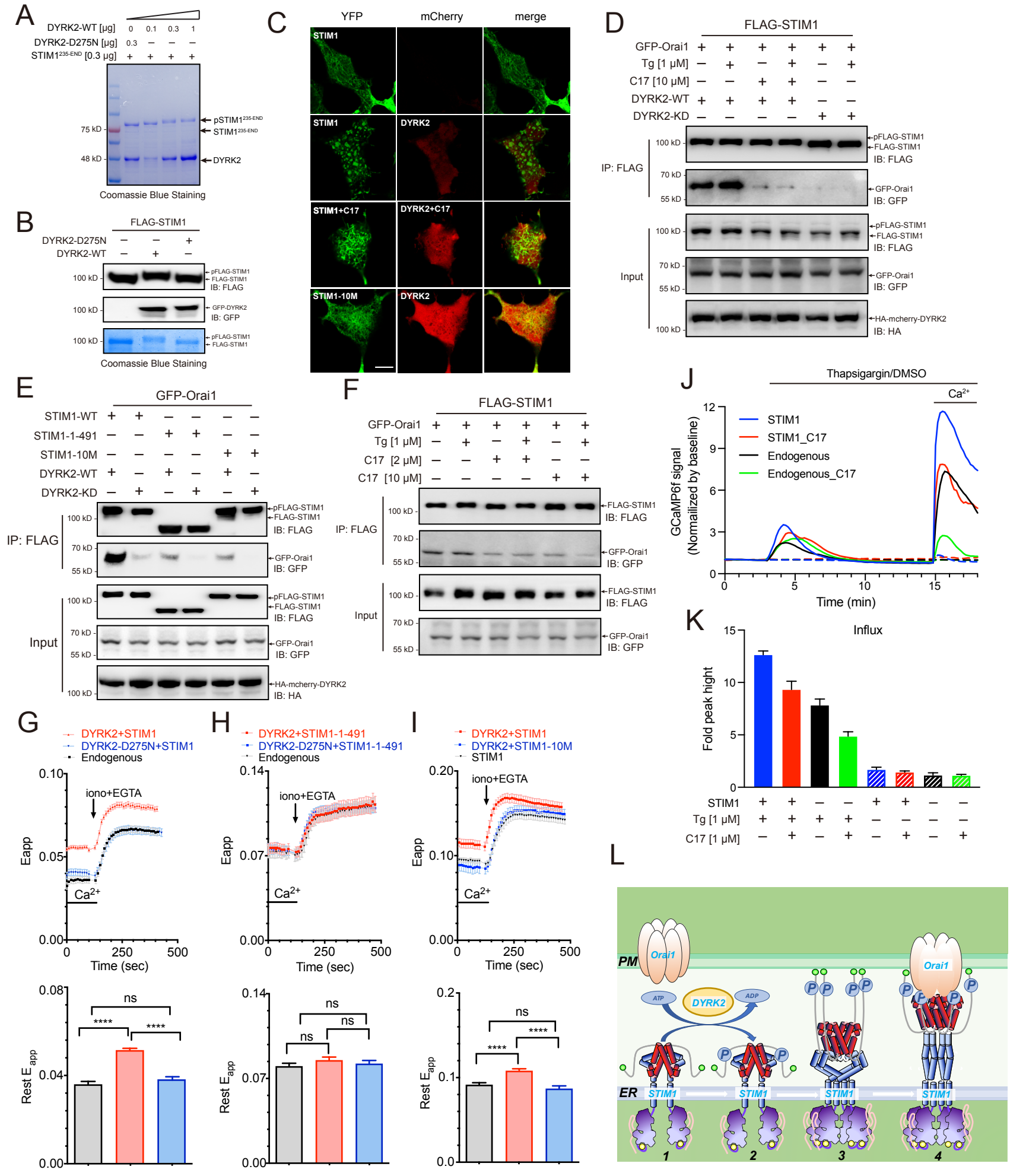
**G**

AKTi-1/2 [1 μ M]	-	+	-	-	-	-	+	+
AKTi-1/2 [10 μ M]	-	-	+	-	-	-	-	-
PD0325901 [50 nM]	-	-	-	+	-	-	+	+
PD0325901 [1 μ M]	-	-	-	-	+	-	-	-
Compound 17 [1 μ M]	-	-	-	-	-	+	-	+

**H**

AKTi-1/2 [1 μ M]	-	+	-	-	-	-	+	+
AKTi-1/2 [10 μ M]	-	-	+	-	-	-	-	-
PD0325901 [50 nM]	-	-	-	+	-	-	+	+
PD0325901 [1 μ M]	-	-	-	-	+	-	-	-
Compound 17 [1 μ M]	-	-	-	-	-	+	-	+



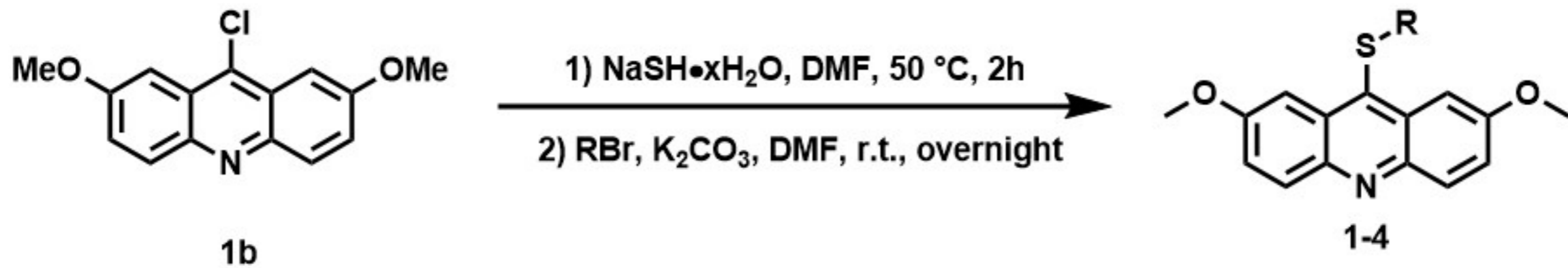
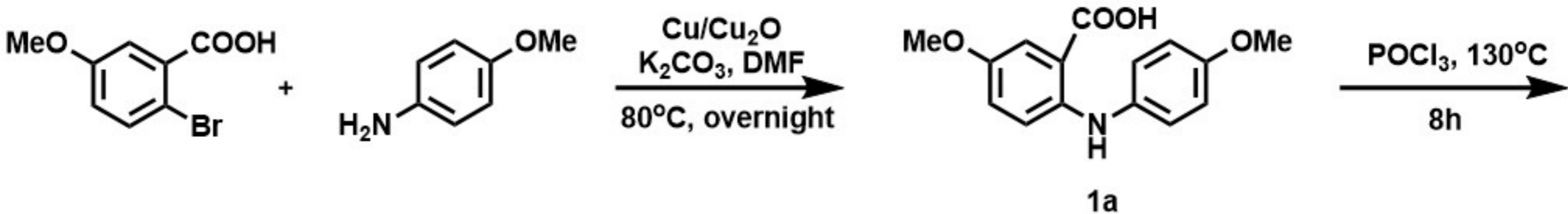


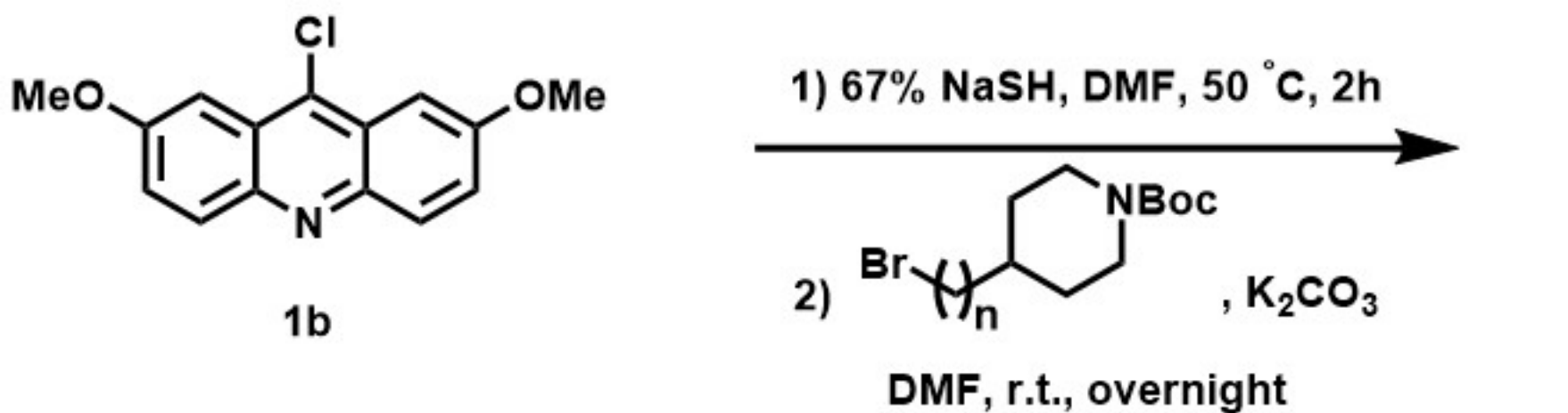
shRNA sequence

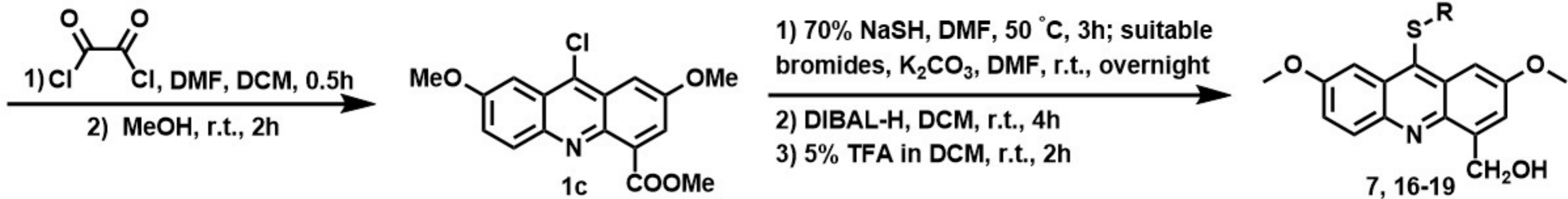
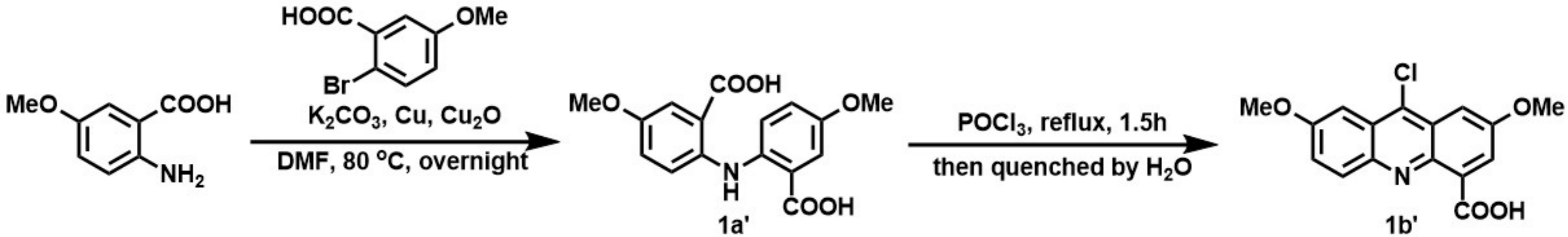
Name	Sequence
DYRK2 shRNA	gaacaagcaatgaagcaat

qRT-PCR primers

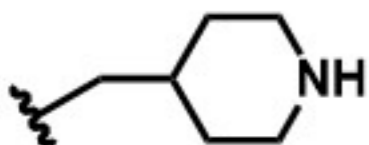
Name	Sequence
DYRK2-qPCR-Forward	TGCATTTTCCTCTCCAGCG
DYRK2-qPCR-Reverse	ACTGTTGAACCTGGATCTGTC
GAPDH-qPCR-Forward	CAAGCTCATTTCCTGGTATGACA
GAPDH-qPCR-Reverse	GGGAGATTCAGTGTGGTGGG



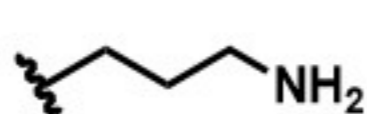




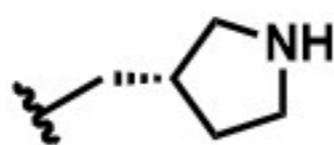
R = 7



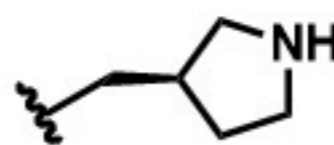
16



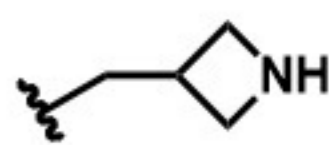
17

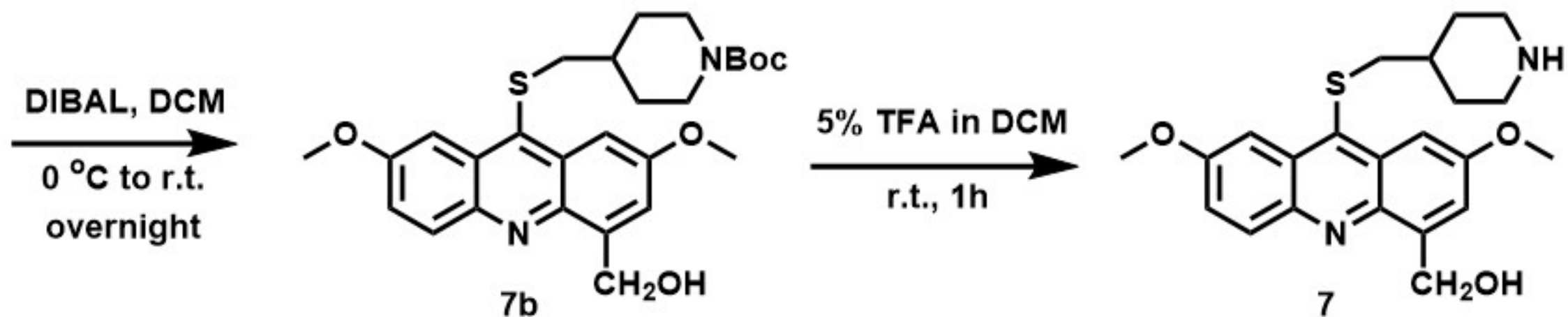
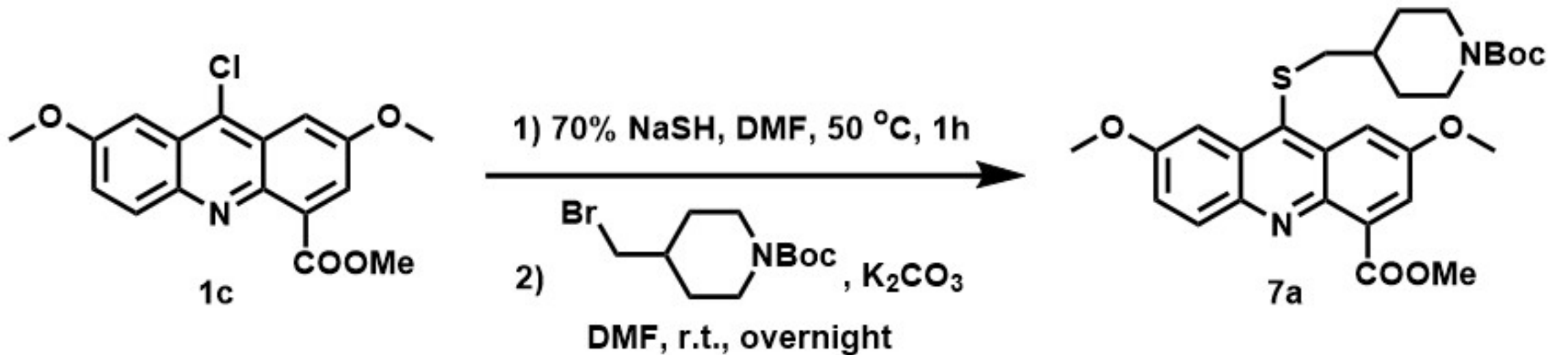


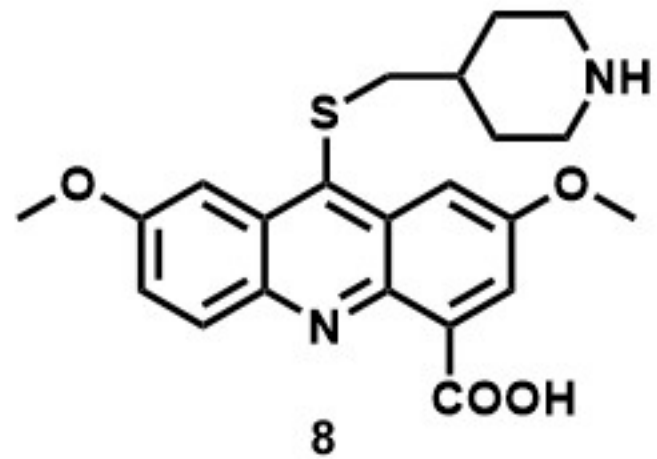
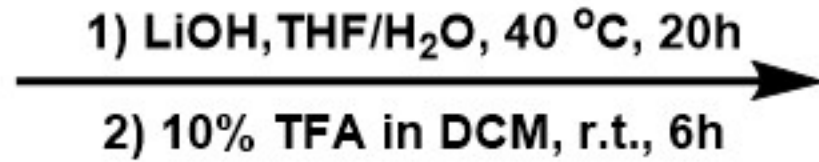
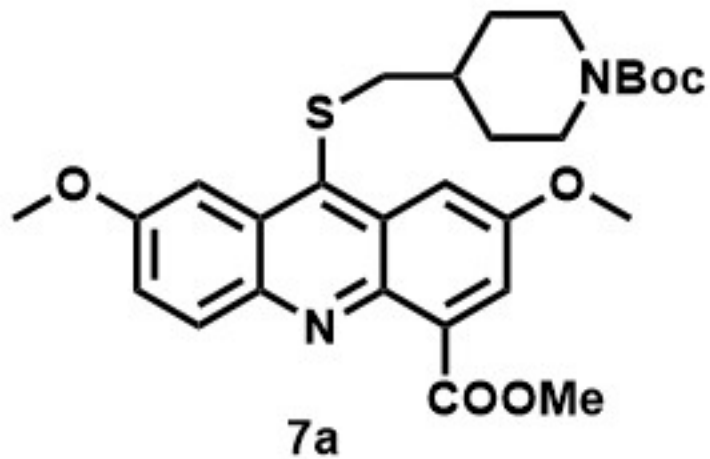
18

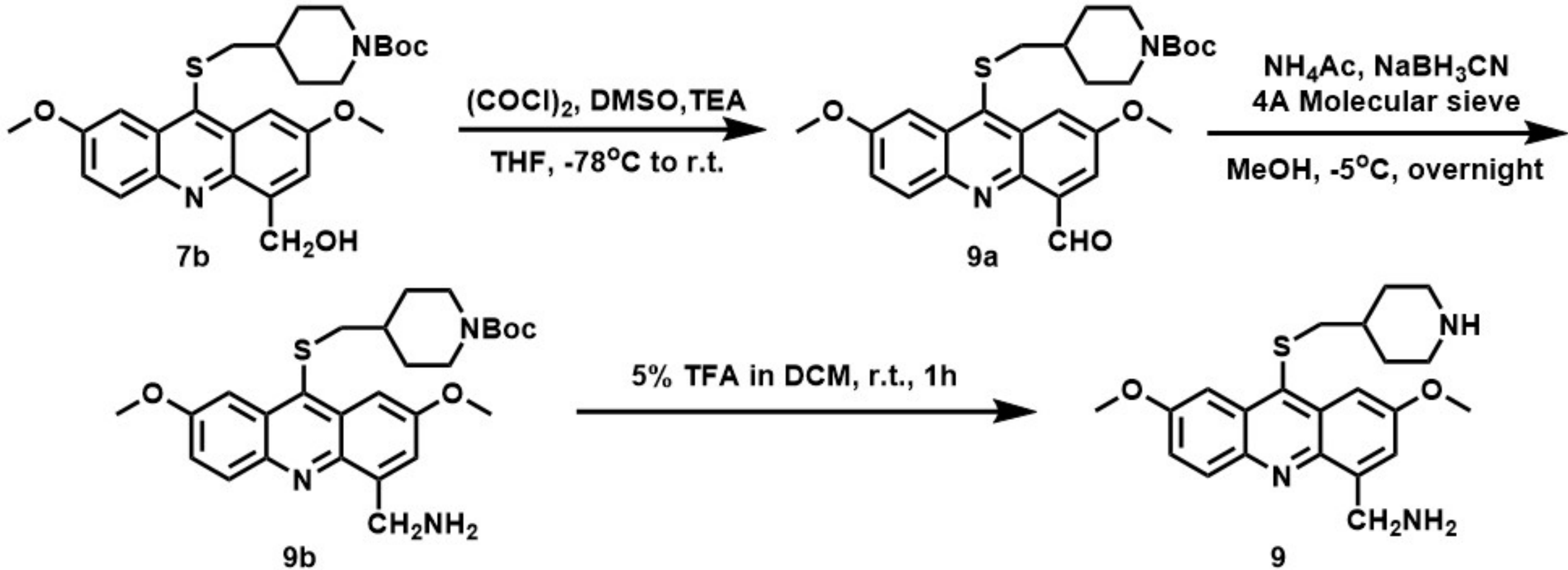


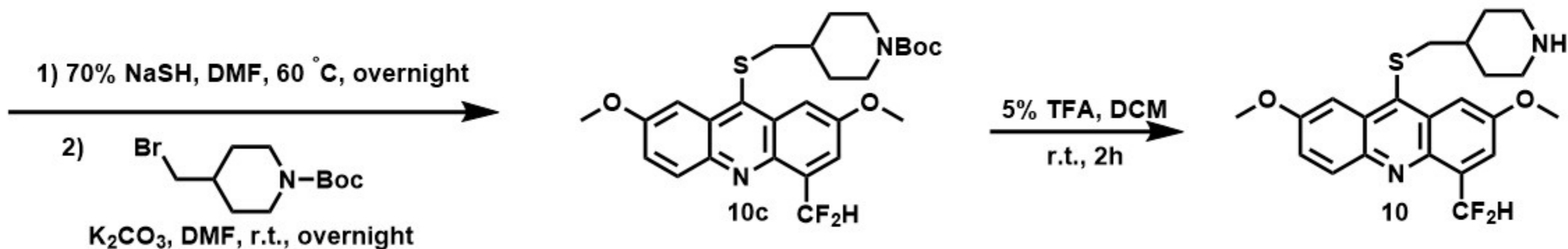
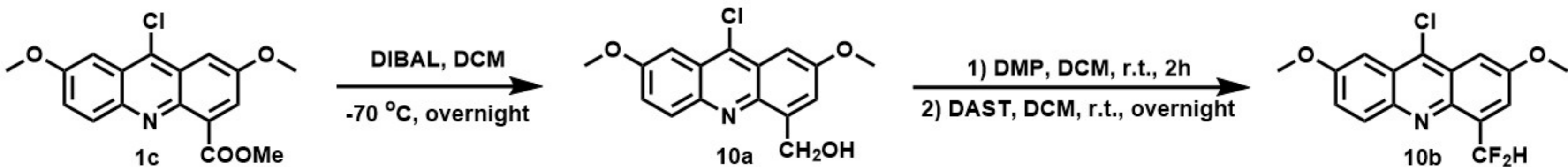
19

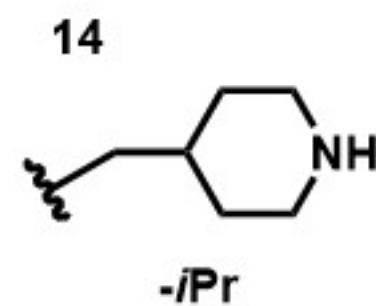
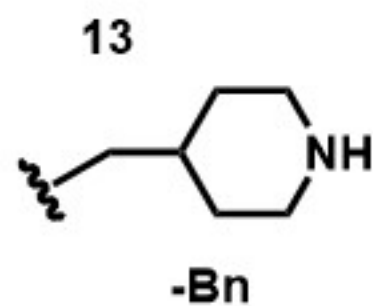
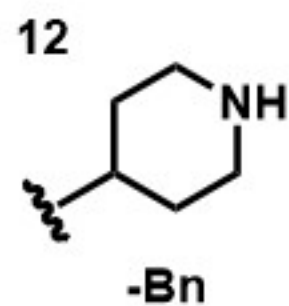
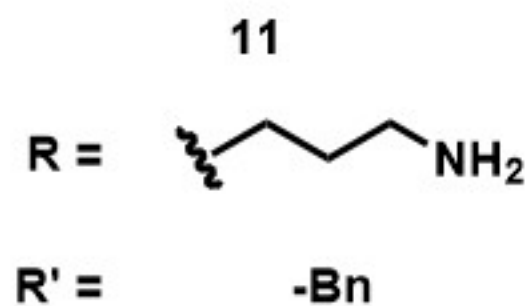
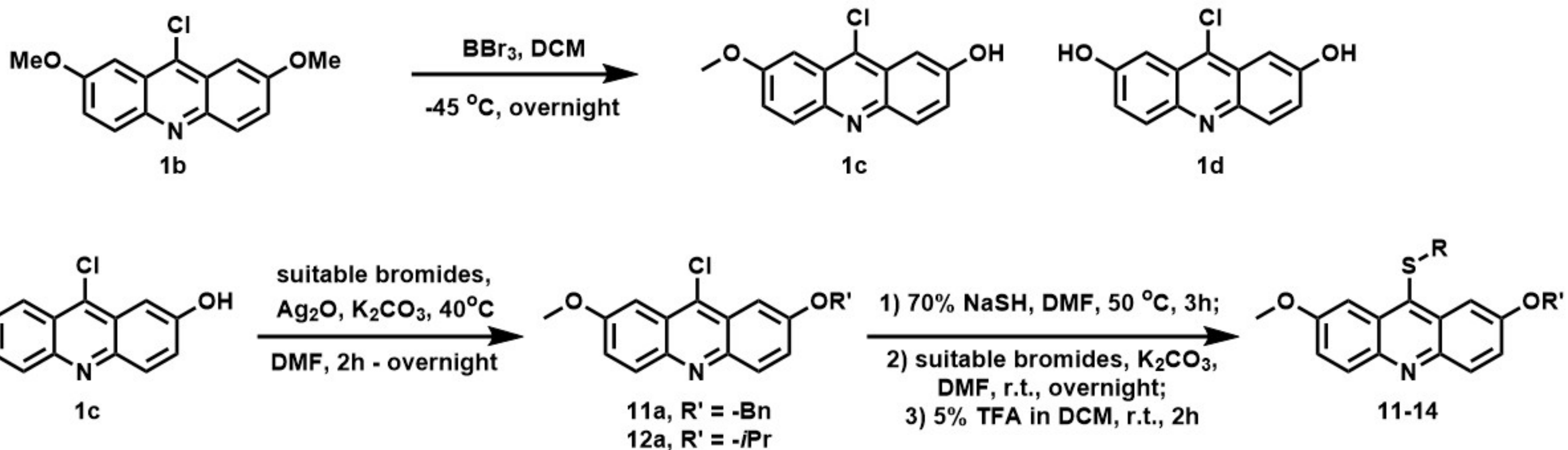


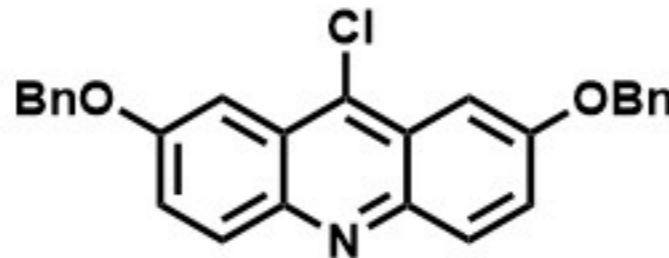
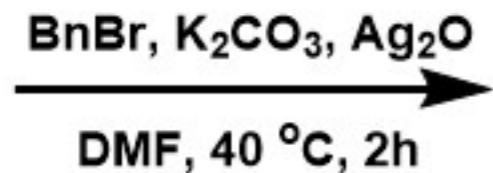
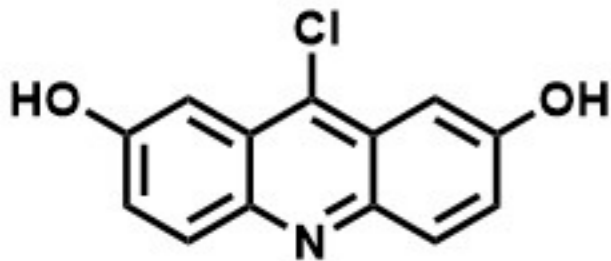




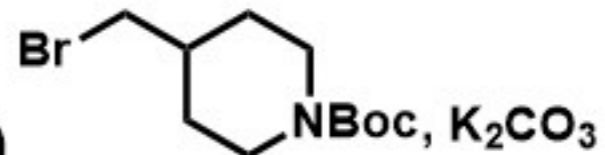








1) 70% NaSH, DMF, 50 °C, 2h



3) 5% TFA in DCM, r.t., 2h

